Doctoral theses at NTNU, 2019:213

Daniel Rohde

Dynamic simulation of future integrated energy systems

Doctoral Thesis

NTNU
Norwegian University of
Science and Technology
Faculty of Engineering
Department of Energy and Process Engineering

NTNU
Norwegian University of
Science and Technology

Daniel Rohde

Dynamic simulation of future integrated energy systems

Thesis for the degree of Philosophiae Doctor

Trondheim, September 2019

Norwegian University of Science and Technology
Faculty of Engineering
Department of Energy and Process Engineering

NTNU
Norwegian University of
Science and Technology

Acknowledgments

First of all, I would like to sincerely thank my supervisors Natasa Nord and Trond Andresen for their valuable support and guidance during the last five years. You both contributed to the fulfillment of this thesis in very different ways and I certainly benefited from the advantages of both.

Thank you also to all the co-authors of my papers, especially Hanne Kauko and Brage Rugstad Knudsen, for the fruitful collaboration. To all other colleagues/friends who know who they are: I very much appreciated the brain center talks, sports activities, countless cakes and coffees, and the almost philosophical discussions about modeling, simulation, and optimization with you.

I would also like to acknowledge the Norwegian Research Council and the staff at NTNU for providing the funding and the resources that made this work possible.

Last but not least, special thanks to Mareike and our daughters for always reminding me of the important things in life as well as to everyone who helped us during the stressful days before my final deadline.

Summary

The building sector is responsible for a large part of the world's total energy use. More than half of building energy use is needed for space heating, domestic hot water heating, and space cooling. Thermal energy supply systems are used to cover these thermal energy demands and are an integral part of new buildings and neighborhoods. These systems are becoming increasingly more complex due to the inclusion of renewable energy sources and thermal storages. Advanced simulations are required to analyze the design and the operation of these complex systems in detail and are thus an important part of the transition to new and improved building energy systems.

In this work, component and system models for thermal energy supply systems were developed in the modeling language Modelica. Numerical efficiency was an important part of the development process because the aim was to analyze long periods of time. In addition, the different requirements for simulation and optimization had to be considered during model development. Detailed description of all the developed Modelica models are given in this thesis. The models were used for dynamic simulations with Dymola as well as dynamic optimizations with JModelica.org, of which the latter proved to be more challenging. The optimization approach is therefore also described in detail in this thesis.

The design and the operation of two case study systems were analyzed in this work: 1) an existing integrated heating and cooling system at Vulkan, Oslo and 2) a planned local district heating grid at Brøset, Trondheim. The main components of the integrated heating and cooling system at Vulkan were heat pumps, plate heat exchangers, flat plate solar collectors, water storage tanks, ice thermal energy

storage, and borehole thermal energy storage. The system supplied a total floor area of 38 500 m^2 and is described in detail in this thesis. The main components of the local district heating grid at Brøset were a heat central, distribution pipes, and customer substations. The system was assumed to supply a total floor area of 178 000 m^2 and the different system design concepts that were analyzed are described in this thesis.

The main focus of this work was the case study system at Vulkan. The simulation results showed that the current operation of this system might be unsustainable due to an unbalanced long-term storage. Sustainable operation was possible in the simulations by increasing the number of solar collectors or the amount of imported heat from the district heating grid. The optimization results showed that variable setpoints for the heating and cooling supply temperatures could reduce the electricity use of the system. However, this would require the implementation of an advanced control system. The installation of larger storage tanks combined with optimal control was also investigated. It was shown that this combination could reduce the electricity costs of the system. However, the savings were not large enough to make an installation seem profitable with the current pricing scheme. Higher peak load tariffs and/or an increased variability of the electricity price might change this conclusion in the near future.

The analyses of the different system design concepts for the local district heating grid at Brøset showed that low-temperature grids were more environmentally-friendly than high-temperature-grids. This was mainly due to lower heat losses in the grid and the ability to include waste heat sources. The diameters of the district heating distribution pipes were shown to be important for the heat losses of the pipes and the required pumping power.

Several Modelica libraries with similar component models as the ones presented in this thesis are available. However, the system model development and the dynamic optimizations proved to be the most challenging tasks in this work. These tasks require a rather high level of user experience, but are expected to be increasingly important in the near future. This prediction is supported by the coordinated efforts that are currently going on in the IBPSA Project 1, which has a scope similar to the one of this thesis.

Table of contents

List of figures

List of tables

Nomenclature

Abbreviations

BAU	Business as usual
BTES	Borehole thermal energy storage
COP(s)	Coefficient(s) of performance
DAES	Differential algebraic equation system
DH	District heating
DHW	Domestic hot water
DS	Dymola screenshot
GHG	Greenhouse gas
GSHP(s)	Ground source heat pump(s)
HP(s)	Heat pump(s)
HVAC	Heating, ventilation, and air conditioning
HX	Heat exchanger
IHCS	Integrated heating and cooling system
ITES	Ice thermal energy storage
LMTD	Logarithmic mean temperature difference
LTDH	Low-temperature district heating
MPC	Model predictive control
MSL	Modelica standard library
NLP	Nonlinear programming
NTU	Number of transfer units
PRBC	Predictive rule-based control
TES	Thermal energy storage

Symbols

a_1	Linear heat loss coefficient $\left(\mathrm{W}/(\mathrm{m}^2 \cdot \mathrm{K})\right)$
a_2	Quadratic heat loss coefficient $\left(\mathrm{W}/(\mathrm{m}^2 \cdot \mathrm{K}^2)\right)$
A	Area (m^2)
c_p	Specific heat capacity at constant pressure $\left(\mathrm{J}/(\mathrm{kg} \cdot \mathrm{K})\right)$
c_v	Specific heat capacity at constant volume $\left(\mathrm{J}/(\mathrm{kg} \cdot \mathrm{K})\right)$
C	Heat capacity flow rate (W/K)
Δp	Pressure difference (Pa)
ΔT	Temperature difference (K)
δ	Slack parameter $(-)$
ε	Heat exchanger effectiveness $(-)$
η	Efficiency $(-)$
e	Electricity price (NOK/MWh)
E	Electricity use (kWh)
FtP	Flow-to-power coefficient ($\mathrm{MW} \cdot \mathrm{s}^2/\mathrm{m}^6$)
$\dot{m}$	Mass flow rate (kg/s)
Nu	Nusselt Number $(-)$
NTU	Number of transfer units $(-)$
P	Power (W)
q	Exponent for calculation of the heat transfer coefficient $(-)$
Q	Heat (kWh)
$\dot{Q}$	Heat flow rate (W)
ρ	Density (kg/m^3)
R	Solar radiation per square meter (W/m^2)
t	Time (s)
T	Temperature (K)
U	Heat transfer coefficient $\left(\mathrm{W}/(\mathrm{m}^2 \cdot \mathrm{K})\right)$
v	Variability $(-)$
V	Volume (m^3)
$\dot{V}$	Volume flow rate (m^3/s)

Subscripts

amb	Ambient
ann	Annual

avg	Average
col	Solar collector
cold	Cold side
cond	Condenser
const	Constant
cool	Cooling
del	Delivered
dem	Demanded
evap	Evaporator
heat	Heating
hot	Hot side
HP(s)	Heat pump(s)
HX	Heat exchanger
in	Inlet
L	Lorentz
LM	Logarithmic mean
max	Maximum
meas	Measured
min	Minimum
nom	Nominal
opt	Optical
out	Outlet
pump(s)	Circulation pump(s)
r	Ratio
ret	Return
SC	Space cooling
sec	Secondary
SH	Space heating
sim	Simulated
SM	Snow melting
sup	Supply
sys	System
sys+BTES	System and BTES
tot	Total

1 Introduction

1.1 Motivation

The building sector is responsible for a large part of the world's total energy use, with a share of around 40 % in the European Union [1] and the United States [2]. This energy use is responsible for significant greenhouse gas (GHG) emissions, which contribute to global warming. Emission reduction of building energy systems is therefore a goal of many research and development initiatives.

More than half of building energy use is needed for space heating, domestic hot water (DHW) heating, and space cooling. These thermal energy demands *"represent the single largest opportunity to reduce buildings energy consumption in most regions of the world"* according to the International Energy Agency [3]. In non-residential buildings, other thermal energy demands can also occur, e.g. heating of water in swimming halls, cooling of food products in supermarkets, cooling of medical products in hospitals, or cooling of IT equipment in data centers. In Norway, heating is sometimes also applied to highly frequented walking areas or stairs to melt snow and ice to ensure a safe environment for pedestrians during the winter.

Thermal energy supply systems are used to cover the thermal energy demands described above and are an integral part of new buildings and neighborhoods. Many different system solutions exist throughout the world due to the abundance of building types and climatic conditions, which influence the heating and cooling demands significantly. In addition, various solutions exist for different system scales, reaching from small private installations to large city-wide systems.

In Norway, electric heating and wood burning have long been the dominant choices for space heating and DHW heating due to the availability of cheap electricity and firewood. However, due to higher electricity prices and stricter legislation, more efficient solutions like heat pumps (HPs) [4] and district heating (DH) [5] have become more popular in recent decades. The development of low-temperature district heating (LTDH) grids [6], low- or zero-energy buildings [7], and even zero emission neighborhoods [8] has gained much attention recently. Future thermal energy supply systems are thus significantly different from traditional systems. To meet the strict targets for energy efficiency, system integration and "smart" control are prerequisites. System integration means the coupling of thermal systems for efficient interaction of heating and cooling demands as well as thermal energy storage (TES) and renewable energy sources. "Smart" control means using predictive control strategies and thermal energy storages to reduce energy use and/or operating costs. This development is heavily driven by coming dynamic tariff structures for electricity and district heating in Norway. Future thermal energy supply systems are thus more complex and flexible than traditional single-purpose systems and require a holistic design and control approach to make use of their flexibility in an optimal way.

Computer simulations are required to analyze the design and the operation of these complex systems in detail [9]. The simulation capability has increased significantly during the last decades due to the increase in available computational power. Many different software solutions exist, both for dedicated applications as well as sophisticated multi-purpose tools [10]. Using advanced computational methods for the design and analysis of future integrated energy systems is thus an important part of the transition to new and improved building energy systems.

1.2 Aim of study

The main aim of this work was the analysis of both the design and the operation of thermal energy supply systems on neighborhood scale to make these systems more energy- and/or cost efficient. Due to the importance of storages for such systems, focus was on both long- and short-term thermal energy storage. Dynamic simulations were chosen as computational method due to the inherent dynamics of thermal energy storages and flexible systems. The high level of com-

plexity and individuality of future integrated energy systems makes it difficult to draw general conclusions from case studies. The goal was therefore to develop simulation models, which can be reused easily and to apply them to selected case studies. Although closely related, building performance simulation, i.e. the calculation of the energy demands of buildings, was outside the scope of this work. To achieve the aim of this study, the following objectives were defined:

- Development of component models for dynamic simulation, which enable the analysis of future integrated energy systems. All the component models should have a similar level of detail and be accurate enough to include relevant component characteristics, but also fast enough to enable long-term simulations in reasonably short time.
- Development of system models for dynamic simulation, representing case study systems. This includes data acquisition for the heating and cooling demands, the coupling of component models, and the implementation of a control system.
- Development of component and system models for dynamic optimization. This should enable the detailed analysis of system control for one of the case study systems.
- Recommendations for the design and the operation of the case study systems. In particular, design suggestions for the planned system and retrofitting options as well as operating suggestions for the existing system.

1.3 Thesis content

This thesis is structured as follows: Chapter 2 gives information about thermal energy supply systems, modeling and simulation, as well as optimization. The case study systems that were analyzed are introduced and explained in Chapter 3. Afterwards, the simulation model development is described in detail in Chapter 4, which was the main task of this work. The optimization model development is described in Chapter 5 followed by results from the two case studies in Chapter 6 and Chapter 7. Concluding remarks and suggestions for further work are given in Chapter 8.

1.4 List of publications

The author of this thesis contributed to six scientific papers during his thesis work. The relation between the content of the thesis and the papers will be explained where necessary. Author contributions for each paper based on the CRediT taxonomy [11] are given below.

Paper I

D. Rohde, M. Bantle, T. Andresen, and N. Nord (2015). "Documentation of an Integrated Thermal Energy System for a Building Complex." In: *Proceedings of the 24th International Congress of Refrigeration, Yokohama, Japan.* DOI: 10.18462/iir.icr.2015.0445.

Author contributions: Conceptualization: D.R., N.N., Investigation: D.R., T.A., N.N., Resources: M.B., Writing – Original Draft: D.R., Writing – Review & Editing: D.R., T.A., N.N., Visualization: D.R., Supervision: T.A., N.N., Funding acquisition: N.N.

Paper II

D. Rohde, T. Andresen, and N. Nord (2016). "Interaction Between a Building Complex with an Integrated Thermal Energy System and a District Heating System." In: *Proceedings of the 12th REHVA World Congress, Aalborg, Denmark.*

Author contributions: Conceptualization: D.R., N.N., Methodology: D.R., T.A., Investigation: D.R., Resources: D.R., Writing – Original Draft: D.R., Writing – Review & Editing: D.R., T.A., N.N., Visualization: D.R., Supervision: T.A., N.N., Funding acquisition: N.N.

Paper III

H. Kauko, K. H. Kvalsvik, D. Rohde, A. Hafner, and N. Nord (2017). "Dynamic modelling of local low-temperature heating grids: A case study for Norway." *Energy* 139, pp. 289–297. DOI: 10.1016/j.energy.2017.07.086.

Author contributions: Conceptualization: H.K., A.H., N.N., Methodology: H.K., K.H.K., D.R., Investigation: H.K., K.H.K., D.R., Resources: H.K., Writing – Original Draft: H.K., K.H.K., Writing – Review & Editing: H.K., K.H.K., D.R.,

N.N., Visualization: H.K., Supervision: H.K., A.H., Project Administration: H.K., Funding acquisition: H.K., A.H.

Paper IV

H. Kauko, K. H. Kvalsvik, D. Rohde, N. Nord, and Å. Utne (2018). "Dynamic modeling of local district heating grids with prosumers: A case study for Norway." *Energy* 151, pp. 261–271. DOI: 10.1016/j.energy.2018.03.033.

Author contributions: Conceptualization: H.K., N.N., Å.U., Methodology: H.K., K.H.K., D.R., Investigation: H.K., K.H.K., D.R., Resources: H.K., Å.U., Writing – Original Draft: H.K., Writing – Review & Editing: H.K., K.H.K., D.R., N.N., Å.U., Visualization: H.K., Supervision: H.K., N.N., Project Administration: H.K., Funding acquisition: H.K.

Paper V

D. Rohde, T. Andresen, and N. Nord (2018). "Analysis of an integrated heating and cooling system for a building complex with focus on long–term thermal storage." *Applied Thermal Engineering* 145 (7), pp. 791–803. DOI: 10.1016/j.applthermaleng.2018.09.044.

Author contributions: Conceptualization: D.R., T.A., N.N., Methodology: D.R., T.A., Investigation: D.R., Resources: D.R., Writing – Original Draft: D.R., Writing – Review & Editing: D.R., T.A., N.N., Visualization: D.R., Supervision: T.A., N.N., Funding acquisition: N.N.

Paper VI

D. Rohde, B. R. Knudsen, T. Andresen, and N. Nord (2020). "Dynamic optimization of control setpoints for an integrated heating and cooling system with thermal energy storages." *Energy* 193, p. 116771. DOI: 10.1016/j.energy.2019.116771.

Author contributions: Conceptualization: D.R., B.R.K., N.N., Methodology: D.R., B.R.K., Software: D.R., B.R.K., Investigation: D.R., Resources: D.R., B.R.K., Writing – Original Draft: D.R., Writing – Review & Editing: D.R., B.R.K., T.A., N.N., Visualization: D.R., Supervision: T.A., N.N., Funding acquisition: N.N.

2 | Background

The aim of this work was to study thermal energy supply systems by means of computational system analysis. Therefore, background information on these topics is given in the following sections.

2.1 Thermal energy supply systems for neighborhoods

2.1.1 Definition and system scale considerations

In order to cover the heating and cooling demands of large buildings, building complexes, or neighborhoods, the required thermal energy has to be delivered to the buildings and then be distributed to several areas and rooms within each building. In this work, only the supply system side was analyzed, the distribution system side was excluded. As mentioned in the introduction, different system solutions exist for different scales. The scale can roughly be divided into detached houses with individual systems, building complexes or neighborhoods with integrated thermal energy supply systems, and small cities or districts with district heating and cooling systems. The scale relevant for this work was the neighborhood scale, i.e. building complexes or small districts with a designated thermal energy supply system.

Such systems can show a high degree of individuality, especially when different heating and cooling demands at various temperature levels are present and when fluctuating renewable energy sources and storages are included. Such systems are therefore not standardized and need to be adapted to the neighborhood at hand. Other terms used for this kind of system are “smart thermal grid”, “ther-

mal network", "thermal micro-grid", "integrated energy system", "hybrid energy system", and "large-scale heating and cooling system" with definitions varying from source to source. In this thesis, the terms "integrated heating and cooling system" and "local district heating grid" are used for the two case study systems.

2.1.2 Key components for thermal systems

The key components for the thermal energy supply systems that were analyzed in this work are described in this chapter. Key components means that they are important for system performance, but not all of them are required for each system. The component choice is part of the system design phase and depends on the neighborhood at hand.

Heat exchanger A heat exchanger is used to transfer heat from a warmer fluid (liquid or gas) to a colder fluid. Heat exchangers are used in many different engineering applications and several different types have been developed. Heat exchangers are usually customized for their designated operating conditions so that a good trade off between heat transfer, pressure drop, and cost can be found. A very common type for heating, ventilation, and air conditioning (HVAC) systems is the counterflow plate heat exchanger, which is compact, cost effective, and readily available. This type of heat exchanger was the only type used for the case study systems in this work.

Heat pump A heat pump transfers heat from a colder environment to a warmer environment via a closed thermodynamic cycle by using work. The heat pump process includes evaporation and condensation of the working fluid. Depending on the application, the heat released during condensation of the working fluid is used for heating purposes, or the heat taken up during evaporation of the working fluid is used for cooling purposes. The coefficient of performance (COP) of a heat pump is an efficiency measure and depends significantly on the heat pump's temperature lift, i.e. the temperature difference between the evaporation temperature and the condensation temperature. High temperature lifts require more compressor power and lead to lower COPs. The COP of air source heat pumps thus depends highly on the outdoor temperature and is lowest on cold days when the most heating energy is needed. Ground source heat pumps

(GSHP) have therefore become increasingly popular in cold regions due to their higher COPs during the winter. However, the installation costs for GSHPs are high due to expensive drilling and can thus be critical for small residential applications. For larger installations, GSHPs are a promising choice and are often combined with seasonal thermal energy storage as described in one of the case study systems in this thesis.

Solar collectors Solar collectors are used to heat a fluid by radiation from the sun. Different types of solar collectors for different temperature levels exist. The most common type for building applications is the flat plate solar collector, which was the only type used for the case study systems in this work. The number of collectors to be installed depends on the available area and the expected heating demands. There is often a mismatch between the availability of solar heat and the heating demands, which is why the collectors are usually coupled to a storage tank. Seasonal storage of solar heat is also a common solution [12].

Thermal energy storage Thermal energy storage allows, to a certain extent, to decouple thermal demand and supply. This decoupling can be used to integrate fluctuating energy sources, e.g. solar heat, or to reduce expensive peak demands [13]. A classification of storage types is shown in Figure 2.1. Common storage components of thermal energy supply systems are water tanks for short-term storage and borehole thermal energy storage (BTES) for long-term (seasonal) storage. These were the only types used for the case study systems in this work. Phase change materials and thermochemical storage are emerging technologies which are not widely implemented yet [14]. An important aspect for the inclusion of thermal storages is the control strategy, i.e. when the storages should be charged or discharged and which temperature levels should be obtained. Different strategies are presented in Section 2.1.3.

Pipes The importance of pipes for thermal energy supply systems depends on the distance between the location of the heat source and the heating demand, i.e. the customer (for cooling demands, the distance between the heat sink and the cooling demand). They are thus less relevant for dense building complexes compared to larger neighborhoods. For district heating and cooling systems with

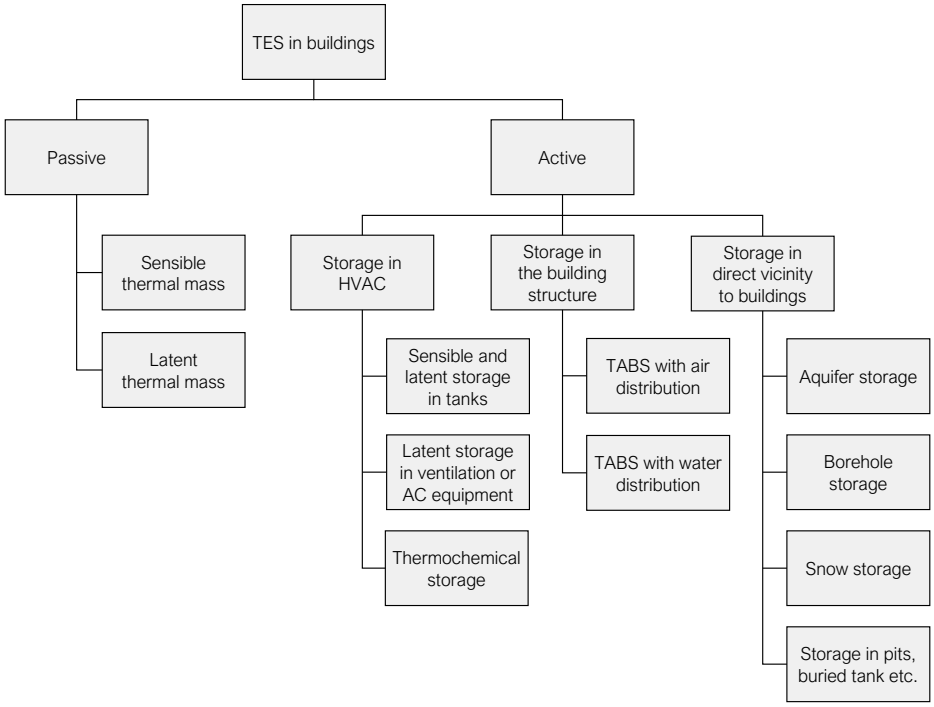

Figure 2.1: Classification of TES techniques [14].

several kilometers of buried pipes, the pipe selection is a crucial aspect. Especially the diameter of the pipes has to be chosen carefully to find a good trade-off between heat losses, required pump power, and cost in each branch. Different pipe materials and insulation thicknesses are available. Common for new grids are twin pipes, where both supply and return pipe are enclosed in the same insulation layer to reduce the grid's heat losses [15]. Both single and twin pipes were studied in this work.

2.1.3 The importance of system control

The operating performance of a thermal energy supply system does not only depend on the installed components, but also on the implemented control system. A classification of control methods is shown in Figure 2.2.

Classical control, see Figure 2.2, is the simplest and by far the most commonly used control method. With on/off control, a component is switched on and off depending on a measured variable that is to be kept between a lower and an

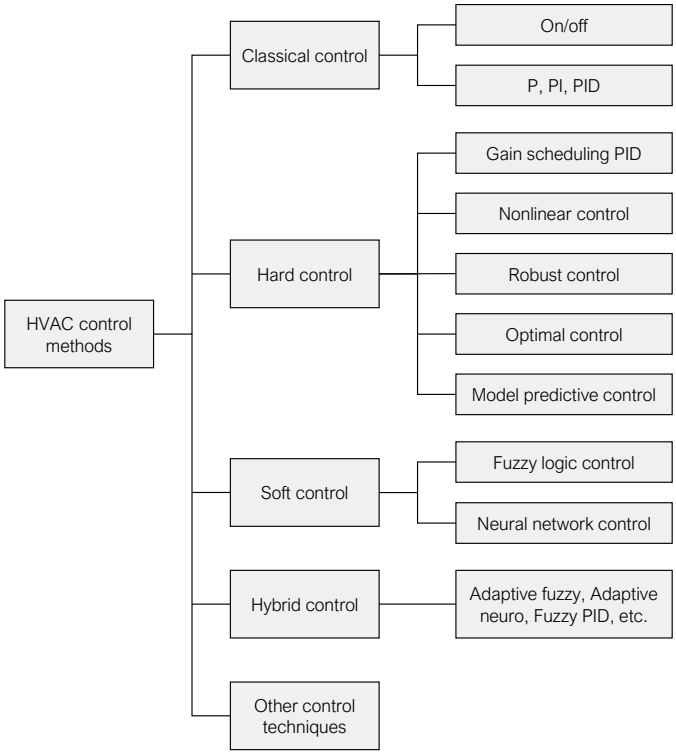

Figure 2.2: Classification of HVAC control methods [16].

upper threshold. This approach is very simple because only the two thresholds need to be defined. However, this control method is unsuitable for processes with large time delays because time delays can lead to large deviations between desired setpoint and measured variable. The aim of P, PI, or PID control is to keep a measured variable at a certain setpoint. The output of the controller is continuously adjusted based on the controller parameters and the control error, i.e. the difference between the measured value and the setpoint value. The parameters for the proportional (P), integral (I), and derivative (D) term have to be tuned for each application to achieve good results. This can be difficult in practice, especially when the operating conditions of the process change and thus differ from the tuning conditions. The other control methods shown in Figure 2.2 are more advanced. They may therefore lead to better results, but also require more implementation effort.

Apart from the control method, a control strategy also has to be defined, i.e.

how the thresholds and/or setpoints for the controllers are chosen and potentially changed during operation. This is especially important for systems with storages because it has to be determined when the storages should be charged or discharged. A good control strategy is crucial for efficient storage operation and different strategies exist. A classification of control strategies is shown in Figure 2.3.

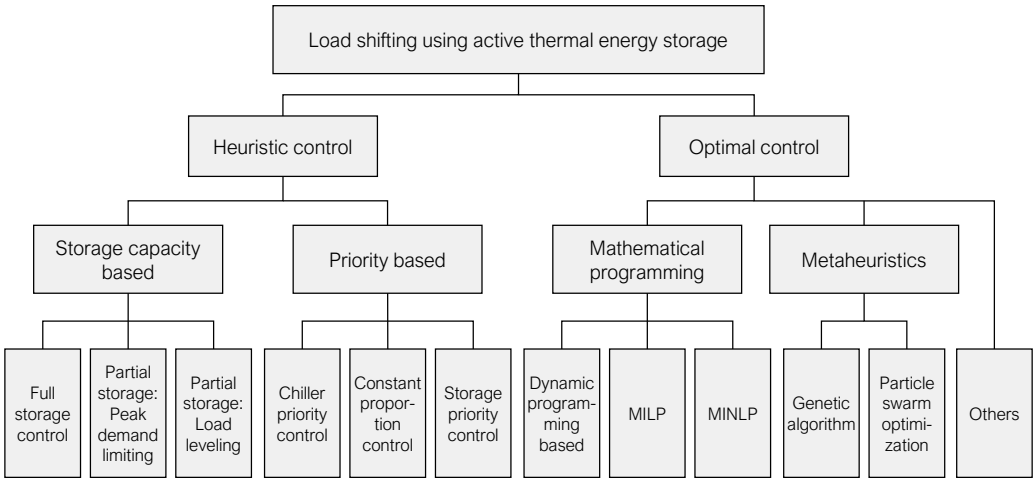

Figure 2.3: Classification of active TES control strategies [17] (MILP = Mixed integer linear programming, MINLP = Mixed integer nonlinear programming).

Recently, predictive control has received much attention because the implementation of forecasts for weather, demands, and prices can lead to improved operation. Two common approaches are predictive rule-based control (PRBC) and model predictive control (MPC). With PRBC, the setpoints for the local controllers are adjusted based on a set of heuristic "if-then-else" rules. PRBC is relatively easy to implement, but the performance depends highly on the rules, which can be difficult to define for complex systems or changing operating conditions [18]. With MPC, a system model is used to repeatedly solve an optimal control problem over a receding horizon, with the first control action of the optimal solution being implemented before re-optimization. MPC is more difficult to implement than PRBC and the performance is very dependent on the optimization model of the system [19]. Note that both MPC and optimal control are also listed as control methods in Figure 2.2. However, the control strategy is defined in the objective function of the optimal control problem, which is why they are

also treated as control strategies here. Typical objectives for optimal control are the minimization of energy use or operating costs. Optimal control is treated in this thesis and is explained in Section 2.2.3 and Chapter 5.

2.2 Methods for computational system analysis

Significant advances have been made in microprocessor performance during the last decades, see Figure 2.4.

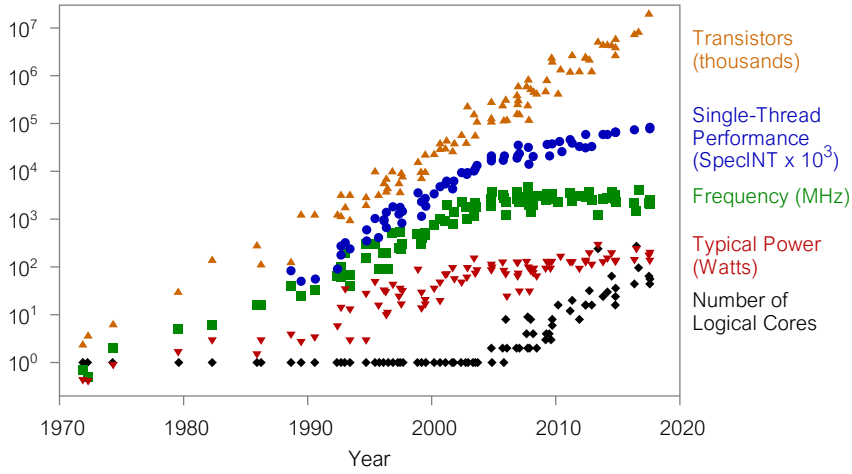

Figure 2.4: 42 years of microprocessor trend data [20].

The performance advances shown in Figure 2.4 have enabled the development of sophisticated computer simulation tools. However, computational performance is still a limiting factor for these tools and can restrict their simulation capability. Keeping computation times within reasonable limits is important and should be kept in mind during simulation model development. As G. Augenbroe stated in a book about building performance simulation [21]:

> "The art of modeling and simulation is leaving things out that don't affect the answer." – G. Augenbroe

Computation time obviously depends on the type of hardware used. Apart from that, the level of detail, the number of components, and the simulated time influence the computation time as shown in Figure 2.5.

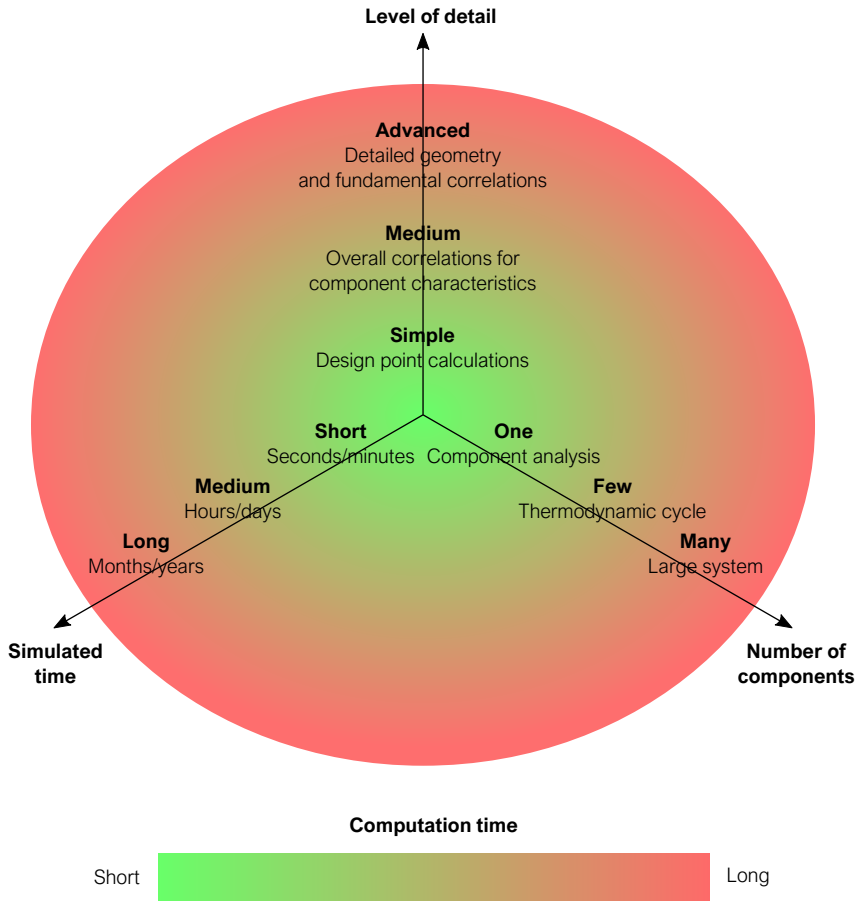

Figure 2.5: Computation times for system analysis.

Figure 2.5 is a very general representation. Other factors can also influence the computation time, e.g. the complexity of the system, i.e. the number of interactions between components, or the efficiency of the software used.

The number of components of a system and the simulated time for the specific analysis are usually known beforehand. The level of detail and the simulation software can also be predefined, but are often more free. The right choice depends first of all on the aim of the analysis, but in practice also to a high degree on the available resources and the experience of the user. The scope of work was to analyze the annual performance of systems with many components. Therefore, the level of detail of the component models was chosen to be "medium", see Figure 2.5. A higher level of detail could lead to unacceptably long computation

times and would also require much more user input data. Unless these inputs are available and can be specified at a sufficiently high level of certainty, the results would not necessarily be more correct with more detailed component models as shown in Figure 2.6.

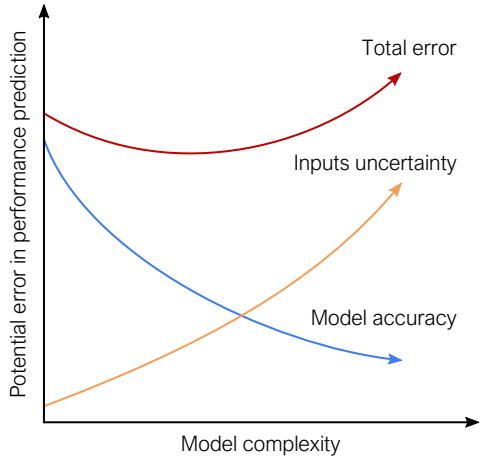

Figure 2.6: Potential error vs. model complexity [22].

2.2.1 Modeling with Modelica

Modeling is a broad term. In this thesis, modeling refers to the mathematical description of a component or a system. This mathematical description can be used in a computer simulation to study the behavior of the modeled component or system.

Originally, modeling and simulation were closely linked because programming languages were used for both modeling and simulation. Modeling was thus mainly writing code that a computer could execute. However, this approach suffered from several disadvantages. For one, the required explicit formulation of equations made it cumbersome to describe the component's or system's behavior in an intuitive way. In addition, small changes in the system to be modeled could lead to large changes in the computer code. Reusing the same model for different use cases was therefore limited.

A different approach are equation-based languages, which separate the modeling from the numerical solution. This allows to write implicit model equations,

i.e. relations between variables, and apply advanced computer algebra to create efficient simulation code from those equations afterwards [23]. Modelica is an equation-based, object-oriented modeling language, which has been developed because the 1990s and is widely used today. It is open-source and is under continuous development by the non-profit organization The Modelica Association. Modelica was chosen for this work and is therefore described below. For a full documentation of the Modelica language, the reader is referred to [24].

Models A model is the most generic type of definition in the Modelica language. It defines the name of the model as well as its variables, parameters, equations, and connectors. These elements are described below. Modelica uses the basic data types "Real" for floating point numbers, "Integer" for integer values, "Boolean" for true/false expressions, and "String" for text.

Variables Variables are usually time-varying and are calculated during a simulation based on the model equations. They are generally continuous, but may also contain discontinuities. Variables of type Real are used for physical variables, e.g. the mass flow rate of a fluid or the temperature of a thermal capacity. Attributes can be assigned to variables to define their usage. Two commonly-used attributes for variables of type Real are "unit", used to assign a physical unit to that variable and enable unit checking in the equations, and "start", used to set initial conditions for state variables. Variables of type Integer can be used for control purposes, e.g. the number of active parallel components. However, it is more common to use the type Boolean for control purposes, e.g. to define the mode of operation or to activate/deactivate components. Variables in Modelica are scalars by default but can also be defined as vectors or matrices/arrays.

Parameters Variables can be defined as parameters when they do not change during a simulation. Parameters need to be defined beforehand and are typically user input data, which define a specific model instance. Parameters of type Real can be used for component specifications, e.g. the length of a pipe or the volume of a tank. Parameters of type Integer can be used for discretization or to define a number of components, e.g. the number of fluid layers in a tank model or the number of series/parallel collectors in a solar collector model. Parameters of type Boolean can be used to activate/deactivate certain model parts, e.g. choosing

between a constant and a variable heat transfer coefficient or deciding if an input signal or a parameter should be used in the model.

Equations Modelica supports algebraic, differential, and discrete equations. Partial differential equations are not supported, i.e. Modelica is not suitable for finite element methods or computational fluid dynamics. Equations define the actual behavior of the model and are simply written as "left hand side" = "right hand side". Equations can be written implicitly due to the acausal structure and will be rearranged by the simulation tool afterwards. Therefore, the models have no input-output structure and can be simulated as long as the number of equations and unknown variables are equal. Special types of equations are initial equations, used for initialization of differential equations, conditional equations, i.e. if-then-else equations, and connect-equations, which are used to define connections between models.

Connectors Models can be connected in Modelica using connectors. Connectors can have a predefined input-output direction, e.g. for control signals or input data which need to be passed to component models. However, connectors can also be acausal to represent a physical connection, e.g. the junction of two pipes or the thermal connection of two fluid streams. In such a connection, the direction of flow is not defined beforehand, but instead calculated during the simulation. Flow reversal during a simulation is also possible. These physical connectors can contain "potential variables", "flow variables", and "stream variables", which trigger the automatic generation of balance equations when two or more connectors are connected. Potential variables are equal in connected connectors, e.g. pressure or temperature. The sum of all the flow variables in connected connectors is zero, e.g. the sum of all mass flow rates or heat flow rates. Stream variables are calculated based on the flow direction and the product of the flow variable and the stream variable, such that the sum of these products is zero. An example is the energy balance with mass flow rate as flow variable and enthalpy as stream variable.

The object-orientation of Modelica has several advantages. It ensures that models can contain other models and makes models extensible, i.e. one model can inherit the structure and behavior from another model. This is very useful

for hierarchical library structures, where a so-called "base class" can be used as basis for many other models. A model with four fluid ports can for example be used for a heat pump model and a heat exchanger model via the extends-clause. Such a base class can be a "partial model", i.e. it can have an unbalanced number of equations and variables and thus be unsuitable for simulation. The required additional equations can then be added in the model derived from the base class. This approach also allows to build models with different levels of detail from the same base class and ensures that these models can easily be exchanged in e.g. a system model. This inheritance structure and easy model exchange lead to a high degree of reusability, which is especially important for the development of comprehensible model libraries. Such libraries usually have a hierarchical model structure organized in packages. Many Modelica libraries are available, both commercial and open-source [25].

2.2.2 Dynamic simulation with Dymola

Simulation means using a mathematical model of a system to predict the system's behavior. Simulations can thus be used to compare different scenarios and thus help both during system design and during system operation. There are three different approaches to represent the dynamics of a system dynamics, i.e. how the system's state changes over time. The simplest is "steady-state", i.e. all variables are assumed constant over time. This approach is only suitable for rough calculations. In "quasi-steady-state" simulations, the simulated time (see Figure 2.5) is divided into a certain number of intervals or time steps. The states/variables are assumed constant in each time step, but can change from one time step to the next. The accuracy of this approach depends highly on the chosen time step. In "dynamic" simulations, differential equations can be used to describe how variables change over time. Thus, a numerical integration algorithm (often called "solver") is required to run a simulation. The scope of this work was dynamic simulation due to the increased flexibility and inherent dynamics of future thermal energy systems as mentioned in Section 1.2.

Different tools for dynamic simulations exist, which have individual strengths and weaknesses. The most common tools for dynamic simulation of energy systems are TRNSYS, IDA ICE, MATLAB/Simulink, and Modelica/Dymola. These are briefly described here. TRNSYS (Transient System Simulation Tool) is a

graphically based software environment for the simulation of transient systems with focus on thermal and electrical energy systems. It is widely used, but was not chosen for this work due to its causal modeling approach, which requires that the in- and outputs of models are predefined. IDA ICE (IDA Indoor Climate and Energy) is a simulation tool for building performance simulation. It employs acausal equation-based modeling of buildings and building energy systems. It also has many preconfigured subsystems available, but focus is more on single buildings rather than neighborhoods [26]. Since it is not open-source, the model equations in IDA ICE cannot be edited by the user easily, which is why it was not chosen for this work. MATLAB (MATrix LABoratory) has its origin in control engineering and strong support for optimization. Graphical energy system modeling is possible with Simulink, but as for TRNSYS, the modeling approach is causal, making MATLAB unsuitable for this work.

Models written in Modelica can be simulated by different simulation environments and both commercial and open-source tools are available [27]. To simulate a model, the Modelica model descriptions have to be translated into executable code and be linked with numerical solvers. To do so, the Modelica code is first flattened, which means that the hierarchical structure is broken up. All the required model equations are inserted during flattening, e.g. inherited equations from extends-clauses or equations resulting from connections. This leads to an unstructured set of differential, algebraic, and discrete equations. This set can then be sorted, simplified, and optimized by the application of advanced mathematical techniques. Afterwards, the optimized set of equations is used to generate executable code [23]. Dymola is a commercial Modelica-based tool developed by Dassault Systèmes. It is widely used for modeling and simulation due to its superior performance and efficient solvers. Dymola was chosen for this work and some aspects regarding its numerical performance are discussed in Section 4.2.

2.2.3 Dynamic optimization with JModelica.org

Simulations can be used to study system performance by comparing different system design concepts or control strategies. However, the best possible solution might not be among the ones that were selected for the study. To find the best possible solution, optimization has to be applied. The general concept of optimization is finding a vector of variables ($\mathbf{x}$) that minimizes a defined objective

function $f(\mathbf{x})$ subject to certain constraints $c(\mathbf{x})$

$$\begin{aligned} &\underset{\mathbf{x} \in \mathbb{R}^n}{\text{minimize}} && f(\mathbf{x}) \\ &\text{subject to} && c_i(\mathbf{x}) = 0, \quad i \in \mathcal{E} \\ &&& c_i(\mathbf{x}) \geq 0, \quad i \in \mathcal{I} \end{aligned}$$

with $\mathcal{E}$ and $\mathcal{I}$ being the sets of indices for equality and inequality constraints, respectively. This concept is applied in many different fields and a variety of optimization problem types and solution algorithms exist. A classification of optimization problems is shown in Figure 2.7.

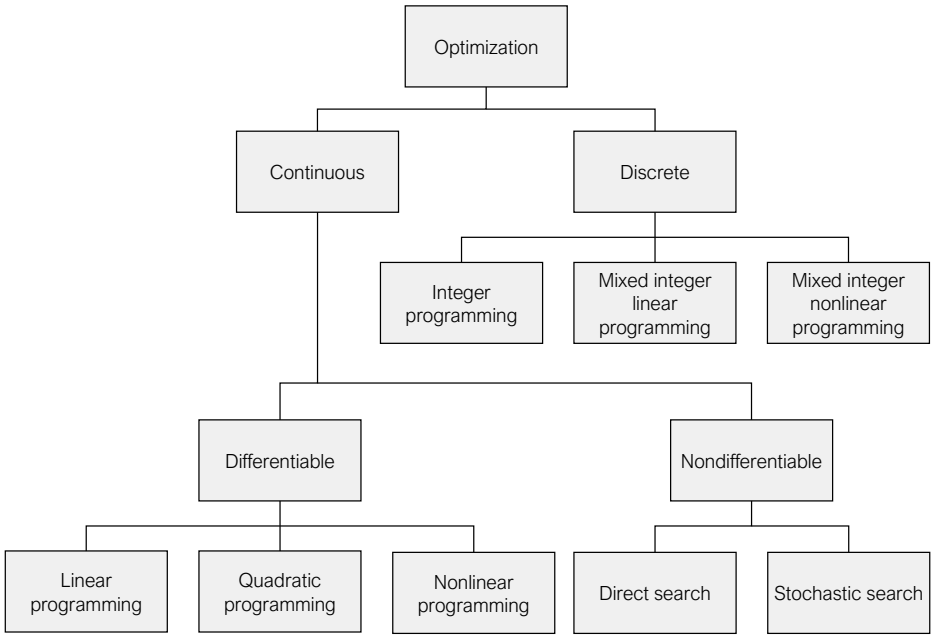

Figure 2.7: Classification of optimization problems [28].

Optimization algorithms are used to find the solution of an optimization problem. They are iterative, i.e. they need a starting point and stopping criteria. Different methods of how to move from one iterate to the next have been developed and an algorithm is usually only suitable for a certain problem type. This is known as the "No Free Lunch" theorem, which states that *"for any algorithm, any elevated performance over one class of problems is offset by performance over*

another class" [29]. A distinct difference can be made between algorithms that use gradient information during the iteration (gradient-based) and those that do not use it (derivative-free). Obtaining the first or second order derivatives of the objective function and the constraint functions can be difficult to obtain. However, algorithms using this information are usually much more efficient. In addition, the gradient information allows the definition of optimality conditions, which can confirm that the optimal solution has been found.

Optimization is a vital part of optimal control and MPC, see Figure 2.2. Optimal control is also called "trajectory optimization" and is used to find the best possible control sequence for a process over a given time horizon. This is very useful when different system design concepts are to be compared, i.e. different component sizes or different component combinations, because a fair comparison can only be made when the control strategy is equally well adapted for each of the design concepts. The more dynamic a system behaves, the more challenging it is to ensure equally good control with constant or rule-based setpoints for different system design concepts. Thus, optimal control is required for a fair comparison.

The optimization of a dynamic system, i.e. a system whose state changes over time, requires dynamic optimization techniques. Dynamic optimization problems, e.g. optimal control, are infinite-dimensional and can therefore not be solved directly. They can be transformed into a finite-dimensional problem by means of collocation on finite elements [30]. The continuous time horizon is then discretized into a finite number of elements in which the state profiles, i.e. the dynamic model variables, are approximated by polynomials. This yields a finite-dimensional nonlinear programming (NLP) problem, which can be solved. The size of this NLP depends on the equations of the system model to be optimized, the length of the time horizon, the number of finite elements, and the number of collocation points in each finite element, i.e. the degree of the polynomial approximation.

JModelica.org is an open-source platform for simulation and optimization of complex dynamic systems [31]. It is based on Modelica and the Functional Mock-up Interface standard, enabling coupling to different software packages. Two vital packages that are implemented are CasADi, which is used for the computation of derivatives using algorithmic differentiation [32], and IPOPT, which is used to solve the NLP. IPOPT stands for "Interior Point OPTimizer" and is an open-

source state-of-the-art solver for large scale sparse optimization problems [33]. JModelica.org also uses the language extension Optimica, which enables high-level formulation of optimization problems [34]. JModelica.org has recently been used for several optimization studies [35–40] and is also a key part of several compound tools [41–44]. JModelica.org was chosen for this work due to the Modelica-based approach. The optimization procedure used in this work is described in more detail in Section 5.1.

3 Description of the two case study systems

Two case study systems from Norway were analyzed for this thesis: an existing integrated heating and cooling system in Oslo and a planned local DH grid in Trondheim. The Oslo case study was part of the research project "Efficient interaction between energy demand, surplus heat/cool and thermal storage in building complexes" (INTERACT), which was the main funding source of this work. The Trondheim case study was part of the research project "Development of Smart Thermal Grids" (DSTG), to which the author of this thesis contributed due to the similar modeling and simulation requirements. However, the focus of this work was the Oslo case study, which is therefore described in more detail.

3.1 Integrated heating and cooling system at Vulkan, Oslo

The thermal energy supply system at Vulkan is called "integrated heating and cooling system" (IHCS) in this thesis due to its high level of integration with the buildings and the fact that it delivered both heating and cooling energy. The main aim of this case study was to analyze the design and the operation of the IHCS, especially the performance of the long- and short-term thermal energy storages.

3.1.1 Vulkan area and building stock

An area of about 100 by 200 meters in the Norwegian capital Oslo was renewed with several buildings and the IHCS. Construction was completed in 2014 and the

IHCS supplied a total floor area of 38 500 m^2. The area and the supplied buildings are shown in Figure 3.1. The total floor areas of the different building types are listed in Table 3.1.

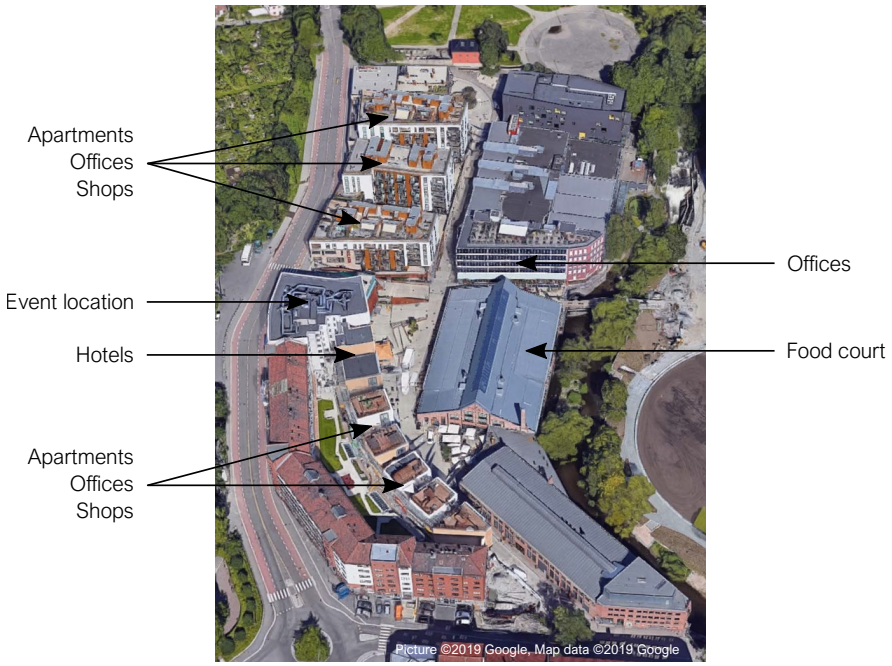

Figure 3.1: Overview of the Vulkan area and the existing buildings (arrows show the buildings that are connected to the IHCS).

Table 3.1: Building types and total floor areas at Vulkan.

Building type	Total floor area m^2
Offices	15 000
Shops	6 650
Hotels	7 600
Apartments	3 900
Food court	3 500
Event location	1 850
Total	38 500

3.1.2 The integrated heating and cooling system

The demands covered by the IHCS were space heating, DHW heating, snow melting, space cooling, and product cooling. Snow melting was applied to the walkways between the buildings and product cooling was delivered to the food court. The IHCS had separate heat exchangers for each building and demand type, which were connected to the heating and cooling loops of the IHCS in parallel. These parallel heat exchangers are shown as one heat exchanger with the corresponding total area of the parallel heat exchangers in Figure 3.2, which shows a schematic of the IHCS.

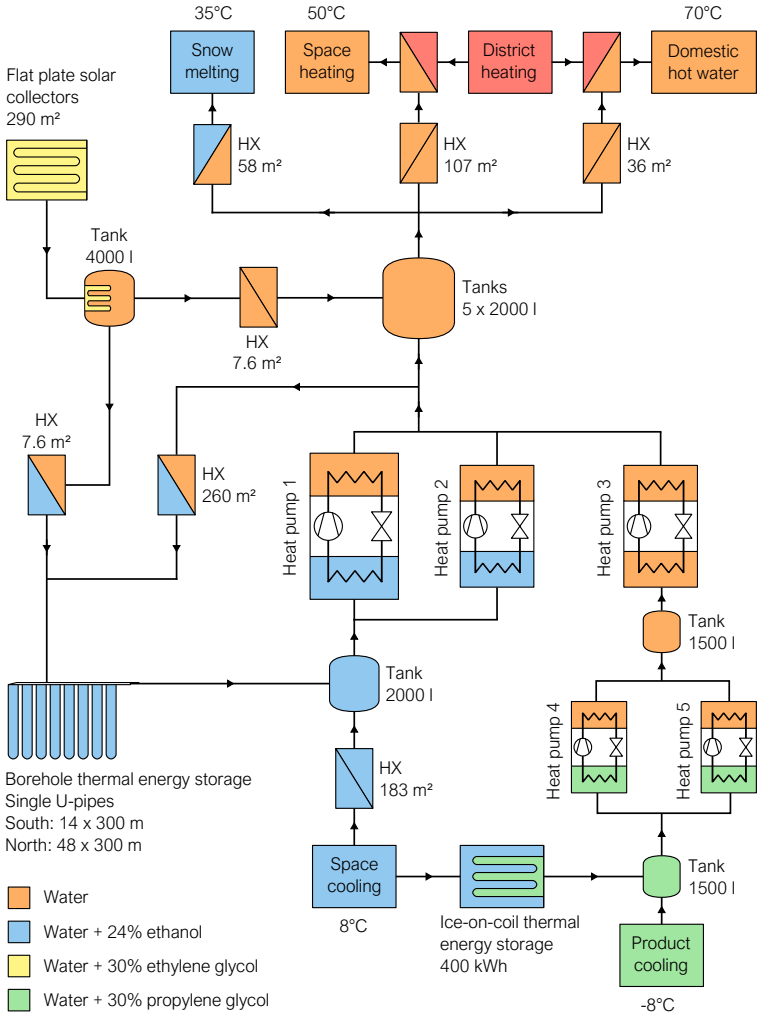

Figure 3.2: Schematic of the IHCS with main specifications.

The main components of the IHCS shown in Figure 3.2 were heat pumps, plate heat exchangers, flat plate solar collectors, storage tanks, ice thermal energy storage (ITES), and borehole thermal energy storage. The heat pump specifications are listed in Table 3.2.

Table 3.2: Heat pump specifications.

	HP 1	HP 2	HP 3	HP 4 & 5
Type	WSA2802X	WSA1602X	WSA0701X	NXW0600X
Working fluid	R134a	R134a	R134a	R410a
Compressor	Screw (2)	Screw (2)	Screw	Scroll
Design data cooling (evap/cond)				
Temperatures (°C)	4.5/48	4.5/48	20/55	-8/25
Capacities (kW)	595/772	334/436	224/283	87/110
COP (-)	4.36	4.27	4.8	4.78
Design data heating (evap/cond)				
Temperatures (°C)	0/50	0/50		
Capacities (kW)	473/652	264/365		
COP (-)	3.64	3.61		

The heat pumps were designed to deliver heat at a temperature of around 50 °C, see Table 3.2, so they could only cover parts of the DHW heating demand by preheating the DHW up to around 50 °C. Heat from Oslo's DH grid was then used to lift the DHW temperature to the required 70 °C. The space heating loops were also connected to the DH grid as backup system in case of very high space heating demands or heat pump failure.

During heating season, the BTES and the surplus heat from space cooling and product cooling were used as heat sources on the evaporator side of the heat pumps. The condenser heat from the heat pumps was sent to space heating, DHW preheating, and snow melting. During cooling season, a lot of surplus heat was available from the cooling systems, which needed to be released on the condenser side of the heat pumps, and the solar collectors. Only a part of this heat was needed for space heating and DHW preheating. Therefore, heat was injected into the BTES during cooling season. The ITES was used to reduce space cooling

peak demands during the summer. The ITES was charged during the night and discharged during the day.

3.1.3 Input data for the case study Vulkan

A simulation model of the IHCS described in the previous section was developed, see Section 4.5.1. The different heating and cooling demands as well as outdoor temperature and solar radiation were required as input data for the simulation model. An input file was created with hourly values of these variables, which were retrieved as explained below.

The IHCS was equipped with a control and monitoring platform. Energy meters were installed to measure the delivered energy for heating and cooling in each connected building. Aggregated daily demand data for 2015 and 2017 are shown in the figures 3.3 and 3.4, respectively. Data for 2016 were excluded from the analyses because long periods of data are missing from that year due to a server change.

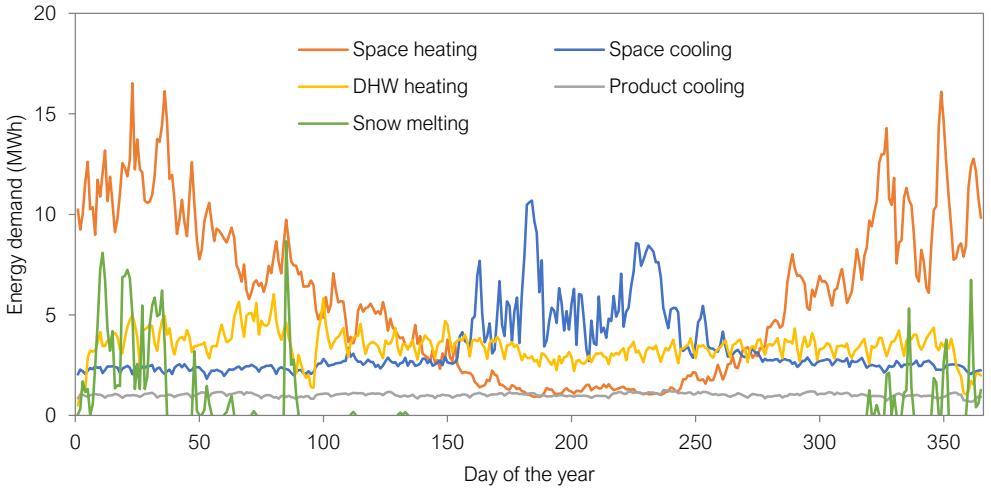

Figure 3.3: Measured daily heating and cooling demands in 2015 (hourly values were used as input data, daily values are shown for better readability).

The figures 3.3 and 3.4 show typical seasonal variations of the space heating, space cooling, and snow melting demands. The product cooling and DHW heating demands were relatively constant throughout the year.

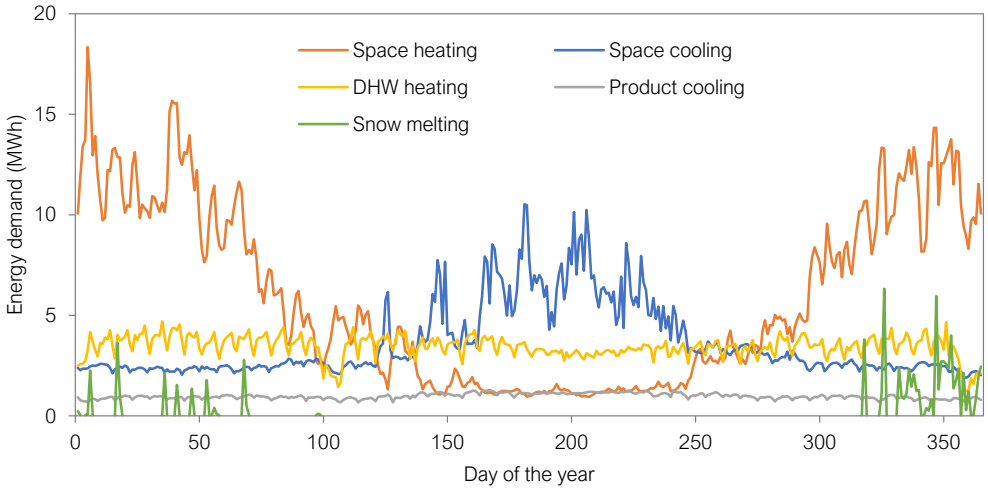

Figure 3.4: Measured daily heating and cooling demands in 2017 (hourly values were used as input data, daily values are shown for better readability).

Daily demand profiles for the different seasons are shown in the figures 3.5, 3.6, and 3.7, which show an average winter day, an average spring/fall day, and an average summer day, respectively (the same y-axis range was chosen for all three figures for better comparability).

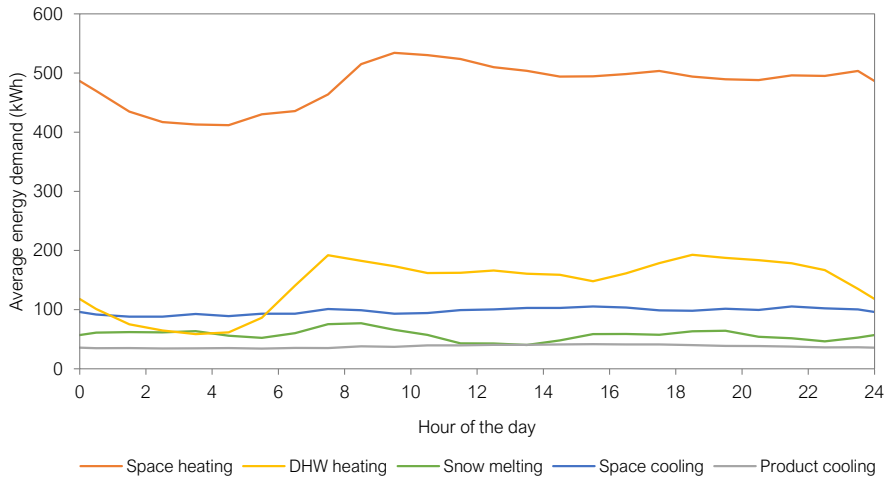

Figure 3.5: Average heating and cooling demands for a winter day.

The figures 3.5, 3.6, and 3.7 show that the product cooling and DHW heating demand did not change significantly during the year. The DHW heating demand

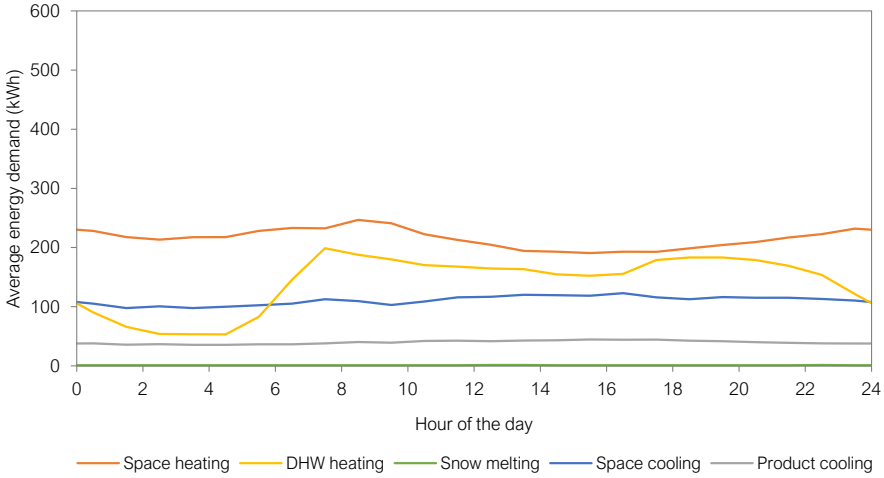

Figure 3.6: Average heating and cooling demands for a spring/fall day.

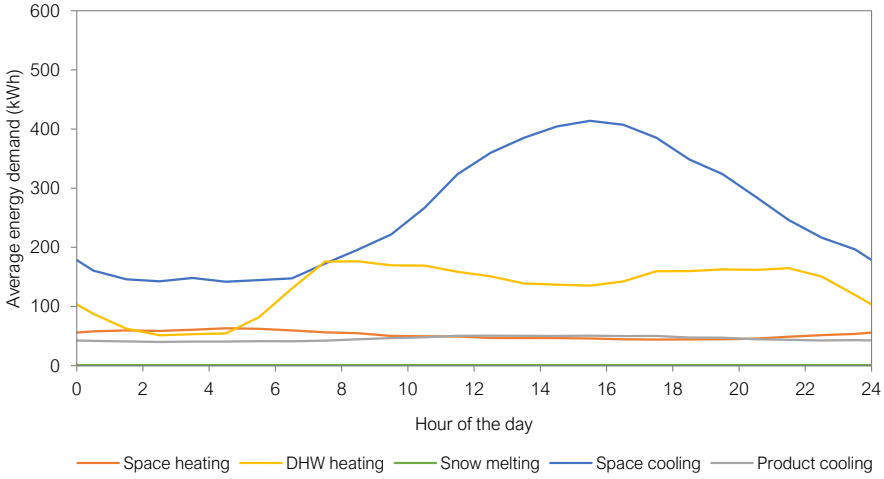

Figure 3.7: Average heating and cooling demands for a summer day.

showed a peak in the morning due to people taking showers and was the lowest during the night. Product cooling and snow melting did not show typical hourly variations. On the contrary, the space heating and space cooling demands showed large differences between the seasons. Especially the space cooling demand depended highly on the outdoor temperature during the summer, see Figure 3.7.

Unfortunately, no energy meters were installed to measure the energy exchange with the BTES or the performance of the solar collectors. In addition, only the total electricity use of the system was measured, the electricity use of single

components was not available. The amount of DH import was measured for each building. Daily total values for DH import and electricity use for the two years are shown in Figure 3.8.

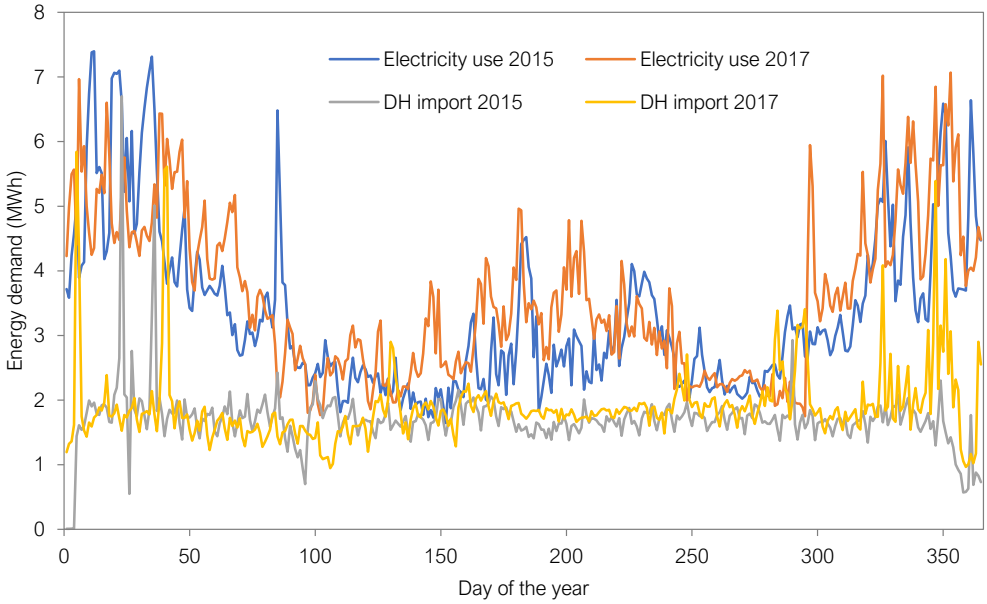

Figure 3.8: Measured daily electricity use and DH import in 2015 and 2017.

Figure 3.8 shows that the electricity use was the highest during winter and the lowest during spring and fall. The DH import was relatively constant during the years because it was mainly used for DHW heating. The peaks in DH import were caused by high space heating demands. In total, there was no significant difference between the measured energy amounts of the two years, see Figure 3.9.

The on-site temperature was only measured by one sensor and solar radiation was not measured at all. Therefore, outdoor temperature and solar radiation data from nearby weather stations were retrieved from [45]. The on-site temperature measurement was found to be around 5 K higher than nearby measurements, see Paper I. This might be due to the location of the sensor or an offset error. Therefore, 5 K were subtracted from the on-site temperature measurement values when they were used as input data. These corrected temperature values are shown in Figure 3.10.

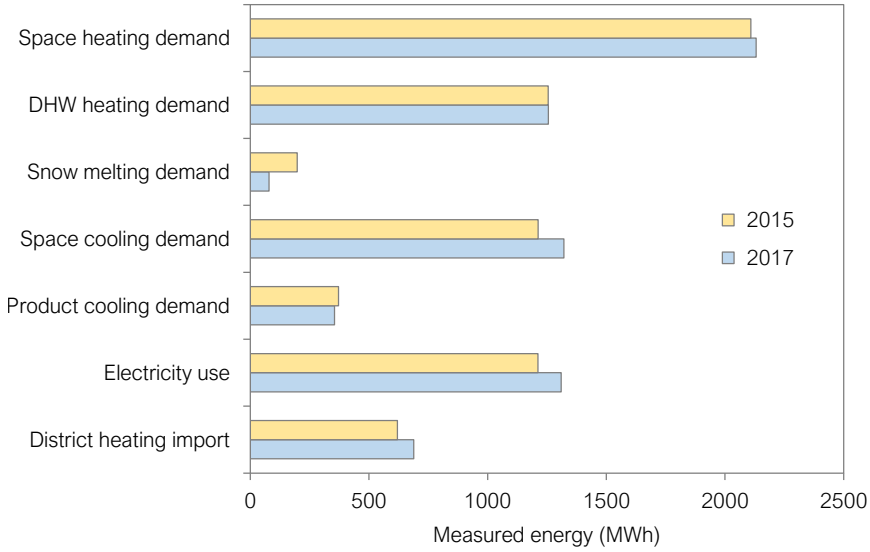

Figure 3.9: Total measured energy amounts in 2015 and 2017.

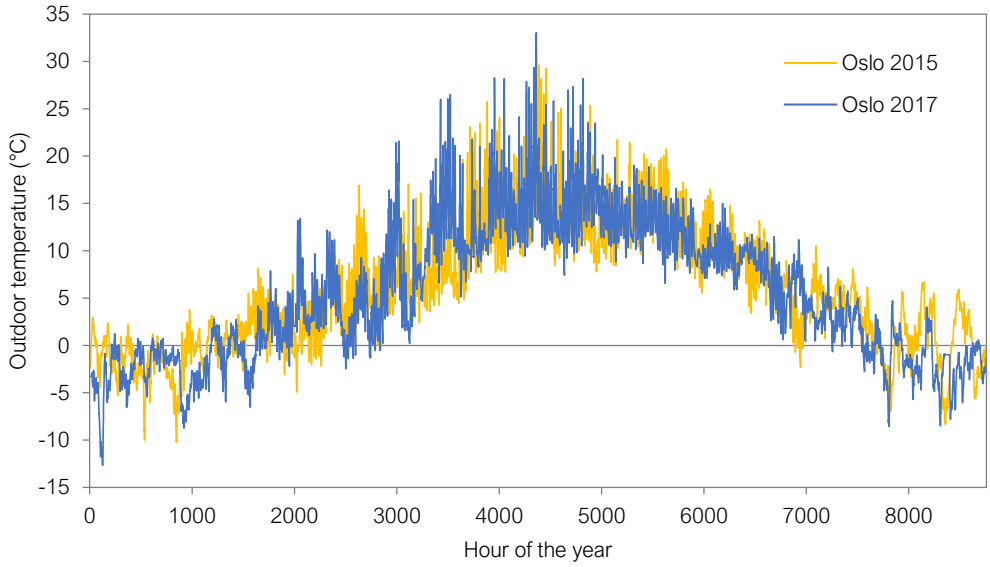

Figure 3.10: Input data for the case study Vulkan: Outdoor temperature.

Figure 3.11 shows the measured solar radiation from the nearest weather station for the years 2015 and 2017.

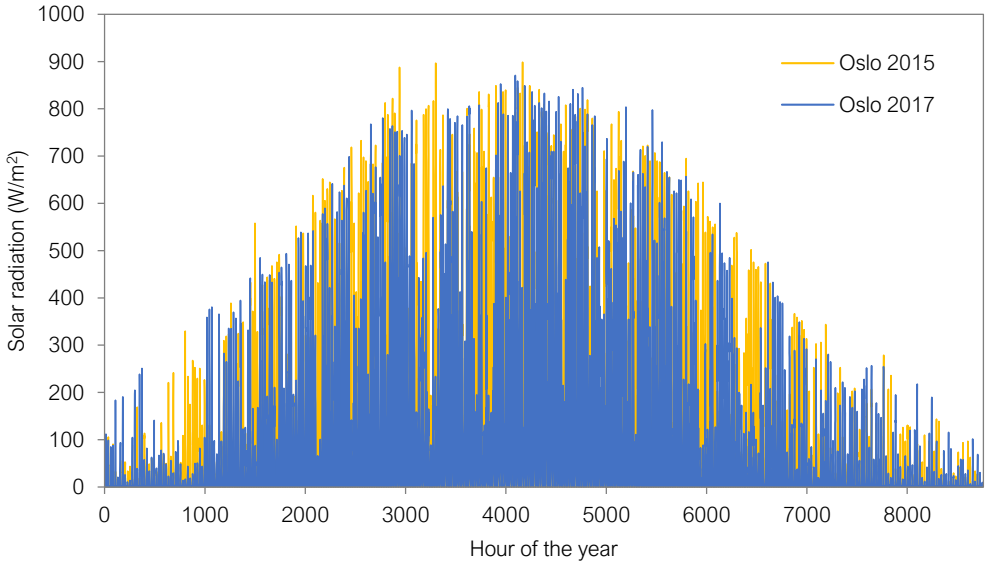

Figure 3.11: Input data for the case study Vulkan: Solar radiation.

3.2 Local district heating grid at Brøset, Trondheim

The main aim of this case study was to increase knowledge about the design of local DH grids and to investigate different solutions for the given area. As mentioned above, the author of this thesis contributed mostly to the modeling and simulation part of this case study, see also the author contributions listed in Section 1.4.

3.2.1 Brøset area and building stock

In 2013, Trondheim Municipality made plans to develop a new neighborhood at Brøset, which is a part of the city of Trondheim. The size of the available area was about 344 000 m^2 and the aim was to develop a low-emission neighborhood. The area and a development plan are shown in Figure 3.12.

Based on the existing buildings and the development plan shown in Figure 3.12, the building stock listed in Table 3.3 was assumed for this case study. This building stock was used as basis for the calculation of the heating demand profiles.

Figure 3.12: Overview of the Brøset area (left) and the planned buildings (right [46]).

Table 3.3: Building types and floor area at Brøset.

Building type	Number of buildings	Total floor area (m^2)
Apartment block (type A)	4	31 000
Apartment block (type B)	6	41 000
Apartment block (type C)	8	59 000
Kindergarten	3	4 400
Nursing home (old)	2	4 000
Nursing home (new)	1	12 600
Sports hall	1	10 000
School	1	6 000
Library	1	5 850
Office	1	4 000
Total	28	177 850

3.2.2 The local district heating grid

Trondheim Municipality wanted the CO_2 footprint of the new neighborhood to be considerably lower than the Norwegian average [47]. An efficient thermal energy supply system for the neighborhood was therefore sought. This system is called "local district heating grid" in this thesis due the fact that it delivered only heating energy and that the supplied area was relatively small. The total pipe

length was estimated to be around 7 km.

The existing DH grid in Trondheim delivers heat at supply temperatures between 75 °C and 115 °C as explained in Paper IV. LTDH with supply temperatures below 70 °C has recently received much attention [5, 48]. There are a number of benefits and some drawbacks related to LTDH. The main advantages are that the heat losses from the grid are reduced and that more renewable and waste heat sources can be included, leading to higher energy efficiency and lower emissions. The main disadvantages are that measures have to be taken to avoid the risk of Legionella bacteria in DHW systems and that existing buildings/substations might not be suitable for heat supply at such low temperatures [49]. Therefore, LTDH is especially relevant for new building areas.

Several design concepts for local DH grids with different temperature levels have been compared for this case study with focus on LTDH. The main heat supply was assumed to come from Trondheim's existing DH grid. The inclusion of prosumers, i.e. customers that can also deliver heat, was also analyzed. Several other solutions for increased energy efficiency of the neighborhood were originally discussed, e.g. heat recovery from waste water, solar collectors combined with thermal energy storage, heat pumps, and the use of geothermal energy [47]. These additional design concepts were not analyzed in this work due to time limitations.

3.2.3 Input data for the case study Brøset

Simulation models of the local DH grids described in the previous section were developed, see Section 3.2.2. Hourly values for space heating and DHW heating demand of the different building types were required as input data for the simulation models. An input file was created for each of the building types listed in Table 3.3. The DH demand data in each input file were based on DH use data from existing buildings of similar type and building code. These use data were retrieved from the local DH company and Trondheim Municipality. The DH use data only showed the total DH demand, i.e. both space heating and DHW heating. Therefore, generic DHW profiles were created and used to split the total DH demand data into space heating demand and DHW heating demand. Apartment blocks represented by far the largest share of floor area, see Table 3.3. Therefore, three different input files, based on DH use data from three

different buildings, were created. Daily values for the heating demands of the entire building stock (excluding prosumers) are shown in Figure 3.13.

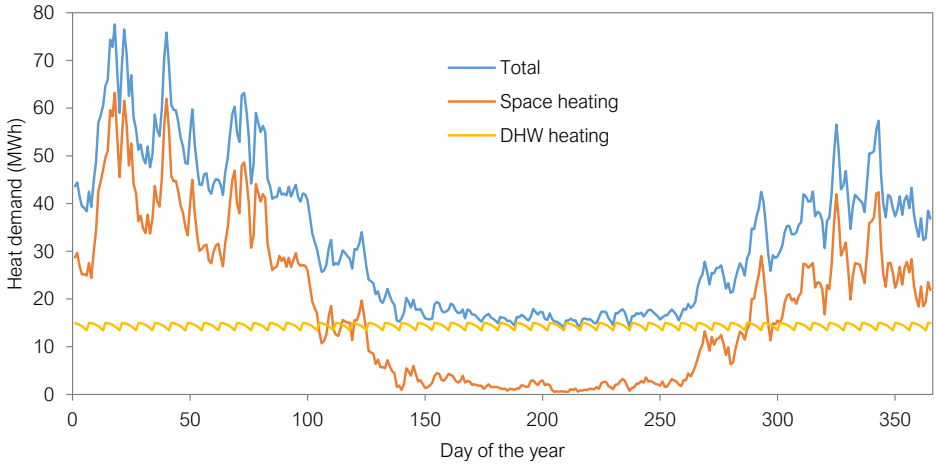

Figure 3.13: Input data for the case study Brøset: Daily heat demands (hourly values were used as input data, daily values are shown for better readability).

The total calculated heating demand shown in Figure 3.13 was 11 940 MWh, with 6 680 MWh required for space heating and 5 260 MWh required for DHW heating. The DH use data included the outdoor temperature for the year 2013, which was also used as input and is shown in Figure 3.14.

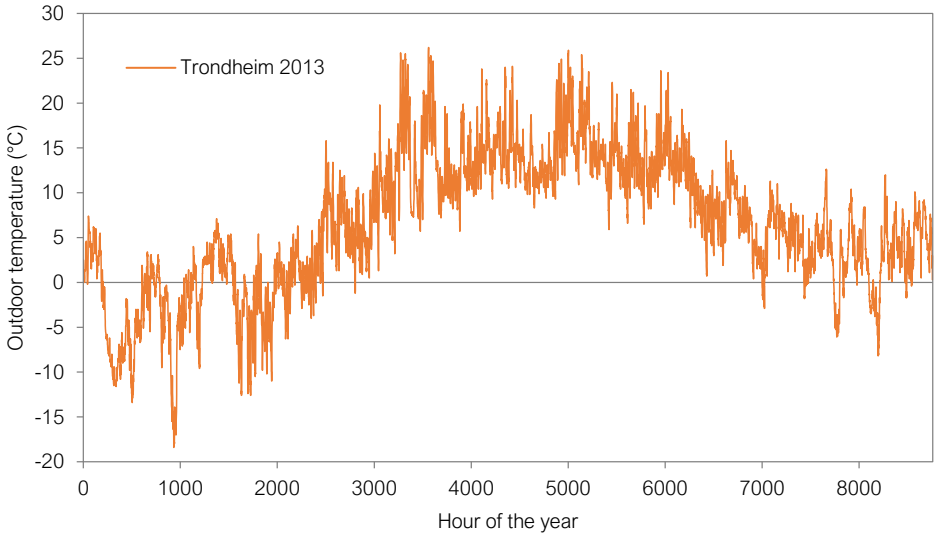

Figure 3.14: Input data for the case study Brøset: Outdoor temperature.

Two different prosumer heat profiles were created, which represented different types of prosumers and were used to study the effect of prosumers in the DH grid. These types were a data center and a supermarket. Their capacities were chosen based on values found in the literature and their heat profiles depended on the outdoor temperature, see Paper IV. The resulting heat profiles for the prosumers, which were based on the outdoor temperature shown in Figure 3.14, are shown in Figure 3.15.

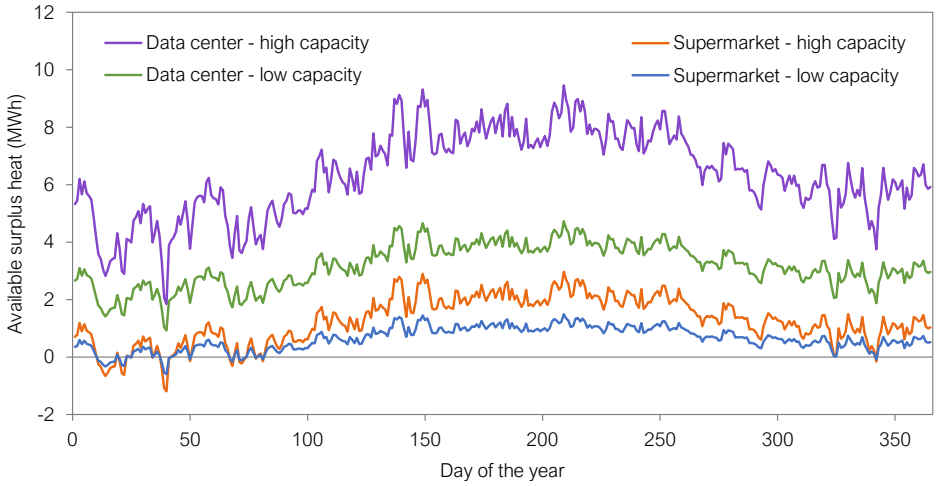

Figure 3.15: Input data for the case study Brøset: Prosumer heat profiles (hourly values were used as input data, daily values are shown for better readability).

It can be seen from the heat profile in Figure 3.15 that the supermarket was a customer, i.e. it required heat from the DH grid, on the coldest days of the year. However, for most part of the year it was a producer, i.e. it delivered heat to the DH grid. The data center was actually not a prosumer because it always delivered heat to the DH grid and could therefore be seen as decentralized renewable heat source.

4 Simulation models for future integrated energy systems

The simulation model development is explained in detail in this chapter. Simple models were used as starting point and were continuously extended and improved. This evolution of the simulation models over the course of this work will be explained where appropriate.

The term "model" has various meanings and it is therefore important to clarify the usage in this thesis. As described in Section 2.2.1, a model is the most generic type of definition in the Modelica language. It defines the name, input parameters, connections, variables, and equations of the specific model. In the following chapters, the term model refers to a Modelica model. Since Modelica is object-oriented, models can contain other models, e.g. a system model usually contains several component models.

4.1 Choice of Modelica library for simulation model development

To recall, sufficiently accurate but also fast models were sought as the scope of this work was the analysis of systems with several components and long simulated times. Therefore, the level of detail had to be limited to ensure reasonable computation time. However, the important characteristics of the components had to be represented by the models. At an early stage of this work, the use of component models from existing Modelica libraries was evaluated. The commercial library TIL from TLK-Thermo GmbH [50] and the open-source library Buildings

from Lawrence Berkeley National Laboratory [51] were selected as potential candidates. Both libraries seemed to be targeted at a higher level of detail than required for this work and were thus deemed unsuitable. Modifying the existing models in the libraries or building own models from the libraries' base classes was considered. However, the libraries are under constant development and modifications could lead to compatibility issues when library updates are released. The library Thermal from the Modelica Standard library (MSL) provides simple components for one-dimensional incompressible thermo-fluid flow models. It is also called library, but is very basic compared to TIL or Buildings and does not contain components like heat pumps or heat exchangers. It can be seen as a base class library and it has not been further developed since 2010. This library was chosen as basis for model development because the level of detail was suitable and no compatibility issues were expected to arise.

4.2 Numerical performance with the DASSL solver in Dymola

As described in Section 2.2.1, modeling and simulation are separate tasks. However, the numerical performance of the simulation depends highly on the simulation models, i.e. the modeling part. Thus, simulation-friendly modeling is desirable to achieve good numerical performance. This means that the simulation terminates successfully, i.e. the solver does not fail, and that the computation time is sufficiently low. Several reasons can cause the solver to fail, e.g. a division by zero, or lead to unacceptably long computation times, e.g. algebraic loops or chattering, which are explained below. Many different Modelica-based simulation tools and solvers exist, making it impossible to ensure good numerical performance for all simulation possibilities. Dymola was used for this work with the solver DASSL. Some aspects regarding the numerical performance of this choice are given below.

Numerical integration algorithms in Dymola Several different solvers, i.e. algorithms for numerical integration, are included in Dymola. Most solvers in Dymola are variable step size algorithms. These algorithms calculate the local error at each trial step and proceed if the error is lower than the defined tolerance.

At an early development stage, test runs were performed to compare the solvers in Dymola. The standard solver DASSL showed by far the best performance in terms of robustness and computation time. It was therefore chosen for all simulations in this work. DASSL is a multi-step solver, which means that it uses information from more than one previous step to calculate the solution of the next step. The way this is done cannot be changed in Dymola, the only allowed user input for the solver is the integration tolerance. The integration tolerance was set to 10^{-4} during model development and to 10^{-5} for result production. A diagnostics file of the solver's integration error can be obtained in Dymola. This file contains all state variables and lists the number of times that each variable

- Limits the solvers step size
- Dominates the integration error
- Exceeds 10% of the integration error

thus providing useful information for debugging slow or unstable simulations.

Algebraic loops As briefly explained in Section 2.2.2, Dymola processes the Modelica code to generate a differential-algebraic equation system (DAES). This DAES is then further processed to generate an efficient executable file. The statistics of this translation are available in Dymola's message window and contain important information about the size and structure of the DAES. Dymola lists the sizes of linear systems of equations before and after manipulation as well as the sizes of nonlinear systems of equations before and after manipulation. These sizes have significant influence on the computation time, especially the sizes after manipulation. If they are not zero, then Dymola could not break all algebraic loops, which means that the equation systems are still coupled. Solving these coupled systems of equations is more challenging, especially with nonlinear equations. It is sometimes possible to take measures in the Modelica models that reduce these algebraic loops [52]. These measures can affect the model behavior so an implementation should be carefully evaluated.

Time and state events Events are used to handle discontinuities in Dymola and can play an important role for the numerical performance. Discontinuities are defined by conditional expressions and can lead to abrupt changes in

the behavior of a system. If the conditional expression is related to time, e.g. `if time > 10 s`, then the event is called "time event". If the expression is based on a system variable, e.g. `if temperature > 50 °C`, then the event is called "state event". Due to the possibility of abrupt changes in system behavior, variable step size solvers take an iteration step up to the time of the event and restart the integration with new starting conditions afterwards. This slows down the simulation for several reasons: 1) events limit the step size of the solver by enforcing a step to be taken at the time of the event, 2) finding consistent restart conditions can be challenging, depending on the changes triggered by the event, and 3) for state events, the time of the event must be detected. The time at which a time event occurs is obviously known beforehand, but costly iterations can be necessary to detect the exact time of a state event, e.g. the time at which a temperature crosses a certain threshold. For good numerical performance, unnecessary events should be avoided and continuous behavior at events should be ensured. This is especially relevant for control structures, where conditional expressions often are used to activate/deactivate components or to adjust setpoints. A well-known effect that can occur in such situations is "chattering". Chattering describes a situation in which the numerical performance is degraded due to the generation of many state events. This can occur if the change introduced by a conditional expression leads to a change in the expression itself, leading to a loop of true/false solutions for that expression and thus the generation of many state events. The noEvent() operator can be used to suppress state events, allowing the solver to step past the event instead of determining its exact time of occurrence. This can avoid chattering and lead to improved numerical performance in some cases. However, events are also valuable for a solver because they inform about discontinuities. Without knowing about the event, the solver might struggle to find appropriate time steps, due to the discontinuity and its impact on system behavior. This can lead to simulation performance issues.

4.3 Handling of input data and results

The type and the amount of required input data depends on the type of simulation and the modeled system at hand. Input parameters, e.g. for system and component specification, are often manual user input unless automated parame-

ter studies are run. Time-varying input variables, e.g. outdoor temperature or energy demands, need to be specified by data containing the value of the variable at certain simulation times. In this work, the system boundary was set at the customer substation level, i.e. distribution systems and buildings were not modeled. Thus, all heating and cooling demands were required input data for the system models. The outdoor temperature and solar radiation were also required for the solar collector model. Hourly data points for the demands and weather data were stored in a file and read by the model `CombiTimeTable` from the MSL. The model offers several interpolation methods for the data points, e.g. linear segments and spline interpolation. Spline interpolation led to lower computation times compared to linear interpolation and was therefore chosen in this work. However, at the beginning of this work, the only spline interpolation method was `ContinuousDerivative`, which led to over- and undershoots as shown in Figure 4.1.

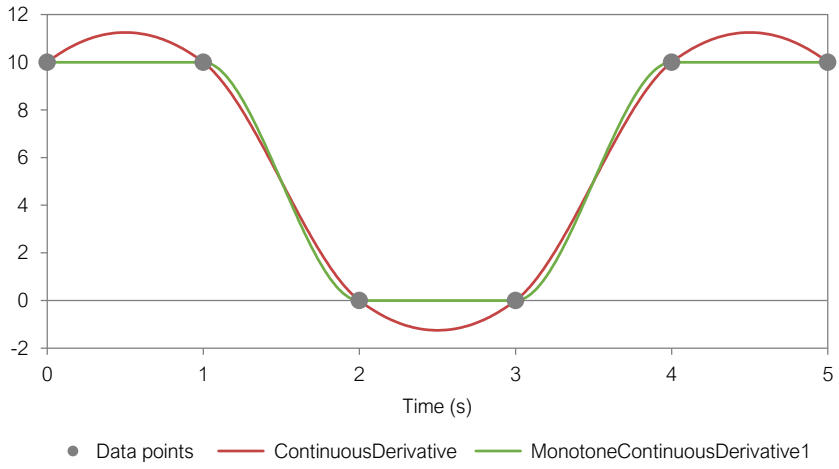

Figure 4.1: Different spline interpolations in Modelica.

As can be seen in Figure 4.1, negative energy demands could occur with this interpolation method, which led to numerical instabilities. Therefore, max() operators were used to avoid negative demands. In a later version of the model `CombiTimeTable`, new spline interpolation methods were available which did not overshoot. The method `MonotoneContinuousDerivative1`, see Figure 4.1, was therefore used in the final system models.

Another aspect that deserves attention for dynamic simulations is the plotting and saving of the results. Values for the variable trajectories are stored at certain

simulation times called “result points”, which can easily be plotted in Dymola. The user can specify the number of result points and also chose if variables should additionally be stored at events or not. Storing result points comes at a computational cost, but this is often insignificant. However, for models with many variables, storing many result points can lead to large result files and a noticeable increase in computation time. This can be avoided by only storing selected variables or by decreasing the number of result points. However, large output intervals can be misleading as shown in Figure 4.2.

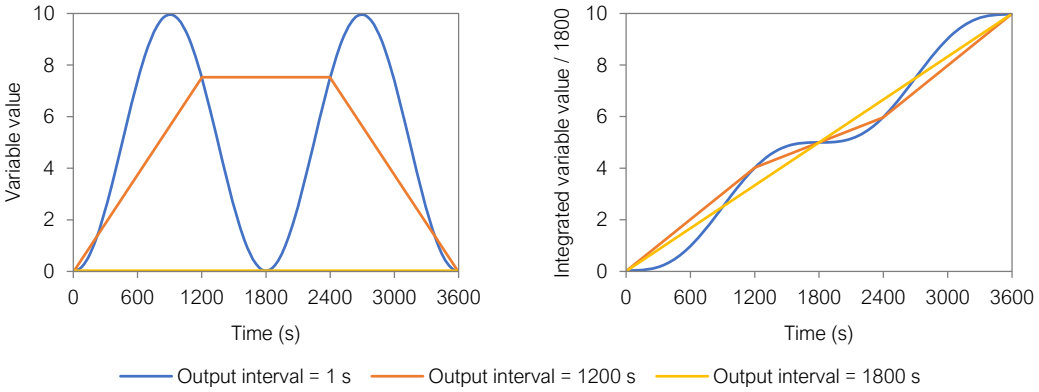

Figure 4.2: Same simulation with different output intervals.

Figure 4.2 shows that small time steps should be chosen for the investigation of fast dynamics, e.g. when tuning the output of a controller. Figure 4.2 also shows that the result points should not be used as average value when large output intervals are chosen. Instead, the variable of interest should be sent to an integrator model so that the average can be calculated precisely from the stored result points. In this work, the output interval was set to one hour for result production and all result variables were integrated.

4.4 Component models

The component models developed during this work are explained in this section. Reusability and a common level of detail were important aspects to enable the analysis of different case study systems. As explained in Section 4.1, the library Thermal from the MSL was used as basis for component model development. Icons of frequently used models and connectors in this work are shown in

Figure 4.3.

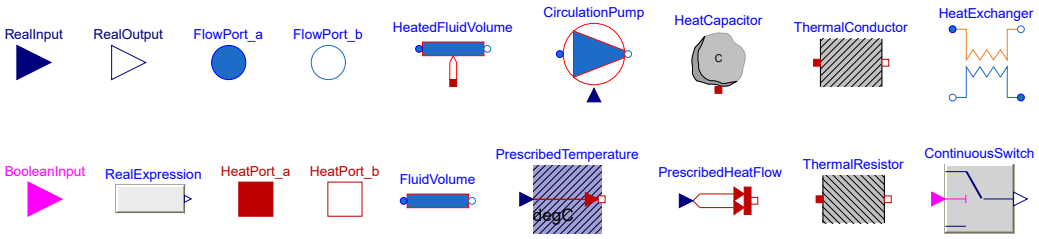

Figure 4.3: Icon legend for simulation model screenshots from Dymola.

The base class of this library is called `TwoPort` and contains two fluid flow connectors, which enable the connection to other models. The energy balance equation included in the model is shown in Equation (4.1).

$$\dot{m} \cdot c_p \cdot (T_{\text{in}} - T_{\text{out}}) + \dot{Q} = V \cdot \rho \cdot c_v \cdot \frac{dT_{\text{out}}}{dt} \tag{4.1}$$

The volume (V) and the type of fluid were input parameters of the `TwoPort` model. The fluid's density (ρ) and specific heat capacities (c_p and c_v) were assumed constant. Their values were calculated with Excel using the add-in CoolProp [53] and were stored in the Modelica class "Record". Since these properties are temperature-dependent, they were calculated for different temperature levels for each fluid. In the system models, the Record with the temperature closest to the expected average temperature in that loop was selected. Minimum and maximum allowed temperatures were also stored in the Records and were used to print warning messages when the fluid temperature was outside these limits.

The `TwoPort` model was used as basis for the models `FluidVolume` and `HeatedFluidVolume`, which were needed in all the component models described below. The models `FluidVolume` and `HeatedFluidVolume` were extensions of the `TwoPort` model and additionally contained equations to define the pressure drop in the fluid volume. The heat flow rate ($\dot{Q}$) in Equation (4.1) was set to zero for the model `FluidVolume`. The model `HeatedFluidVolume` had a thermal connector called `HeatPort`, which enabled heat transfer to and from the fluid.

4.4.1 Circulation pump model

The model `CirculationPump` was an extensions of the `TwoPort` model with a `RealInput` connector. This connector defined the mass flow rate in the `CirculationPump` model and typically originated from PI-controllers in the system model. The required power (P_{pump}) was calculated based on Equation (4.2) assuming a constant wire-to-fluid efficiency (η), which was an input parameter of the `CirculationPump` model.

$$P_{\text{pump}} = \frac{\dot{V} \cdot \Delta p}{\eta} \tag{4.2}$$

Defining the mass flow rate as input signal and the power as output variable avoided numerically expensive iterations that would otherwise be needed to find the interdependent variables $\dot{V}$ and Δp at a given power input. This enabled stable control of the system and kept computation times low. However, this could also lead to nonphysical solutions such as negative pressures, especially at high mass flow rates. The choice of a reasonable mass flow rate limit was therefore required and resulting pressure levels had to be checked for plausibility.

4.4.2 Continuous switch model

As explained in Section 4.2, discontinuities can lead to problems for the solver during simulation. The model `Switch` from the MSL switches discontinuously. Therefore, the model `ContinuousSwitch` was developed, which switches continuously between two inputs over a certain time interval. This interval was an input parameter called transitionTime. Setting this parameter to zero gives a discontinuous signal as in the `Switch` model from the MSL. Example graphs for the model output for three different cases are shown in Figure 4.4.

Different transition times can be defined for switching from Input 1 to Input 2 and vice versa for better usability. A `ContinuousSwitch` model with continuously differentiable output was also tested, but did not lead to better performance and was therefore not used.

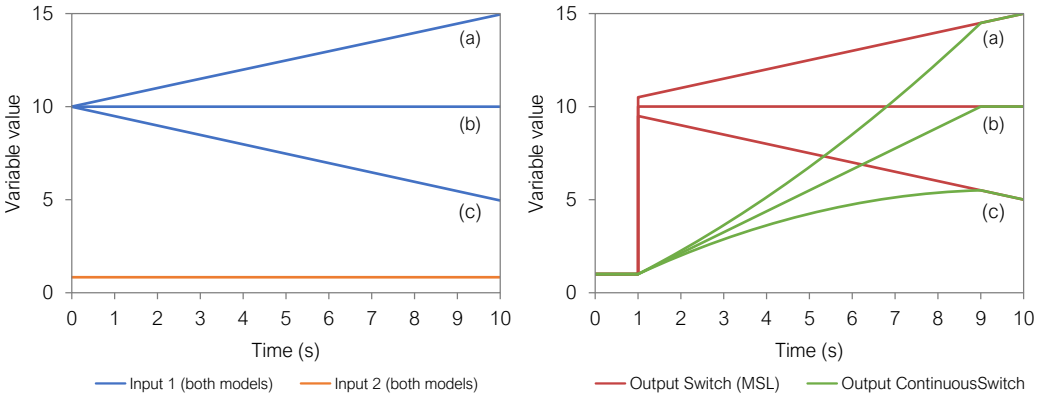

Figure 4.4: Switch model comparison (switch from Input 2 to Input 1 at t = 1 with transitionTime = 8 s).

4.4.3 Controller model

The model `Controller` was developed and included the PID-controller model `LimPID` from the MSL. However, several features for better usability and numerical performance were added over the course of this work. The derivative part of the `LimPID` model was not used in this work, i.e. all controllers were PI-controllers. A Dymola screenshot (DS) of the `Controller` model's parameter window is shown in Figure 4.5 and the parameters "use_activation_input" and "delay_measurement" are described below because they were important for the simulation performance.

Parameter use_activation_input, see Figure 4.5: setting this parameter to false deactivated the activation input connector. The measurement and setpoint signals were then always sent to the included `LimPID` model and its output was always used as output from the model `Controller`. Setting this parameter to true allowed to deactivate the use of the `LimPID` model via a Boolean signal. When deactivated, the value of the parameter output_inactive was used as output from the `Controller` model, which was typically set to zero. In addition, the input signals for the measurement and the setpoint value of the included `LimPID` model were set to zero to avoid unnecessary calculations. The integrator of the `LimPID` model thus received zero as input leading to a constant output value. When the controller was activated, this constant value affected the response of the `Controller` model. This was undesired, so the integrator input of the `LimPID` model was modified to reset the output to zero when the controller was deacti-

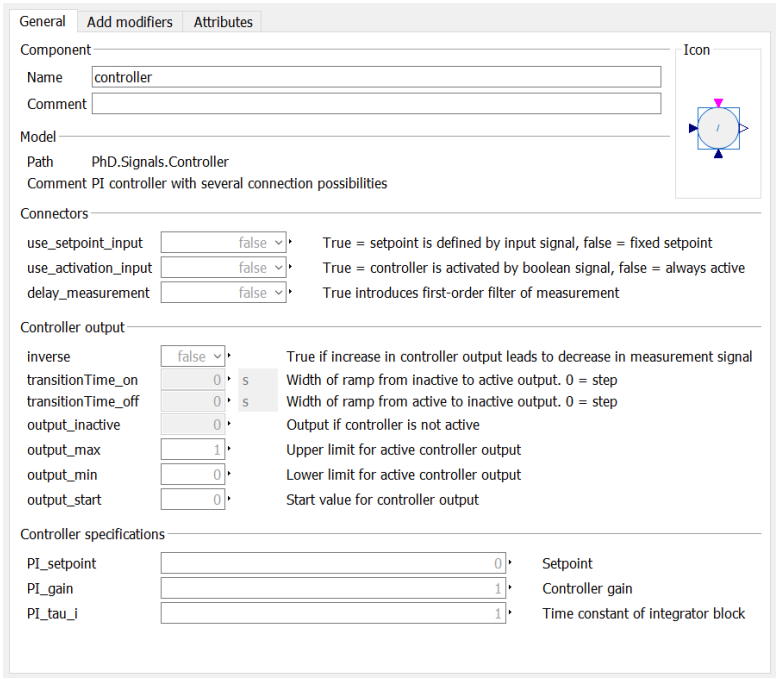

Figure 4.5: Parameter window of the `Controller` model (DS).

vated. When the activation signal became true, the `LimPID` model was used. A `ContinuousSwitch` model was used to switch between the output of the `LimPID` model and the value of the parameter output_inactive to define the output of the `Controller` model. This required the definition of the two input parameters transitionTime_on and transitionTime_off.

Parameter delay_measurement, see Figure 4.5: setting this parameter to true could break algebraic loops resulting from feedback control by delaying the measurement signal with a `FirstOrder` model from the MSL. This introduced an additional state but could still lead to more stable simulations and significantly lower computation times.

4.4.4 Heat pump model

Four heat pump models were developed in this work. Since calculating the heat pump's thermodynamic cycle was outside the scope of this work, all developed heat pump models consisted of two `HeatedFluidVolume` models, which represented the secondary fluid in the condenser and the evaporator of the heat

pump.

In the first heat pump model, `HeatPump1`, an input signal of type Real defined the heat pump power P_{HP}. The COP of the heat pump was an input parameter of the model and the heat flow rates in the condenser and the evaporator were calculated with the equations (4.3) and (4.4).

$$P_{\mathrm{HP}} \cdot \mathrm{COP}_{\mathrm{HP}} = \dot{Q}_{\mathrm{evap}} \tag{4.3}$$

$$P_{\mathrm{HP}} + \dot{Q}_{\mathrm{evap}} = \dot{Q}_{\mathrm{cond}} \tag{4.4}$$

The second heat pump model, `HeatPump2`, was based on a variable COP. Nominal operating conditions were required as input parameters and the COP depended on the actual operating conditions during the simulations. An advanced circuit simulation and optimization tool was used to generate polynomial coefficients for the COP calculation. These coefficients were included in the model `HeatPump2`, details can be found in Paper II. This model required the calculation of the polynomial coefficients for each heat pump based on detailed manufacturer specifications, which might not always be available. It was therefore decided to develop a more generic heat pump model with less user input requirements.

In the third heat pump model, `HeatPump3`, the COP of the heat pump was calculated based on the Lorentz efficiency (η_{L}) of the heat pump, which was an input parameter of the model. The Lorentz cycle is similar to the well-known Carnot cycle, but does not assume the heat source and sink to be isothermal. Instead, they have a finite heat capacity and thus change temperature during heat addition/extraction [54]. Therefore, the COP of the heat pump depended on both inlet and outlet temperatures of the `HeatedFluidVolume` models as shown in the equations (4.5) to (4.7).

$$T_{\mathrm{L,cond/evap}} = \frac{T_{\mathrm{in,sec,cond/evap}} - T_{\mathrm{out,sec,cond/evap}}}{\ln\left(\dfrac{T_{\mathrm{in,sec,cond/evap}}}{T_{\mathrm{out,sec,cond/evap}}}\right)} \tag{4.5}$$

$$\mathrm{COP}_{\mathrm{L}} = \frac{T_{\mathrm{L,evap}}}{T_{\mathrm{L,cond}} - T_{\mathrm{L,evap}}} \tag{4.6}$$

$$\mathrm{COP_{HP}} = \mathrm{COP_L} \cdot \eta_\mathrm{L} \tag{4.7}$$

An additional change was made for the fourth and final heat pump model, `HeatPumpFinal`. In the first three heat pump models, the power was used as input signal. This signal typically came from a `Controller` model, which controlled the outlet temperature on either condenser or evaporator side. This controller was difficult to tune due to the variations in operating conditions, see Section 2.1.3. In addition, the diagnostics file, see Section 4.2, showed that this controller output was computationally expensive. Therefore, a desired outlet temperature was used as input signal in the model `HeatPumpFinal` and the resulting power was calculated by the model. A Boolean input signal was used to define whether the condenser or evaporator outlet temperature should be set. The model `ContinuousSwitch`, explained in Section 4.4.2, was used to avoid instabilities during switching. A diagram of the model `HeatPumpFinal` and its parameter window in Dymola are shown in Figure 4.6 and Figure 4.7, respectively.

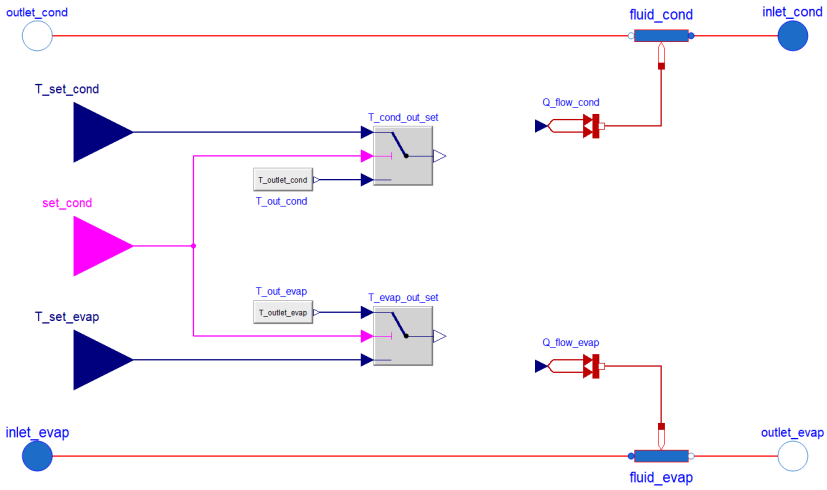

Figure 4.6: Diagram of the model `HeatPumpFinal` (DS).

The model `HeatPumpFinal` was not a physical representation of a real heat pump because of the unrealistic external definition of one of the outlet temperatures explained above. However, this modeling approach only affected the short-term response of the heat pump model. The results from one-year simulations with the third `HeatPump` model were almost identical to simulations with the

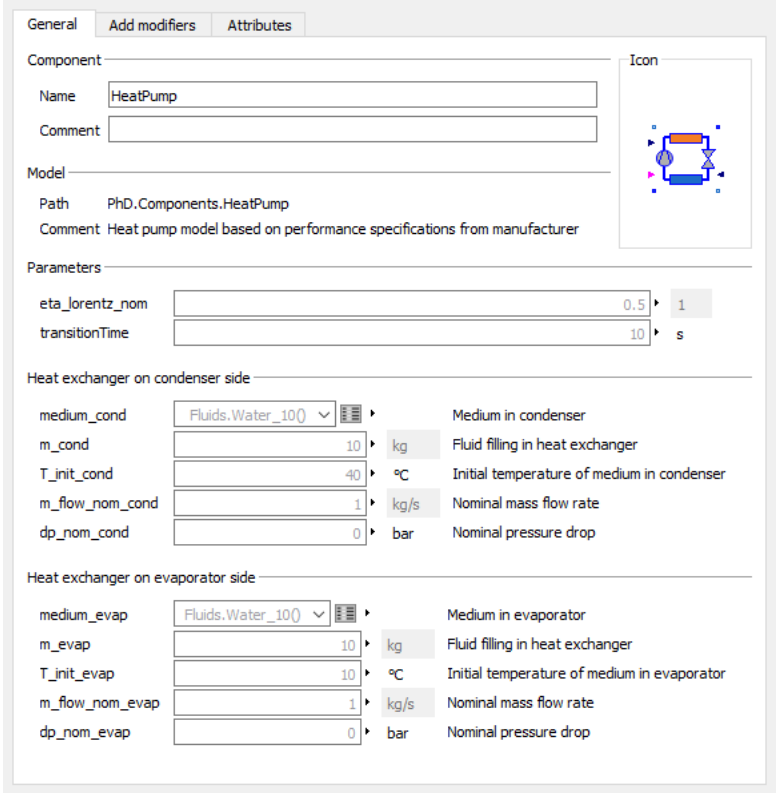

Figure 4.7: Parameter window of the model `HeatPumpFinal` (DS).

model `HeatPumpFinal`. The main difference was that the simulations with the fourth `HeatPump` model were significantly faster and more stable. The only disadvantage of the model `HeatPumpFinal` was that unrealistically high values for P_{HP} could be obtained. In the first three `HeatPump` models, P_{HP} could easily be limited by specifying a maximum output in the `Controller` model, which was used to control P_{HP}. In the model `HeatPumpFinal`, this was not possible and thus the results had to be checked for plausibility.

4.4.5 Heat exchanger models

Three heat exchanger models were developed in this work. All represented plate heat exchangers in counterflow direction. Headers and heat transfer to the ambient were neglected. Nominal values for mass flow rate and pressure drop for both fluid streams were input parameters of the models. Based on these nominal

values, the pressure drop from inlet to outlet could be chosen to be constant or a function of the mass flow rate.

The first heat exchanger model, `HeatExchanger1`, consisted of an array of `HeatedFluidVolume` models, which were connected via an array of `ThermalConductor` models, see Figure 4.8.

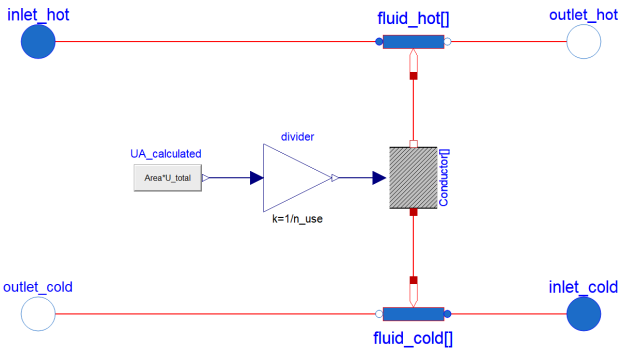

Figure 4.8: Diagram of the model `HeatExchanger1` (DS).

The heat exchange area (A_{HX}), the overall heat transfer coefficient (U_{tot}), and the number of `ThermalConductor` models (n) were input parameters of the model `HeatExchanger1`. This model was used for the simulations for Paper II with $n = 8$. This discretization value was found to give good agreement with logarithmic mean temperature (LMTD) calculations at reasonable computation times.

The discretization approach chosen for the model `HeatExchanger1` led to many state variables in the system models, which increased the computation time. To reduce the number of state variables, the model `HeatExchanger2` was developed, which was based on the widely-used LMTD approach shown in the equations (4.8) and (4.9).

$$\Delta T_{\mathrm{LM}} = \frac{(T_{\mathrm{hot,in}} - T_{\mathrm{cold,out}}) - (T_{\mathrm{hot,out}} - T_{\mathrm{cold,in}})}{\ln\left(\dfrac{T_{\mathrm{hot,in}} - T_{\mathrm{cold,out}}}{T_{\mathrm{hot,out}} - T_{\mathrm{cold,in}}}\right)} \tag{4.8}$$

$$\dot{Q}_{\mathrm{HX}} = U_{\mathrm{tot}} \cdot A_{\mathrm{HX}} \cdot \Delta T_{\mathrm{LM}} \tag{4.9}$$

This approach allowed using only one `HeatedFluidVolume` model for each

fluid stream and led to reduced computation time. However, Equation (4.8) is numerically challenging because the solver can easily take steps into undefined areas of the function during iteration. This led to unstable simulations. Therefore, the model LMTD was developed, which contained a lookup-table from which ΔT_{LM} could be obtained with the input signals dT1 $= T_{\mathrm{hot,in}} - T_{\mathrm{cold,out}}$ and dT2 $= T_{\mathrm{hot,out}} - T_{\mathrm{cold,in}}$ as shown in Figure 4.9.

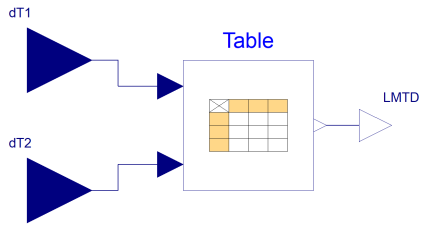

Figure 4.9: Diagram of the model LMTD (DS).

The parameter values for the lookup-table were calculated in Excel and spline-interpolation was used to interpolate between these values in Dymola. The model LMTD was included in the model HeatExchanger2 and led to increased stability of the simulations. However, the LMTD method requires both inlet and outlet temperatures of the fluid streams to calculate the heat flow rate in the heat exchanger, which in turn influences the outlet temperatures of the fluid streams. This interdependence led to long computation times.

The "effectiveness-NTU" method is based on the same theory and assumptions as the LMTD method. However, it only requires the inlet temperatures of the fluid streams to calculate the heat flow rate in the heat exchanger. The effectiveness-NTU method was therefore used in the model HeatExchangerFinal. The NTU-relation for the effectiveness of a counterflow heat exchanger from [55] was implemented in the model HeatExchangerFinal and is shown in the equations (4.10) to (4.15).

$$C_{\mathrm{hot/cold}} = \dot{m}_{\mathrm{hot/cold}} \cdot c_p \tag{4.10}$$

$$C_{\mathrm{min/max}} = \min/\max(C_{\mathrm{hot}}, C_{\mathrm{cold}}) \tag{4.11}$$

$$C_{\mathrm{r}} = \frac{C_{\mathrm{min}}}{C_{\mathrm{max}}} \tag{4.12}$$

$$\mathrm{NTU} = \frac{U_{\mathrm{tot}} \cdot A_{\mathrm{HX}}}{C_{\mathrm{min}}} \tag{4.13}$$

$$\varepsilon = \frac{1 - \exp[-\mathrm{NTU} \cdot (1 - C_{\mathrm{r}})]}{1 - C_{\mathrm{r}} \cdot \exp[-\mathrm{NTU} \cdot (1 - C_{\mathrm{r}})]} \tag{4.14}$$

$$\dot{Q}_{\mathrm{HX}} = \varepsilon \cdot C_{\mathrm{min}} \cdot (T_{\mathrm{hot,in}} - T_{\mathrm{cold,in}}) \tag{4.15}$$

Measures were taken to avoid numerical instabilities for $\dot{m}_{\mathrm{hot/cold}} = 0$ and $C_r = 1$. After the implementation of these measures, the model `HeatExchanger-Final` showed significant improvements in the simulation performance compared to the model `HeatExchanger2`. In addition, the overall heat transfer coefficient U_{tot} could be chosen to be a function of the mass flow rate in the model `Heat-ExchangerFinal`. Nominal conditions for the mass flow rate and the heat transfer coefficient were then required as input parameters and U_{tot} was calculated with Equation (4.16) and q set to 0.63 based on [56].

$$U_{\mathrm{tot}} = U_{\mathrm{nom}} \cdot \frac{(\dot{m}_{\mathrm{hot,nom}})^{-q} + (\dot{m}_{\mathrm{cold,nom}})^{-q}}{(\dot{m}_{\mathrm{hot}})^{-q} + (\dot{m}_{\mathrm{cold}})^{-q}} \tag{4.16}$$

A diagram of the model `HeatExchangerFinal` and its parameter window in Dymola are shown in Figure 4.10 and Figure 4.11, respectively.

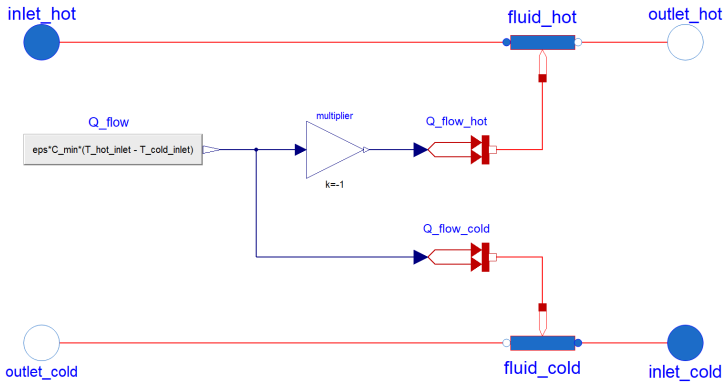

Figure 4.10: Diagram of the model `HeatExchangerFinal` (DS).

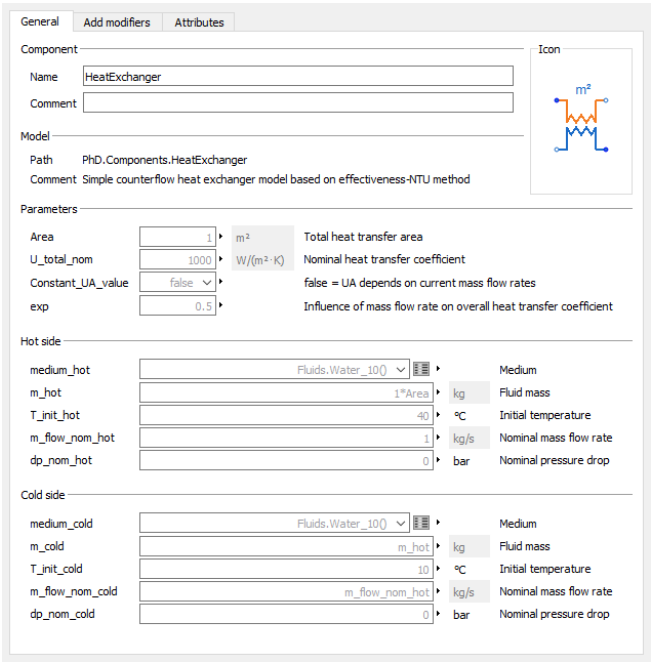

Figure 4.11: Parameter window of the model `HeatExchangerFinal` (DS).

4.4.6 Borehole thermal energy storage model

The model `BTES` represented a BTES with single U-tube pipes. Although a BTES is used as long-term storage, its short-term response can be important for system performance [57]. Therefore, an approach was chosen which included both long- and short-term dynamics in the model. The model `BTESCrossSection` was developed and several of these `BTESCrossSection` models were connected in series in the model `BTES`. The number of `BTESCrossSection` models was an input parameter of the model `BTES`, which is shown in Figure 4.12.

All input values were equal in the `BTESCrossSection` models, e.g. the fluid volume in the pipes or the thermal capacity of the ground. Therefore, the values were calculated in the model `BTES` and defined as "inner" parameters/variables. This way, they could be imported as "outer" parameters/variables in the `BTES-CrossSection` model and did not need to be calculated in each `BTESCrossSection` model. This inner/outer approach avoids duplicate code and should therefore be used when possible. The parameter window of the model `BTES` is shown in Figure 4.13.

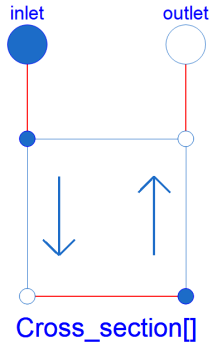

Figure 4.12: Diagram of the model BTES (DS).

General | Add modifiers | Attributes

Component
Name: BTES
Comment:
Icon: BTES

Model
Path: PhD.Components.BTES
Comment: Array of cross sections with single U-tube ground heat exchanger and surrounding ground

Parameters

n_vertical	10		Number of vertical cross sections
n_horizontal	10		Number of (cylindrical) ground shells in each cross section
medium	Fluids.Water_10()		Fluid for the borehole loop
T_init	10	°C	Initial temperature in GHE
T_init_far	10	°C	Initial temperature in far ground
n_boreholes	10		Number of boreholes
depth	100	m	Borehole depth

Ground specifications

d_ground	10	m	Diameter for calculation of ground capacity
rho_ground	1	g/cm³	Density
cp_ground	1000	J/(kg·K)	Specific heat capacity
lambda_ground	2	W/(m·K)	Conductivity

Ground heat exchanger (GHE) specifications

d_GHE	0.1	m	Outer diameter of GHE
s	1e-3	m	Shank spacing (distance between pipe centers)
rho_filling	1	g/cm³	Density of GHE filling material
cp_filling	1000	J/(kg·K)	Specific heat capacity of GHE filling material
lambda_filling	2	W/(m·K)	Conductivity of GHE filling material

Pipe specifications

m_flow_nom	1	kg/s	Nominal mass flow
dp_nom	0	bar	Nominal pressure drop
d_pipe_outer	0.05	m	Outer diameter of pipes in GHE
d_pipe_inner	0.04	m	Inner diameter of pipes in GHE
lambda_pipe	0.5	W/(m·K)	Conductivity of pipe material
Nu_nom	100	1	Nusselt number for nominal conditions

Figure 4.13: Parameter window of the model BTES (DS).

The three main parts of a BTES were included in the BTESCrossSection model: a single U-tube pipe, the borehole with filling material, and the surrounding ground. A schematic of the model and the diagram of the simulation model are shown in the figures 4.14 and 4.15, respectively.

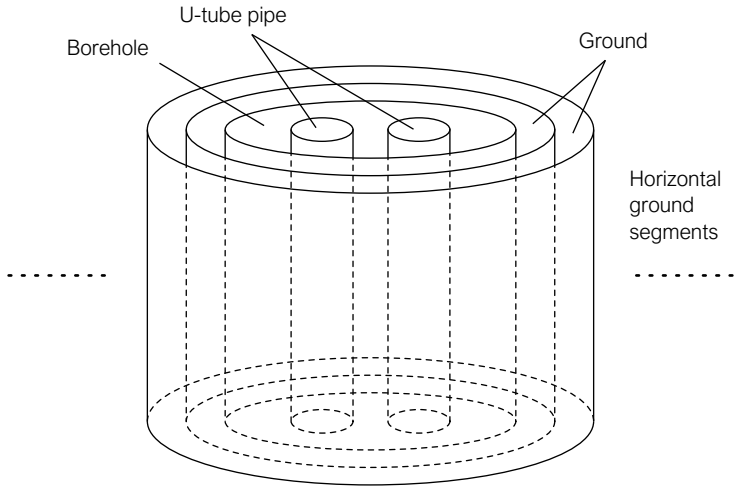

Figure 4.14: Schematic of the model BTESCrossSection.

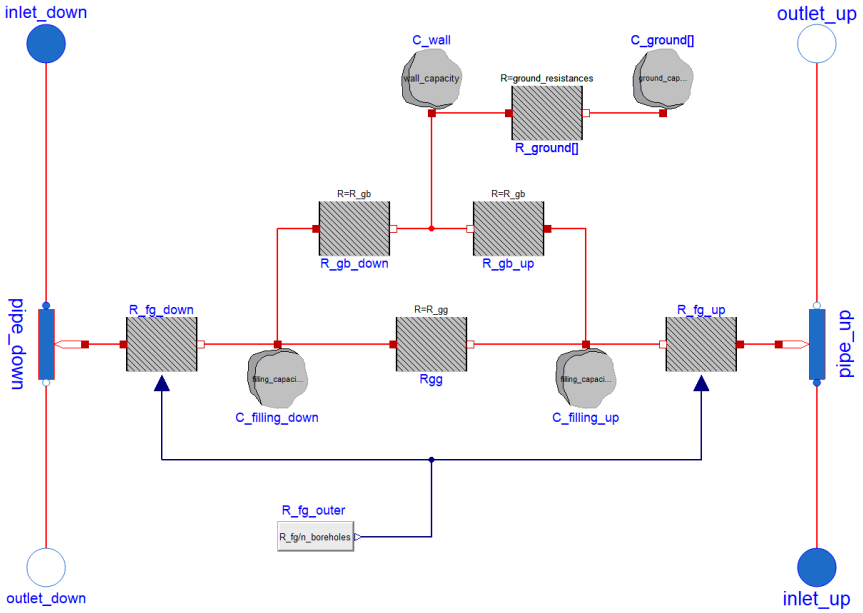

Figure 4.15: Diagram of the model BTESCrossSection (DS).

HeatedFluidVolume models were used to represent the U-tube pipe segments in each BTESCrossSection. The borehole filling and the surrounding ground were modeled with HeatCapacitor models. ThermalResistor models were added to model two-dimensional heat transfer between the fluid in the pipe and the borehole wall according to the methodology published by Bauer et al. [58]. The only variable thermal resistance was between fluid and filling material and depended on the fluid mass flow rate in the pipe due to the convective resistance R_fg, see Figure 4.15. One-dimensional, radial, heat transfer was modeled in the cylindrical ground shells. The capacities and heat transfer coefficients corresponded to the geometry of each shell element according to [59]. The number of ground shells and the ground diameter were input parameters of the model BTES, see the parameter window in Figure 4.13.

Arranging boreholes in a pattern and connecting them in series can increase the performance of a BTES, as described for example in [60]. In this work, it was assumed that all boreholes were connected in parallel with resulting equal mass flow rates. In addition, the thermal properties of the ground were assumed isotropic. These assumptions led to identical temperatures for the outermost ground shell of all boreholes. Thus, no heat was transferred between boreholes in this model and all boreholes showed identical behavior. Thus, they were lumped to one single borehole model with the input parameter n_boreholes, which defined the number of modeled boreholes, see Figure 4.13. All thermal capacities in the model BTES were multiplied by n_boreholes and all thermal resistances were divided by n_boreholes. This lumping reduced the computation time significantly without introducing an additional error. Simulations were performed to validate that the behavior of the lumped model BTES was identical to several individual BTES models.

Beier et al. published experimental data for a 52-hour charging period of a grouted single U-tube borehole heat exchanger surrounded by wet sand [61]. The short-term response of the model BTES developed in this work was validated against this experimental data set. The experimental setup was imitated by setting all input parameters of the model BTES to the respective values of the experimental setup and using the measured inlet temperature and mass flow rate as simulation input. The simulated outlet temperature, the average wall temperature, and three average ground temperatures at different distances from the

borehole were compared to the measured values from [61]. The developed BTES model showed very good agreement with the measurement data as shown in Figure 4.16.

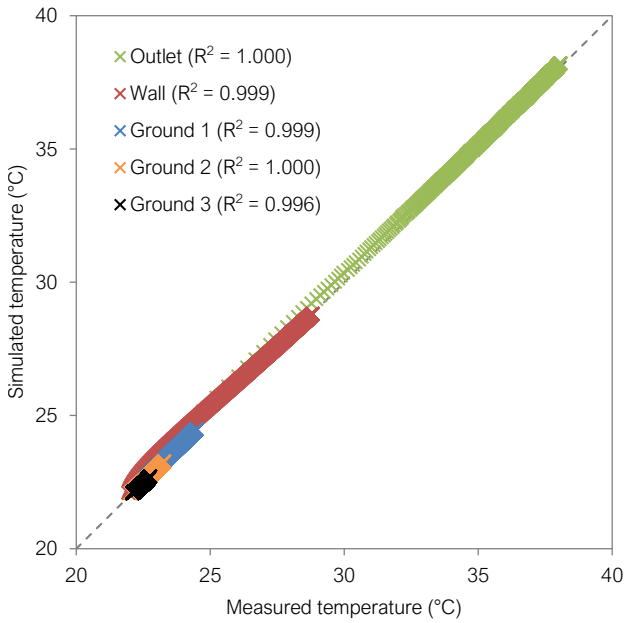

Figure 4.16: Validation of the model BTES with experimental data (data from [61]).

4.4.7 Solar collector models

Three solar collector models were developed in this work. All of them represented flat plate solar collectors and required the ambient temperature and solar radiation as input signal. The outdoor temperature was used as ambient temperature for all simulations. HeatedFluidVolume models were used to represent the fluid in the collectors. The number of serial and parallel collectors, as well as the effective collector area and the optical efficiency were input parameters of the models.

In the model SolarCollectors1, all collectors were lumped into one HeatedFluidVolume. An incoming heat flow was calculated based on the solar radiation, the total area, and the optical efficiency. To account for heat transfer from the fluid to the ambient air, a ThermalConductor model was implemented. The thermal conductance was an input parameter of the model SolarCollectors1.

In the model SolarCollectors2, an array of HeatedFluidVolume models was used. The interaction of parallel collectors was still neglected and parallel collectors were lumped to reduce computation time. However, collectors in series were modeled individually with respective flow connections. This led to a more realistic calculation of the collector outlet temperature compared to the model SolarCollectors1, which was based on only one perfectly mixed HeatedFluid-Volume model.

In the third and final solar collector model, the total heat flow rate $\dot{Q}_{\mathrm{col}}$ in each collector was calculated based on the widely used European Standard EN 12975 1:2006

$$\dot{Q}_{\mathrm{col}} = A_{\mathrm{col}} \cdot \left[R \cdot \eta_{\mathrm{opt}} - a_1 \cdot (T_{\mathrm{col}} - T_{\mathrm{amb}}) - a_2 \cdot (T_{\mathrm{col}} - T_{\mathrm{amb}})^2 \right] \tag{4.17}$$

with R being the solar radiation and T_{col} being the average fluid temperature in the respective collector. The linear and the quadratic heat loss coefficient, a_1 and a_2, respectively, were input parameters of the model SolarCollectorsFinal. A diagram of the model SolarCollectorsFinal and its parameter window in Dymola are shown in Figure 4.17 and Figure 4.18, respectively.

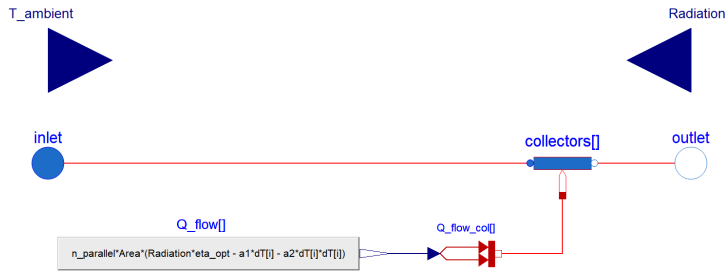

Figure 4.17: Diagram of the model SolarCollectorsFinal (DS).

T_max was an input parameter, which was used to print warning messages when a collector outlet temperature exceeded the maximum temperature. It was also used for the control of the circulation pumps in the solar collector loop.

4.4.8 Storage tank models

Two storage tank models were developed in this work. One-dimensional flow was assumed inside the tank and the tank's volume was an input parameter. Heat

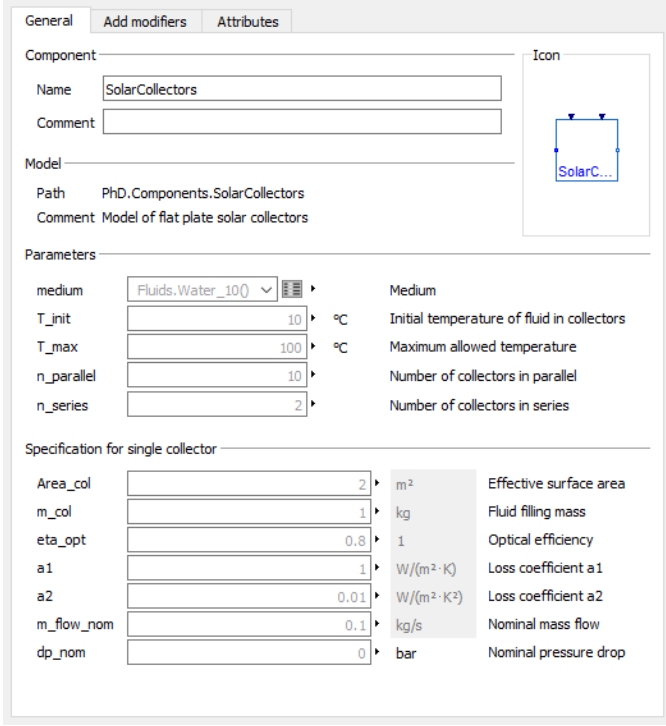

Figure 4.18: Parameter window of the model `SolarCollectorsFinal` (DS).

transfer to the ambient was modeled with a `ThermalConductor` model and the ambient temperature as input signal. Note that this ambient temperature could be different from the ambient temperature of the solar collectors, depending on the location of the storage tank.

In the model `StorageTank1`, only one `HeatedFluidVolume` was used to model the fluid in the tank, i.e. the tank was assumed to be perfectly mixed. In the model `StorageTankFinal`, an array of `HeatedFluidVolume` models was used to represent different fluid layers in the tank. This gave a more realistic temperature profile. However, thermal stratification and heat exchange between the different layers was deemed too detailed and therefore not modeled. The number of `HeatedFluidVolume` models was an input parameter of the model `StorageTankFinal`.

In the model `StorageTankFinal`, an internal heat exchanger could also be added to the tank. This was required for the storage tank in the solar collector loop. An array of `HeatedFluidVolume` models and `ThermalConductor` models

was used to represent the internal heat exchanger, with the array size equal to the number of fluid layers. The fluid in the internal heat exchanger was thermally connected to the fluid in the tank with a constant conductivity in each layer. The conductivity value was an input parameter of the model `StorageTankFinal`, which is shown in Figure 4.19.

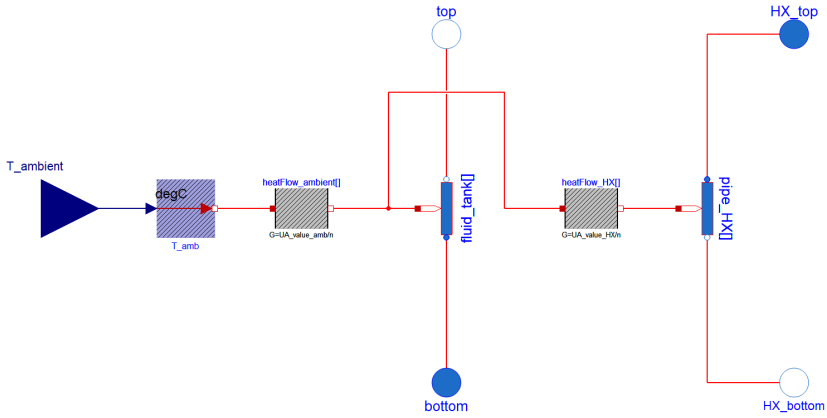

Figure 4.19: Diagram of the model `StorageTankFinal` with internal heat exchanger (DS).

4.4.9 Insulated pipe models

A single pipe model and a twin pipe model were developed in this work. Both consisted of an array of `HeatedFluidVolume` models to represent the fluid inside the pipes. The number of `HeatedFluidVolume` models as well as the pipe dimensions and the insulation properties were input parameters of the models.

The model `SinglePipe` was developed to represent insulated distribution pipes over ground. The ambient temperature was an input signal and was connected to the pipe fluid via an array of `ThermalResistor` models, see Figure 4.20.

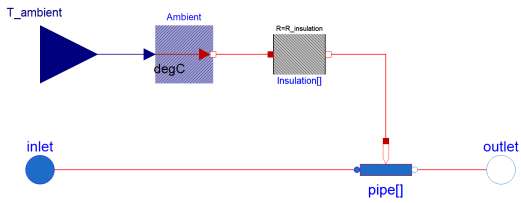

Figure 4.20: Diagram of the model `SinglePipe` (DS).

The model TwinPipe was developed to represent insulated distribution pipes underground because twin pipes are common for new grids, see Section 2.1.2. Correlations for heat losses from twin pipes were implemented in the model TwinPipe, details can be found in Paper IV. Ground specifications were input parameters of the model and the surface temperature of the ground was an input signal. The model TwinPipe is shown in Figure 4.21.

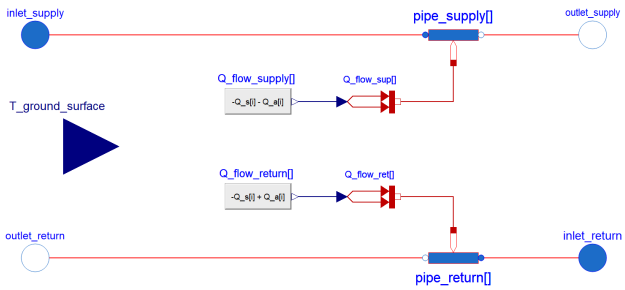

Figure 4.21: Diagram of the model TwinPipe (DS).

4.4.10 Customer substation models

Different customer substation models were developed in this work based on the substation types of the two case study systems, see Chapter 3. The customer substation models were used to model the transfer of heat between a thermal energy supply system and a customer, i.e. the HVAC system of one or several buildings. To recall, these HVAC systems of the buildings were not modeled, i.e. the customer substations were the modeled system boundary. Thus, the heating and cooling demands of the customers were required as input data.

The highly simplified model CustomerSubstation1 was developed first. It consisted of a CirculationPump model and a HeatedFluidVolume model and is shown in Figure 4.22.

The heat flow rate specified in the input data was added to or removed from the fluid and the mass flow rate was controlled by the circulation pump to yield a fixed temperature difference between inlet and outlet of the substation. This temperature difference was an input parameter of the model. The model CustomerSubstation1 was only used for testing purposes and for the very first steps of the system model development.

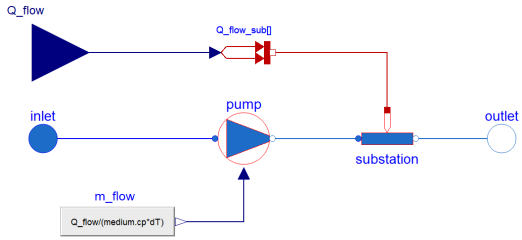

Figure 4.22: Diagram of the model `CustomerSubstation1` (DS).

The model `CustomerSubstationVulkan` was developed for the case study Vulkan and could be used as heating or cooling substation. The inlet temperature on the secondary side, i.e. the return temperature (T_{ret}) from the buildings, was an input parameter of the model. The model `CustomerSubstationVulkan` as used for cooling is shown in Figure 4.23.

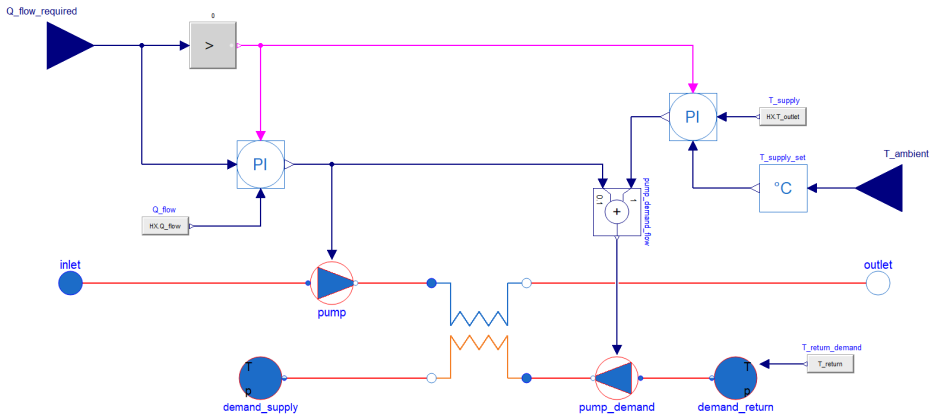

Figure 4.23: Diagram of the model `CustomerSubstationVulkan` (DS).

The model `CustomerSubstationVulkan` contained a heat exchanger and two circulation pumps as can be seen in Figure 4.23. The primary circulation pump, i.e. the one on the thermal energy supply system side, was controlled to deliver the specified heat flow rate. The secondary circulation pump, i.e. the one on the customer side, was controlled to deliver a certain supply temperature to the customer. This temperature could either be constant or outdoor temperature compensated. This supply temperature control could also be deactivated so that both circulation pumps received the same mass flow rate signal. As for the model `HeatPumpFinal`, the model `CustomerSubstationVulkan` was not a physi-

cal representation of a real customer substation because of the unrealistic control approach. However, the model led to fast and stable simulations and the obtained results were reasonable.

A customer substation and a prosumer substation model were developed for the case study Brøset. These are explained in detail in Paper IV and are therefore only briefly introduced here. The model `CustomerSubstationBroeset` had two heat exchangers: one for space heating and one for DHW heating as shown in Figure 4.24.

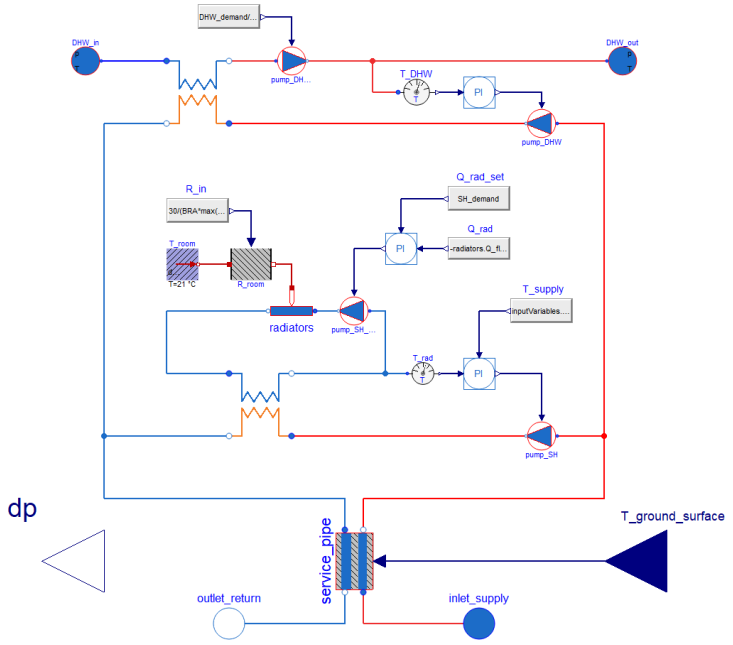

Figure 4.24: Diagram of the model `CustomerSubstationBroeset` (DS).

The model `ProsumerSubstationBroeset` was modeled as return/supply connection for prosumers, i.e. customers that can also deliver heat to the grid. The model is shown in Figure 4.25.

4.5 System models

Several system models were developed for the two case study systems described in Chapter 3. As mentioned before, focus was on the Vulkan case study. The

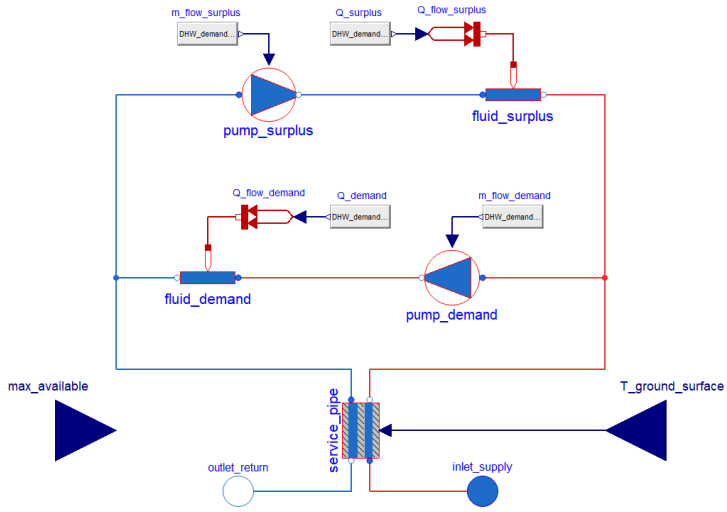

Figure 4.25: Diagram of the model `ProsumerSubstationBroeset` (DS).

author contributed to the Brøset system models by giving general modeling advice, supporting component and system model development, and providing component models for the system model used in Paper IV.

Connecting component models in Modelica is very simple. In Dymola, the graphical user interface allows connecting ports by click and drag. This will automatically create connect-equations in the model. However, implementing a control system can be challenging due to the physical modeling approach, especially for systems with many interconnected components. For such systems, it is advisable to build system models successively, i.e. modeling a part of the system first and adding more components when the control of the modeled part is working satisfactory. However, component models and system models were developed in parallel in this work. Therefore, the system model development was an iterative process and required many adjustments of the control structure.

4.5.1 Integrated heating and cooling system at Vulkan

The system model development for the Vulkan case study was one of the main tasks of this work. The system model has undergone many small and large modifications during the course of this work, but only the two versions that were used for publications, namely Paper II and Paper V, are presented here.

The first system model for Vulkan

The first system model for Vulkan was used for the analysis of heat export to the local DH grid as described in Paper II. The model is shown in Figure 4.26.

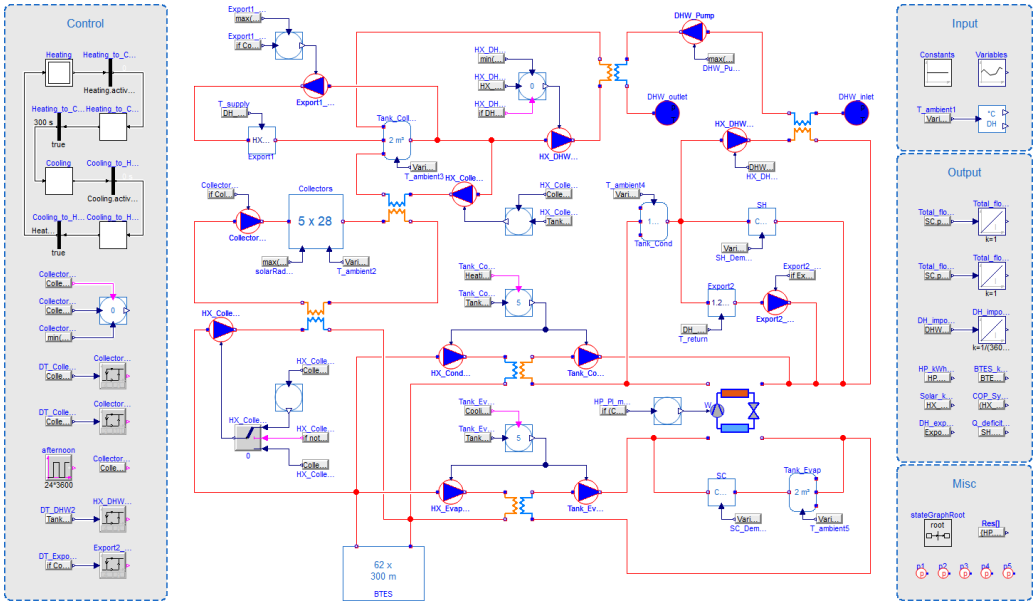

Figure 4.26: Diagram of the first system model for Vulkan as used for Paper II (DS).

The system model shown in Figure 4.26 contained some issues, which are listed below.

- The following non-final component models were used: `StorageTank1`, `HeatExchanger1`, `SolarCollectors1`, and `HeatPump2`, see Section 4.4.
- Only one heat pump was included in the system model. This simplification was made because the condenser heat from all heat pumps was sent to the same secondary fluid loop of the IHCS. The product cooling demand was therefore added to the space cooling demand.
- The snow melting demand and the ITES were neglected.
- The included model `StorageTank1` did not have an internal heat exchanger, so an own loop was modeled to transfer heat from the solar collectors to the tank. Two loops were modeled to transfer heat from the collector tank to the DH grid or to DHW heating.

- A constant initial temperature of the ground was assumed in the model BTES (instead of a linear profile) and the ground radius was set to 5 m (instead of 8 m).
- A heat exchanger was falsely included in the BTES discharging loop on the evaporator side of the heat pump.
- The input data for radiation were retrieved from the software Meteonorm and thus represented a typical year (instead of data for the analyzed year from the nearest weather station).

Due to these issues, the control of this system version is not described in detail here. A short description can be found in Paper II.

The final system model for Vulkan

The issues listed above were fixed in the final system model, in which the final versions of all component models were used. This system model was used for Paper V. A Dymola screenshot of the model and a modified version with selected specifications are shown in Figure 4.27 and Figure 4.28, respectively.

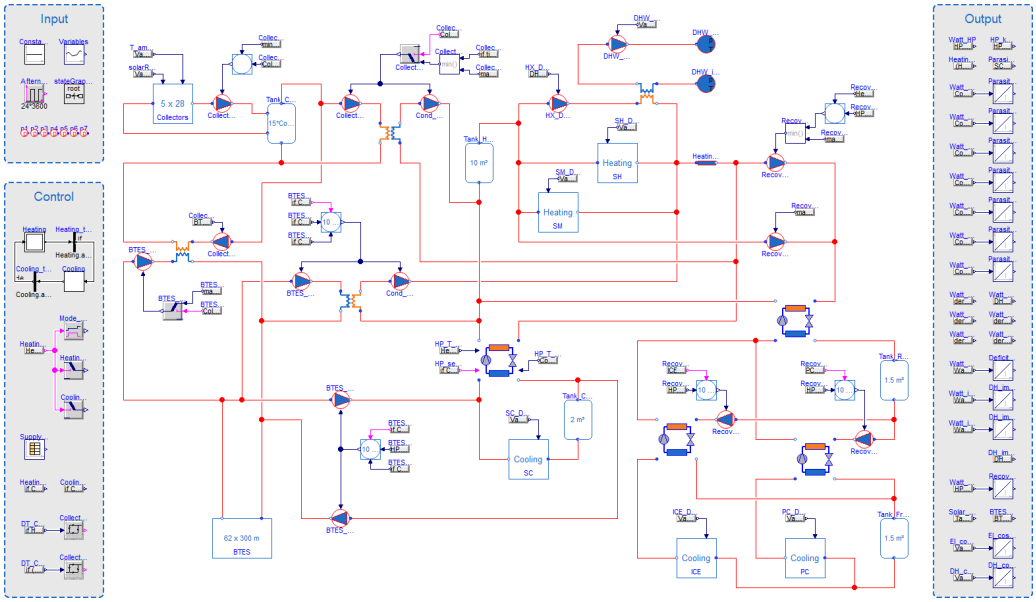

Figure 4.27: Diagram of the final system model for Vulkan as used for Paper V (DS).

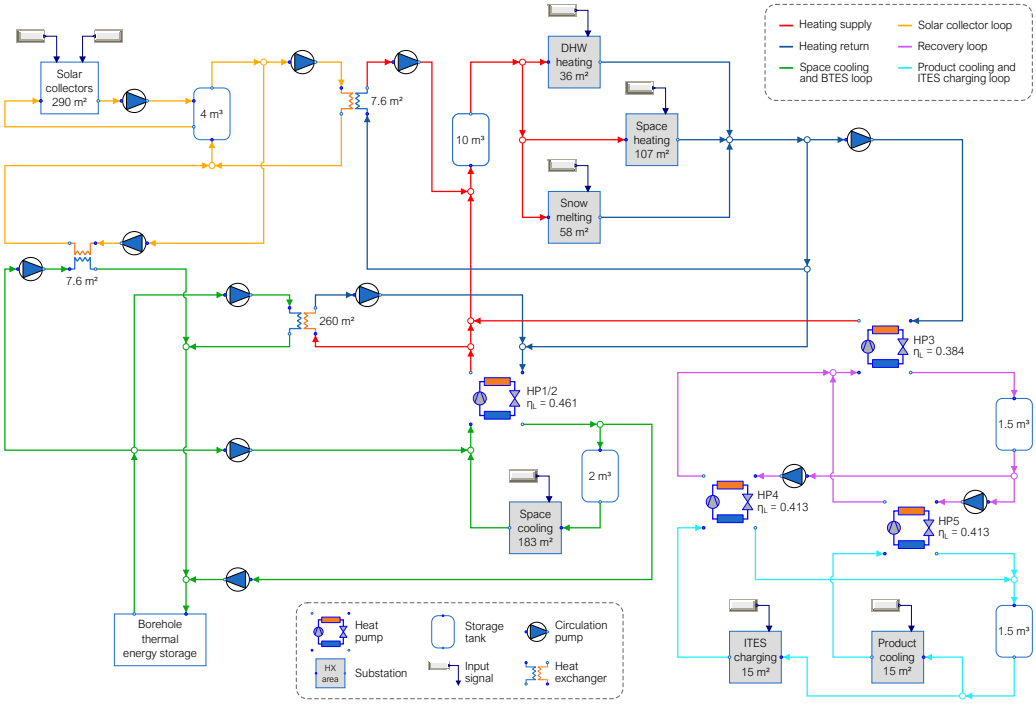

Figure 4.28: Schematic of the final system model for Vulkan with legend and selected specifications.

The main component specifications used for system simulations can be seen in Figure 4.28. Additional specifications are listed in the tables 4.1, 4.2, and 4.3.

The existing IHCS was equipped with a simple control system. The heat pumps received stepwise control signals to activate/deactivate their parallel circuits and compressor stages. These step signals were based on the storage tank temperatures. The circulation pumps were controlled based on pressure difference setpoints or temperature setpoints. The storage tanks were only used as buffers. In the system model, the heat pumps were controlled continuously because the individual compressor stages were not included in the heat developed pump models. The circulation pumps were controlled with PI-controllers based on temperature setpoints. The PI-controller outputs were limited to avoid unrealistically high mass flow rates.

The IHCS had two operation modes: 1) “heating mode” and 2) “cooling mode”. A free cooling mode was originally planned but was not implemented as

Table 4.1: Heat exchanger model specifications used in the final system model.

	Heat transfer area m^2	Nominal heat transfer coefficient $W/(m^2 \cdot K)$	Nominal mass flow rate kg/s
Space heating	107.0	4 400	8.0
Snow melting	58.0	3 300	5.0
DHW heating	36.0	2 700	1.0
Space cooling	183.0	3 300	20.0
Product cooling	15.0	3 500	3.0
ITES loading	15.0	3 500	6.0
Solar to heating	7.6	3 500	0.8
Solar to BTES	7.6	3 500	0.8
HP to BTES	260.0	3 500	10.0

Table 4.2: Solar collector model specifications used in the final system model.

Parameter	Value	Unit
Number of serial collectors	5	-
Number of parallel collectors	28	-
Effective surface area	1.9	m^2
Optical efficiency	0.773	-
Linear heat loss coefficient	3.676	$W/(m^2 \cdot K)$
Quadratic heat loss coefficient	0.0143	$W/(m^2 \cdot K^2)$
Fluid filling	1.2	kg

explained in Paper I. Models from the library StateGraph, which is included in the MSL, were used in the system model to switch between the two operation modes. This operation mode switching was triggered based on the average temperatures in the storage tanks for heating and space cooling as shown in Figure 4.29.

An operation mode switch triggered the activation/deactivation of the BTES circulation pumps, a change in heating supply temperature setpoint, and different control strategies for the solar collectors and the ITES. Details are given in the following paragraphs. The real system required some downtime for an operation

Table 4.3: BTES model specifications used in the final system model.

Parameter	Value	Unit
Number of boreholes	62	-
Vertical discretization	4	-
Horizontal discretization	30	-
Borehole depth	300	m
Borehole diameter	0.14	m
Ground diameter	9	m
Ground density	2 600	kg/m^3
Ground heat capacity	850	$J/(kg \cdot K)$
Ground conductivity	2.75	$W/(m \cdot K)$
U-tube diameter	0.04	m
U-tube conductivity	0.42	$W/(m \cdot K)$
Nusselt number inside borehole	5	-

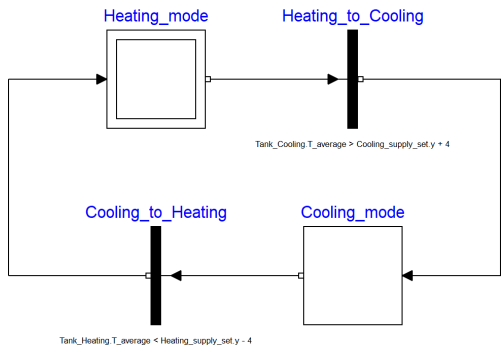

Figure 4.29: StateGraph logic applied for switching between operating modes (DS).

mode switch due to manual valve adjustments. Therefore, only one operation mode switch was performed between heating and cooling season. In the system model, this downtime was neglected and several operation mode switches were allowed.

In heating mode, the outlet temperature of HP 1/2 on the condenser side was set to equal the heating supply temperature of 55 °C. The outlet temperature on the evaporator side of HP 1/2 was controlled by the BTES pump with the space cooling supply temperature of 6 °C as setpoint. When the space cooling demand

increased, less heat had to be extracted from the BTES. At some point, the BTES was not needed as heat source and the temperature in the cooling tank increased. When the average temperature in the cooling tank was higher than 10 °C, an operation mode switch was triggered to ensure that the space cooling demand could be covered. The ITES was not used in heating mode.

In cooling mode, the outlet temperature of HP 1/2 on the evaporator side was set to equal the space cooling supply temperature of 6 °C. The outlet temperature on the condenser side of HP 1/2 was controlled by the BTES pump with a reduced heating supply temperature of 51 °C as setpoint. When the heating demands increased, less heat was available to be injected into the BTES. At some point, the BTES was not needed as heat sink and the temperature in the heating tank decreased due to the increasing heating demands. When the average temperature in the heating tank was lower than 47 °C, an operation mode switch was triggered to ensure that the heating demands could be covered. The ITES was used to reduce space cooling peak demands and was charged by HP 4 during the night.

The heat from the solar collectors was accumulated in a storage tank. The circulation pump was controlled with a floating collector outlet temperature, which was set to 10 °C above the temperature at the top of the solar storage tank, similar to [62]. The accumulated heat could be sent to the heating supply line or to the BTES loop via separate heat exchangers, see Figure 4.28. Rule-based control was applied to decide when the heat should be sent to which heat exchanger. The chosen strategy is described below and shown in Figure 4.30. Boolean signals and hysteresis models were used to implement the strategy in the system model.

In cooling mode, the solar heat was used to charge the BTES because enough condenser heat from the heat pumps was available to cover the heating demands. In cooling mode, sending solar heat to the heating supply line was prioritized. Therefore, the collector tank was charged until the temperature at the top was higher than the heating supply temperature setpoint. The solar radiation peaks around noon, so the temperature in the storage tank was not expected to rise significantly after 1 p.m. The heat was then used to charge the BTES. Most heat was accumulated during the summer when the system was operating in cooling mode. Therefore, around 90% of the heat was used to charge the BTES throughout the year.

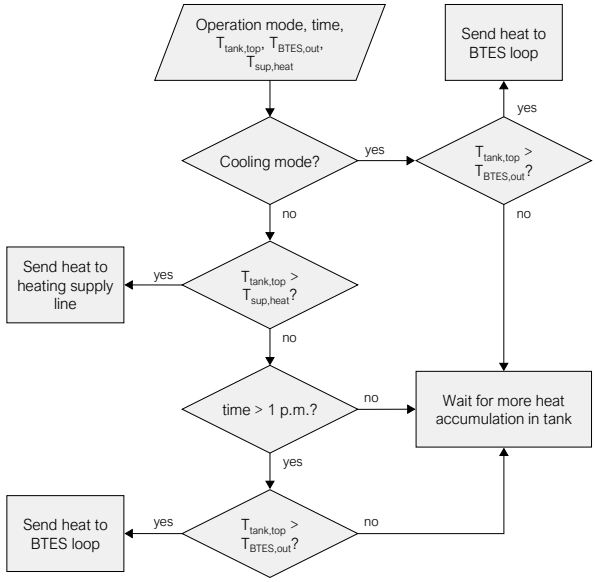

Figure 4.30: Rule-based controller logic for use of the solar heat.

The Dymola statistics of the final system model are shown in Figure 4.31. It can be seen from Figure 4.31 that there were no remaining algebraic loops in the DAES (Sizes after manipulation of the linear systems: $\{0, 0, 0, 0, 0, 0, 0, 0, 0\}$). The computation time for a one-year simulation was about 70 seconds with an Intel© Core™ i7 6700K processor (4 GHz) and 64 GB RAM. Setting the parameter delay_measurement in all `Controller` models to false (see Section 4.4.3) led to remaining nonlinear loops (Sizes after manipulation of the nonlinear systems: $\{9, 4, 10\}$). In this case, the computation time was increased by about 60%. This shows how even small changes in a model can have a large effect on the final DAES and the numerical performance.

The main simplifications and assumptions behind the final system model are summarized below.

- Pipes between components were neglected because no detailed information was available. Distribution heat losses from the IHCS were thus not calculated. However, the losses from the distribution systems of the buildings were included in the measured heating demands. The distances were short compared to the pipe lengths of DH grids due to the small area of the building complex.

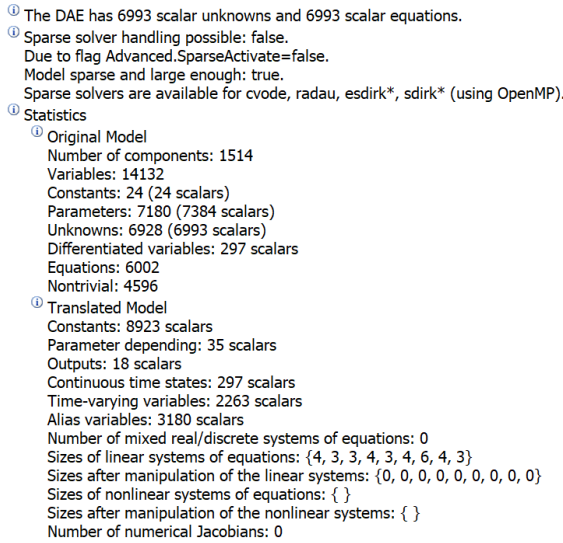

Figure 4.31: Dymola statistics for the final system model for Vulkan (DS).

- Each building substation contained five separate heat exchangers. These were used for space heating from the IHCS and the DH grid, DHW heating from the IHCS and the DH grid, and space cooling from the IHCS. Heat exchangers for the same purpose were lumped in the system model and one substation model for each demand type was used.
- The heat exchangers for heat import from the DH grid were not modeled. Instead, the required heat import was calculated based on the remaining heating demand after the heat exchanger connection to the IHCS.
- The real system required some downtime for an operation mode switch due to manual valve adjustments. Therefore, only one operation mode switch was performed between heating and cooling season. In the system model, this downtime was neglected and several operation mode switches were allowed.
- The return temperature from the buildings was assumed constant because modeling of the building was outside the scope of this work.
- The ITES was not modeled physically. Instead, load profiles were created to represent charging/discharging as explained in Paper V.

- HP 1/2 in Figure 4.28 represented two parallel heat pumps of the same type. These were modeled as one unit because their efficiencies were very similar. Continuous rule-based control was used in the system model although the heat pumps were controlled with stepwise on/off control
- Heat losses from the storage tanks were neglected due to missing temperature measurements at the tank's locations.

4.5.2 Local district heating grid at Brøset

Several system models have also been developed for the case study Brøset, but only the two versions that were used for publications, namely Paper III and Paper IV, are presented here. As mentioned before, the author contributed to the modeling part of these studies, especially Paper IV, but much modeling work has also been done by others.

First system model for Brøset

The commercial library TIL from TLK-Thermo GmbH was initially used for this case study. The first system model for Brøset was therefore developed using this library and was used for the analyses in Paper III. The model is shown in Figure 4.32.

As for the Vulkan case study, the first system model for Brøset was much less mature than the final model. The main issues of the first system model are summarized below.

- The customer substation models (with different building icons in Figure 4.32) were similar to the one shown in Figure 4.22, i.e. extremely simplified.
- Single pipe models were used (similar to the one shown in Figure 4.20) instead of twin pipe models for the DH distribution pipes.
- Only the pipes of the main grid were modeled, the supply pipes to and from the buildings were neglected. The total pipe length was therefore only 3.5 km (compared to 6.8 km in the final system model).

Due to these issues, this system version is not described in more detail here. A description can be found in Paper III. The computation time for a one-year

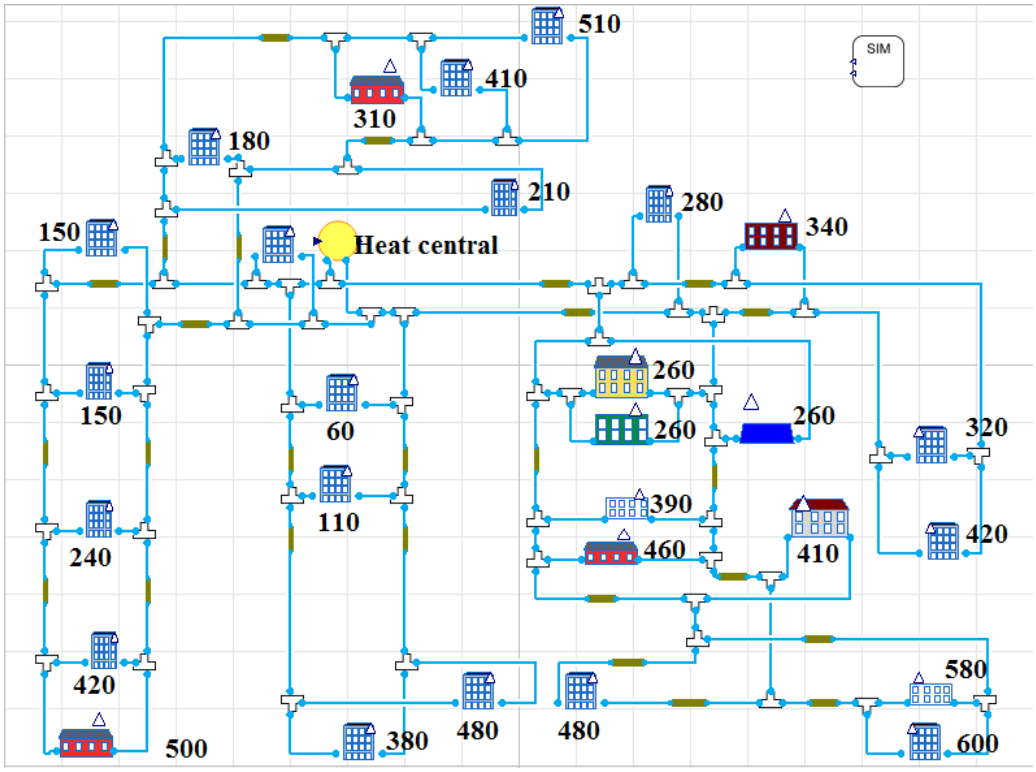

Figure 4.32: Diagram of the first system model for Brøset (taken from Paper III).

simulation with this system model was several hours. The reasons for this were not analyzed in detail. The implementation of a heat exchanger model in the customer substation model was tested, but led to significantly longer computation times and was thus deemed impracticable. It was therefore decided to build a new system model with the simulation models described in this thesis.

Final system model for Brøset

The system model used for Paper IV is shown in Figure 4.33. In this version, the model `CustomerSubstationBroeset`, see Figure 4.24, was used, which had separate heat exchanger models for space heating and DHW heating and a supply pipe. These supply pipes as well as all other pipes in the grid were `TwinPipe` models as shown in Figure 4.21. In addition, several `ProsumerSubstationBroeset` models, see Figure 4.25, were added to the system model.

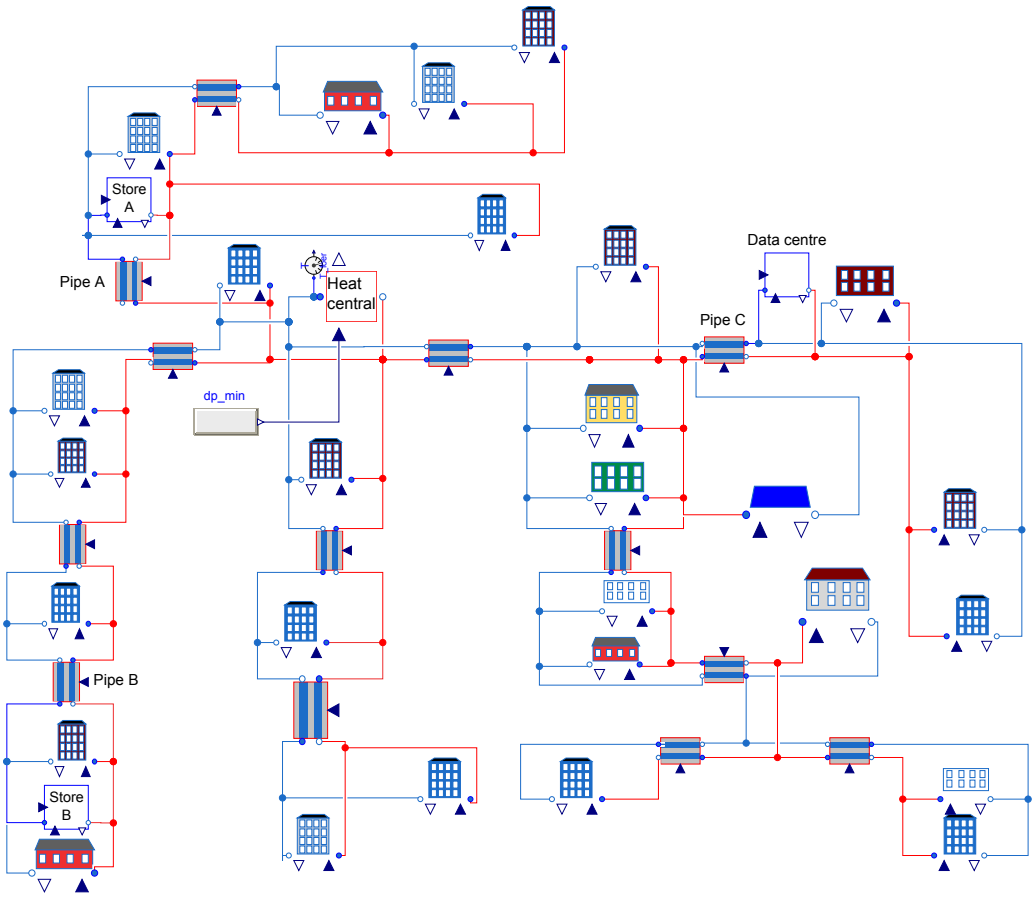

Figure 4.33: The final system model for Brøset (taken from Paper IV).

As explained in Section 3.2.2, the main heat supply was assumed to come from Trondheim's existing DH grid. This connection was not modeled in detail. Instead, the heat central in the system model contained a heat source, which delivered the heat flow rate required to reach the supply temperature setpoint. The pressure lift in the heat central was controlled to ensure a minimum pressure difference of 70 kPa in all the customer substations. The pressure drop in the furthest substation was therefore measured in each branch and the minimum value of these was an input signal of the heat central model, see Paper IV for details.

The Dymola statistics of the final system model are shown in Figure 4.34. It can be seen from Figure 4.34 that there were no remaining algebraic loops in the

DAES of the system model. However, the DAES was much larger compared to the Vulkan system model, see Figure 4.31, which is why computation times were still about two hours for a one-year simulation.

```
The DAE has 21977 scalar unknowns and 21977 scalar equations.
Sparse solver handling possible: false.
Due to flag Advanced.SparseActivate=false.
Model sparse and large enough: true.
Sparse solvers are available for cvode, radau, esdirk*, sdirk* (using OpenMP).
Statistics
  Original Model
  Number of components: 5674
  Variables: 46608
  Constants: 115 (115 scalars)
  Parameters: 24760 (24899 scalars)
  Unknowns: 21733 (21977 scalars)
  Differentiated variables: 558 scalars
  Equations: 19046
  Nontrivial: 15715
  Translated Model
  Constants: 27028 scalars
  Parameter depending: 313 scalars
  Outputs: 2 scalars
  Continuous time states: 558 scalars
  Time-varying variables: 8466 scalars
  Alias variables: 11184 scalars
  Number of mixed real/discrete systems of equations: 0
  Sizes of linear systems of equations: {3, 3, 4, 4, 7, 6, 3, 3, 3, 3, 5, 3, 4, 3, 3, 4, 3, 3, 3, 3, 5, 3, 5, 3, 3, 3, 3, 4, 8, 3, 5, 3, 3, 5, 3, 3, 4, 3, 3, 3, 3, 5, 3, 3, 3, 3, 3, 3, 3}
  Sizes after manipulation of the linear systems: {0, 0, 0, 0, 0, 0, 0, 0, 0, 0, 0, 0, 0, 0, 0, 0, 0, 0, 0, 0, 0, 0, 0, 0, 0, 0, 0, 0, 0, 0, 0, 0, 0, 0, 0, 0, 0, 0, 0, 0, 0, 0, 0, 0, 0, 0, 0, 0, 0}
  Sizes of nonlinear systems of equations: { }
  Sizes after manipulation of the nonlinear systems: { }
  Number of numerical Jacobians: 0
```

Figure 4.34: Dymola statistics for the final system model for Brøset (DS).

5 Approach for optimization-based control of thermal energy systems with storages

The importance of system control has briefly been described in Section 2.1.3. Especially systems with storages require a suitable control strategy to operate efficiently. In this chapter, which is based on Paper VI, an approach for optimization-based control is presented. The main idea of this approach was to find optimized setpoint trajectories for the system's PI-controllers.

The methodology was applied to analyze the case study system at Vulkan, see Section 3.1. The currently used setpoints described in Section 4.5.1 were called "business as usual" (BAU). Optimizations were performed to obtain setpoints for minimized electricity use and minimized electricity costs. Afterwards, these were implemented into the final system model and the simulation results with optimized setpoints were compared to the results with BAU setpoints. This workflow is shown in Figure 5.1.

All elements of the optimization procedure (Part 2 in Figure 5.1) are explained in detail in the next sections.

5.1 Optimization procedure

JModelica.org is an open-source platform for simulation and optimization of complex dynamic systems and is explained in Section 2.2.3. All the optimizations in this work were performed with JModelica.org version 2.2 via 64-bit Python

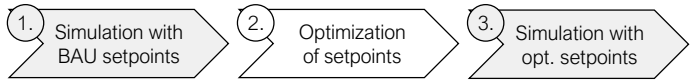

Model	Final system model	Seasonal models	Final system model
Environment	Dymola	JModelica.org	Dymola
Task	Simulation	Optimization	Simulation
Result	Electricity use/costs for the BAU case	Optimized setpoints	Electricity use/costs with improved control

Figure 5.1: Interaction of simulation and optimization.

scripting. It is worth noting that JModelica.org version 2.0 was used initially, which only supported 32-bit Python. The memory usage of a 32-bit Python process is limited to about 2 GB. This was insufficient for the optimizations in this work and led to frequent memory allocation errors. JModelica.org version 2.2 was released in March 2018 and was the first version to support 64-bit Python. The upgrade to version 2.2 was therefore crucial for this work. The main steps of the optimization procedure used to obtain the optimized setpoints are shown in Figure 5.2 and are described below.

Step 1: An initial simulation was required to obtain variable trajectory data for initialization and scaling of the NLP variables in Step 5, see Figure 5.2. To this end, the Modelica model for initialization was compiled into a Functional Mock-Up Unit and simulated using the CVode solver from the SUNDIALS suite [63], which is included in JModelica.org.

Step 2: The Modelica model for optimization and the problem formulation (Optimica code) were compiled and transferred to the CasADi interface of JModelica.org. CasADi was used for the computation of derivatives using algorithmic differentiation [32].

Step 3: Routines for symbolic elimination based on block-triangular ordering are included in JModelica.org and can be applied to reduce the number of algebraic variables as explained in [64]. Symbolic elimination was implemented in this work and was found to be crucial for successful converge as it significantly reduced the size of the resulting NLP.

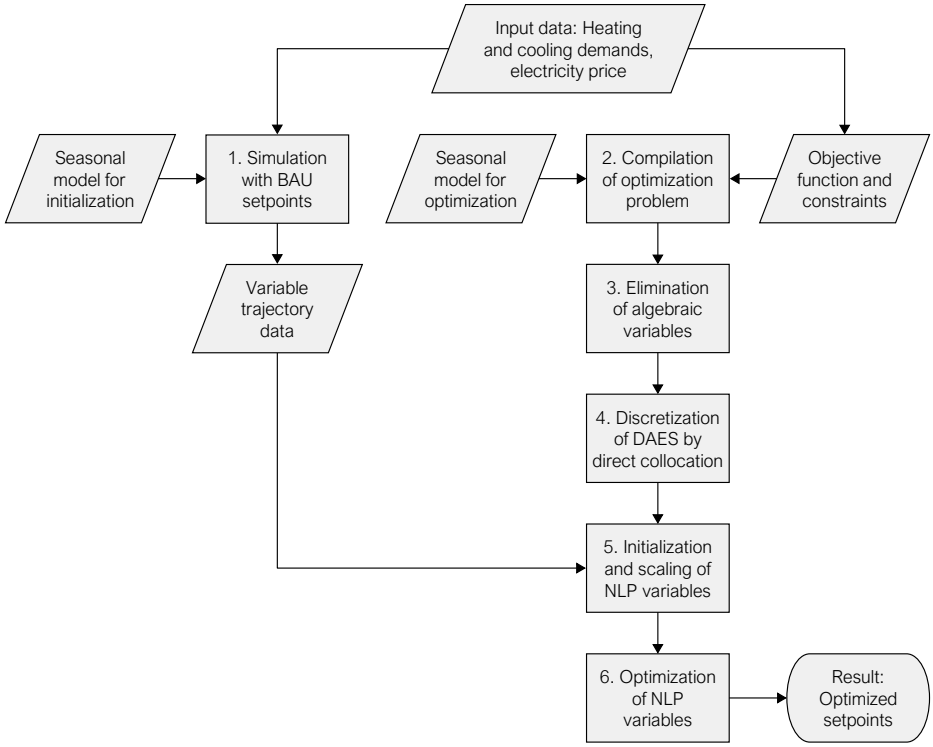

Figure 5.2: Flowchart for main steps of the optimization with JModelica.org.

Step 4: Code for orthogonal collocation on finite elements is included in JModelica.org and was used to transform the infinite-dimensional dynamic optimization problem into a finite-dimensional NLP. The number of collocation elements and the number of collocation points in each element has a strong influence on the size of the resulting NLP. See Paper VI for details.

Step 5: Variable trajectory data obtained during the initial simulation (Step 1) were used for automatic initialization and scaling of the NLP variables.

Step 6: The resulting NLP was solved using version 3.12.4 of the primal-dual interior-point solver IPOPT [33] with linear solver MA57 from HSL [65].

5.2 Adaption of simulation models for optimization

JModelica.org is Modelica-based, which means that simulation models created in Dymola can be used as optimization models in JModelica.org. However, the

different numerical use of the model equations during simulation and optimization often makes it impossible to use simulation models for optimization directly. The adaptions that were required to make the simulation models suitable for dynamic optimization are explained in this section.

5.2.1 Reduction of the final system model

Initial testing showed that the final system model for Vulkan, see Section 4.5.1, could not be used for dynamic optimization due to the large number of components and their interconnections. Therefore, certain parts of the system were removed to reduce the complexity and the size of the resulting NLP. The final system model and the removed parts (covered with gray) are shown in Figure 5.3.

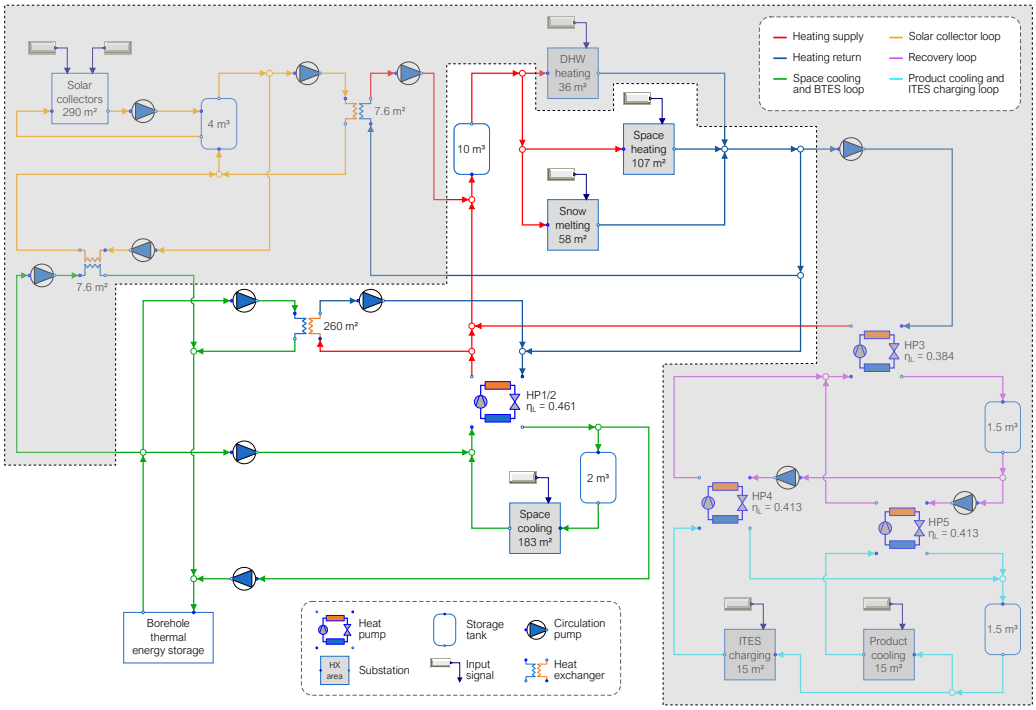

Figure 5.3: Reduction of the final system model (gray part excluded in optimizations).

It can be seen in Figure 5.3 that the solar collector loop, the DHW heating substation, the product cooling and ITES charging loop, and the recovery loop were removed from the final system model. These decisions were based on simulation results, which are presented in Chapter 6. These results showed that the

solar collector loop played a minor role for system performance due to the small total collector area. The DHW heating substation, the product cooling, and the ITES charging loop were removed because the recovered heat from HP 3 was similar to the delivered heat in the DHW heating substation. Removing these parts therefore caused insignificant mismatch in the total heat balance. The simulated electricity use of the removed parts accounted for 18 % of the total electricity use for the BAU case, which showed that the key components of the system were kept. For clarity, a schematic of the reduced system model is shown in Figure 5.4.

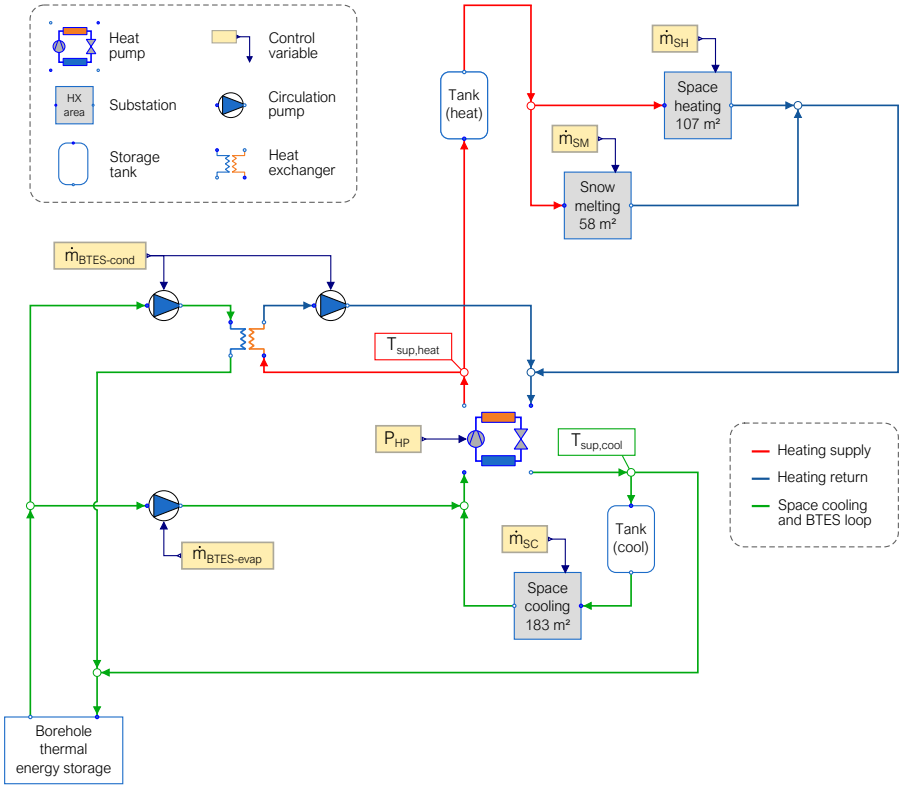

Figure 5.4: Schematic of the reduced system model for optimization.

5.2.2 Modifications of component models

The component models described in Section 4.4 were developed for stable and fast dynamic simulations. However, as mentioned above, some modifications were required to make all the component models suitable for dynamic optimization. These modifications are described below.

The model CustomerSubstationVulkan, see Figure 4.23, received a demanded heat flow rate as input signal, which was sent to the included Controller model. Initial testing showed that this Controller model led to convergence issues. Therefore, the model CustomerSubstationVulkanOpt was developed in which the mass flow rate of the circulation pumps was used as input signal, see the yellow boxes in Figure 5.4. The required heat flow rate in the substation was formulated as a constraint in the optimization problem, see Section 5.3.2. A diagram of the model CustomerSubstationVulkanOpt is shown in Figure 5.5.

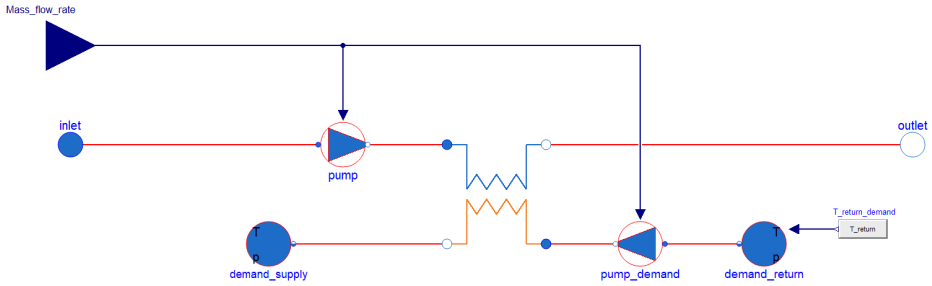

Figure 5.5: Diagram of the model CustomerSubstationVulkanOpt (DS).

The model HeatPumpFinal, see Figure 4.6, contained Boolean signals, which are not suitable for dynamic optimization. In addition, initial testing showed that the calculation of the Lorentz temperature, see Equation (4.5), led to convergence issues. Therefore, the model HeatPumpOpt was developed, which received the heat pump power as input signal and contained an approximation of the Lorentz temperature shown in Equation (5.1). The difference in Lorentz temperature due to this modification was less than 0.1 K for all relevant operating conditions, which was regarded as insignificant.

$$T_{\mathrm{L,cond/evap}} = \frac{T_{\mathrm{in,sec,cond/evap}} + T_{\mathrm{out,sec,cond/evap}}}{2} \tag{5.1}$$

The numerical discretization of the BTES model and the StorageTank model, see Figure 4.12 and Figure 4.19, respectively, had a strong influence on the number of NLP variables. A one-week test optimization was performed to compare the resulting setpoint temperatures with high and low discretization values. The horizontal and vertical discretization of the BTES model was set to 30 and 4 for the high discretization case (as used during simulation) and 10 and 2 for the low

discretization case, respectively. The discretization of the StorageTank models for the heating and cooling tanks was set to 15 and 5 for the high discretization case (as used during simulation) and 5 and 2 for the low discretization case, respectively. The low discretization reduced the number of NLP variables and the solution time of IPOPT by a factor of three and ten, respectively. However, the average absolute difference between the optimized setpoints for the high and low discretization case was less than 0.1 K, which was regarded as insignificant. Therefore, the low discretization values were used for all the optimizations in this work.

5.2.3 Splitting into seasonal models

As mentioned before, the BTES was charged during the summer and discharged during the winter. Thus, the heat exchanger and circulation pumps for BTES charging were not required during the winter and the circulation pump for BTES discharging was not required during the summer. Therefore, the reduced system model for optimization, see Figure 5.4, was split into seasonal models, in which the unused part of the season could be removed. This reduced the optimization problem size significantly. The three seasonal models that were created are listed in Table 5.1 together with the removed parts.

Table 5.1: Seasonal models used for optimization.

Seasonal model	Parts that were removed from the reduced system model
WinterOpt	BTES charging heat exchanger
	BTES charging circulation pumps
SpringFallOpt	Snow melting substation
SummerOpt	Snow melting substation
	BTES discharging circulation pump

An addition, Two versions of each seasonal model were required: one for the initial simulation and one for the optimization, see Figure 5.2. In the initialization models, the component models developed for simulation were used. The component models adapted for optimization were used in the seasonal models for optimization.

5.3 Optimal control problem formulation

To recall, the seasonal models described in the previous section were used to find optimal heating and cooling supply temperature setpoints for simulations with the final system model, see Figure 5.1. The optimization problems for the different seasons were formulated as continuous-time optimal control problems. The control variables, constraints, and objective functions of the optimization problems are explained in the following subsections.

5.3.1 Control variables

The control variables in the optimal-control problems were the heat pump power, P_{HP}, and the mass flow rates for the circulation pumps. These are marked yellow in Figure 5.4 and are written as a vector:

$$\mathbf{u}(t) \coloneqq \left[P_{\mathrm{HP}}(t),\, \dot{m}_i(t)\right]^\top, \qquad i \in \mathcal{P} \tag{5.2}$$

with the definition $\mathcal{P} \coloneqq \{\mathrm{SH},\, \mathrm{SM},\, \mathrm{SC},\, \text{BTES-cond},\, \text{BTES-evap}\}$. The temperatures $T_{\mathrm{sup,heat}}$ and $T_{\mathrm{sup,cool}}$ were not included in the vector $\mathbf{u}(t)$. This was due to the fact that the optimization models did not contain `Controller` models, as explained in Section 5.2.2, so setpoint temperatures were not needed. Instead, the temperatures $T_{\mathrm{sup,heat}}$ and $T_{\mathrm{sup,cool}}$ depended on the control variables and were calculated during the optimizations. The resulting values were then used as input for the new simulations (see Part 3 in Figure 5.1).

5.3.2 Operating constraints

Lower and upper bounds were defined for the control variables based on their operating limits, yielding the following linear inequality constraints:

$$0 \leq P_{\mathrm{HP}}(t) \leq 300\,\mathrm{kW} \tag{5.3}$$

$$0 \leq \dot{m}_i(t) \leq \dot{m}_{i,\max}\,, \qquad i \in \mathcal{P} \tag{5.4}$$

To ensure practically feasible operation, the supply temperatures for heating

and cooling were constrained by:

$$T_{\text{sup,heat}}(t) \leq 65\,^{\circ}\text{C} \tag{5.5}$$

$$T_{\text{sup,cool}}(t) \geq -5\,^{\circ}\text{C} \tag{5.6}$$

Constraints were also added to ensure that the correct amount of energy was delivered by the IHCS to the connected buildings. Enforcing this demand satisfaction as an equality constraint led to convergence issues. Therefore, the following upper and lower bounds were defined for the heat flow rates in the substations, with Qi,dem being the measured values for heating and cooling demands (input data):

$$\dot{Q}_{i,\text{del}}(t) \geq \quad \dot{Q}_{i,\text{dem}}(t), \qquad i \in \mathcal{D} \tag{5.7}$$

$$\dot{Q}_{i,\text{del}}(t) \leq \varepsilon \cdot \dot{Q}_{i,\text{dem}}(t), \qquad i \in \mathcal{D} \tag{5.8}$$

with the definition $\mathcal{D} := \{\text{SH, SM, SC}\}$ and $\varepsilon = 1.005$. This formulation improved the numerical performance significantly. A validation was performed to confirm that the energy demand constraints were not violated during the optimizations. This validation can be found in Paper VI.

5.3.3 Objective function for reduction of electricity use

The simulated electricity use of the IHCS consisted of three parts: the electricity use of the heat pumps, the electricity use of the circulation pumps, and the electricity use of the auxiliary systems. This is explained in more detail in Section 6.2.1. Reducing this total electricity use was defined as the first objective for optimization. Therefore, the following objective function was defined in order to minimize total electricity use

$$\underset{\mathbf{u}(t)}{\text{minimize}} \quad \int_{t_{\text{start}}}^{t_{\text{end}}} \Big(P_{\text{HP}}(t) + P_{\text{pumps}}(t) \Big) dt \tag{5.9}$$

with P_{HP} and P_{pumps} being the heat pump power and total circulation pump power, respectively. The power of auxiliary systems was assumed constant and

thus had no influence on the optimal solution. It was therefore removed from the objective function.

5.3.4 Objective function for reduction of electricity costs

The reduction of electricity costs was defined as the second objective for optimization. Therefore, the following objective function was defined in order to minimize total electricity costs

$$\underset{\mathbf{u}(t)}{\text{minimize}} \quad \int_{t_{\text{start}}}^{t_{\text{end}}} \Big[e(t) \cdot \Big(P_{\text{HP}}(t) + P_{\text{pumps}}(t) \Big) \Big] \, dt \tag{5.10}$$

with $e(t)$ being the time-varying electricity price.

6 Analysis of the case study system Vulkan

The main aim of this case study was to analyze the design and the operation of the IHCS at Vulkan, see Section 3.1. To this end, the simulation models described in Chapter 4 and the optimization approach described in Chapter 5 were used for several analyses. The main results from these analyses are described and discussed in this chapter.

Focus was on the performance of the long- and short-term thermal energy storages. The BTES of the IHCS was used as seasonal thermal energy storage, i.e. heat was injected during the summer and extracted during the winter. The annual heat balance of the BTES (heat injected minus heat extracted) was an important result of the simulations because it affected the average temperature of the surrounding ground. If the ground temperature became too high, the heat injection rate decreased and could lead to operating difficulties during the summer. Similarly, a too low ground temperature could lead to inefficient heat extraction during the winter.

6.1 Heat export to district heating grid

The analysis described in this section was performed when the first system model for Vulkan, see Section 4.5.1, had been developed. The simulation results showed a positive heat balance of the BTES of around 200 MWh for the year 2015. Therefore, the possibility of exporting heat to the local DH grid was analyzed. Two heat export cases were defined and compared to the BAU case, see Table 6.1.

Table 6.1: Defined cases for the analysis of heat export.

Case	Heat export	Number of solar collectors	Solar collector area (m^2)	BTES
BAU	No export	140	290	Unbalanced
Export 1	To DH return line	140	290	Balanced
Export 2	To DH supply and return line	500	1 036	Balanced

For the case Export 1, heat export from the heating tank to the DH return line was simulated. For the case Export 2, heat export from the collector tank to the DH supply line was simulated additionally, see Paper II for details. The amount of exported heat was controlled to yield a balanced BTES at the end of the year for both export cases.

The installed solar collectors at Vulkan are integrated into the facade of one of the buildings. This corresponds to a small fraction of the total roof area. A map showing the solar potential of the roof areas at Vulkan is shown in Figure 6.1, which also shows the location of the installed collectors (blue mark).

Installing more solar collectors was therefore considered as realistic retrofitting option and the number of collectors was increased from 140 to 500 for the case Export 2. In addition, the volume of the collector tank was increased from 2 m^3 to 10 m^3.

To compare the total operating costs of the three cases, relative cost factors were defined for electricity, DH import, DH export to the supply line, and DH export to the return line. Electricity was assumed most expensive and was set to 1. The chosen cost factors for DH import and export are listed in Table 6.2.

All three cases listed in Table 6.1 were simulated with input data for the year 2015. Detailed results can be found in Paper II. The resulting operating costs relative to the BAU case are listed in Table 6.3.

The results showed that the operating costs could be reduced by 5.4 % for the case Export 1 and 8.2 % for the case Export 2. However, these numbers should only be taken as rough indications due to two reasons: 1) the system model used

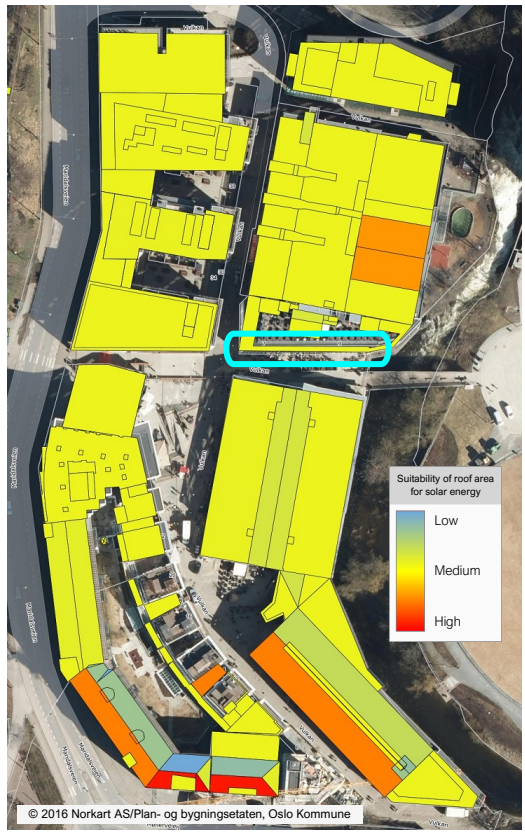

Figure 6.1: Solar potential of the roof area at Vulkan [66].

Table 6.2: Relative cost factors for the different energy types.

Energy type	Cost factor
Electricity	1.00
DH import	0.95
DH export to supply line	0.80
DH export to return line	0.40

for the simulations had several issues, which are explained in Section 4.5.1, and 2) the prices for electricity and DH were assumed constant in this study although they can show large variations over time.

Further development of the component models and the system model led to the final system model for Vulkan, see Section 4.5.1. To increase the reliability of the

Table 6.3: Total operating costs compared to the BAU case.

Case	Relative operating costs (%)
BAU	100.0
Export 1	94.6
Export 2	91.8

results, a calibration of the simulated electricity use was performed. In addition, a sensitivity analysis was performed to study the impact of input parameters on the simulated system performance. The calibration and the sensitivity analysis are described in the next section.

6.2 Calibration and sensitivity analysis

6.2.1 Calibration of the system's electricity use

As explained in Section 3.1.3, only the total electricity use of the system was measured, i.e. the electricity use of components was unknown. The total simulated electricity use of the system ($E_{\text{sim,tot}}$) consisted of three parts: the electricity use of all the heat pumps (E_{HPs}), the electricity use of all the circulation pumps (E_{pumps}), and the electricity use of all auxiliary systems (E_{aux}), see Equation (6.1).

$$E_{\text{sim,tot}} = \underbrace{\int \big(P_{\text{HPs}}(t)\big)dt}_{E_{\text{HPs}}} + \underbrace{\int \big(P_{\text{pumps}}(t)\big)dt}_{E_{\text{pumps}}} + \underbrace{\int \big(P_{\text{aux}}\big)dt}_{E_{\text{aux}}} \tag{6.1}$$

E_{HPs} was calculated by integrating the simulated power of all heat pump models (P_{HPs}) as shown in Equation (6.1). The circulation pump model calculated the required power (P_{pump}) of each circulation pump based on the volume flow rate and the pressure difference, see Equation (4.2). However, the pressure difference was not calculated correctly in the final system model because connecting pipes were neglected and the heat exchangers, solar collectors, and BTES were lumped models. Therefore, P_{pump} was assumed proportional to the squared volume flow rate of the circulation pump in the final system model. This assumption corresponds to a linear relation between pressure drop and volume flow rate in

Equation (4.2). The squared volume flow rate was multiplied with the constant flow-to-power coefficient FtP to calculate P_{pump}, see Equation (6.2).

$$P_{\text{pump}} = 10^{-6} \cdot \text{FtP} \cdot \dot{V}^2 \tag{6.2}$$

The power of the auxiliary systems (P_{aux}) was assumed constant and E_{aux} was calculated by integrating P_{aux}, see Equation (6.1). A system-level approach was chosen to calibrate the values for FtP and P_{aux}. To this end, the monthly difference between the measured electricity use and the simulated electricity use was minimized, see Equation (6.3).

$$\min \sum_{i=1}^{12} \left(E_{\text{tot,meas}} - E_{\text{sim,tot}}\right)^2, \quad i = \text{month of the year} \tag{6.3}$$

The calibration was performed with input data for the year 2015 and yielded values of 70.65 $\text{MW} \cdot \text{s}^2/\text{m}^6$ and 30.5 kW for FtP and P_{aux}, respectively. These values were implemented in the final system model. Monthly values for $E_{\text{meas,tot}}$ and $E_{\text{sim,tot}}$ for the two simulated years are shown in Figure 6.2.

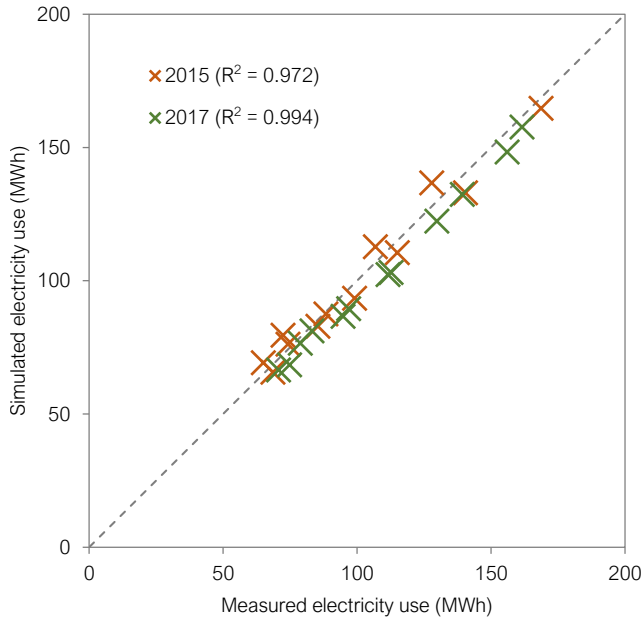

Figure 6.2: Measured and simulated electricity use after the calibration.

It can be seen from Figure 6.2 that the calibration led to good agreement between the measured values and the simulated values.

6.2.2 Sensitivity analysis

A sensitivity analysis was performed to evaluate the influence of selected input parameters on the simulated system performance. Two COPs were defined to measure the system performance: $\mathrm{COP}_{\mathrm{sys}}$ and $\mathrm{COP}_{\mathrm{sys+BTES}}$. These were evaluated at the end of a simulated year. $\mathrm{COP}_{\mathrm{sys}}$ was defined as the ratio of the heating and cooling energy delivered by the IHCS to the electricity use of the IHCS as shown in Equation (6.4). Note that the amount of imported heat from the DH grid was not included in $Q_{\mathrm{heat,tot}}$.

$$\mathrm{COP}_{\mathrm{sys}} = \frac{Q_{\mathrm{heat,tot}} + Q_{\mathrm{cool,tot}}}{E_{\mathrm{sim,tot}}} \tag{6.4}$$

$\mathrm{COP}_{\mathrm{sys+BTES}}$ was similar to $\mathrm{COP}_{\mathrm{sys}}$ but included the annual heat balance of the BTES ($Q_{\mathrm{BTES,ann}}$) in the numerator as shown in Equation (6.5). The heat balance was included because it affected long-term operation as explained above. $\mathrm{COP}_{\mathrm{sys+BTES}}$ thus gave a more holistic indication of system performance by penalizing unsustainable operation.

$$\mathrm{COP}_{\mathrm{sys+BTES}} = \frac{Q_{\mathrm{heat,tot}} + Q_{\mathrm{cool,tot}} + Q_{\mathrm{BTES,ann}}}{E_{\mathrm{sim,tot}}} \tag{6.5}$$

Parameters were changed one at a time during the sensitivity analysis and the difference in COP compared to the BAU case was calculated. A 20 % change was chosen as the default value. However, some parameters were varied by a different percentage as can be seen in Table 6.4 and explained in the notes below:

1. According to [67].
2. ΔT of 3 K chosen instead of default percentage.
3. According to [68].
4. According to manufacturer specifications. All efficiency values were changed at once, see Equation (4.7).
5. See Equation (4.16).

Table 6.4: Parameter values used for the sensitivity analysis (notes on pages 91 & 93).

Parameter	Unit	Lower value	Base value	Upper value	Change %	Note
Numerical discretization						
Factor storage tanks	-	0.8	1.0	1.2	20	
Factor BTES	-	0.8	1.0	1.2	20	
Uncertain inputs						
BTES: Nusselt number	-	3.5	5.0	6.5	30	1
BTES: Initial temp. (near)	°C	22	25	28	12	2
BTES: Initial temp. (far)	°C	7	10	13	30	2
BTES: Ground conductivity	$W/(m \cdot K)$	2.10	2.75	3.40	24	3
Lorentz efficiency HP 1/2	%	41.0	46.1	51.2	11	4
Lorentz efficiency HP 3	%	34.6	38.4	42.2	10	4
Lorentz efficiency HP 4 & 5	%	33.9	41.3	48.7	18	4
Exponent q in HX model	-	0.50	0.63	0.76	20	5
Coefficient FtP	$MW \cdot s^2/m^6$	56.6	70.7	84.8	20	6
Assumed return temperatures						
Space heating	°C	37	40	43	8	7
Snow melting	°C	13	20	27	35	7
Space cooling	°C	13.2	15.0	16.8	12	7
Product cooling	°C	-5.2	-4.0	-2.8	30	7
Heating/cooling demands						
Demand factor all	-	0.8	1.0	1.2	20	8
Demand factor heating	-	0.8	1.0	1.2	20	9
Demand factor cooling	-	0.8	1.0	1.2	20	10
Control setpoints						
Mode switch ΔT	K	3.2	4.0	4.8	20	11
Heating supply	°C	52	55	58	5	12
Space cooling supply	°C	4.2	6.0	7.8	30	12
System design						
Factor HX area	-	0.8	1.0	1.2	20	13
Number of solar collectors	-	110	140	170	21	14
Number of boreholes	-	50	62	74	19	15

6. See Equation (6.2).
7. Secondary side changed to give 20 % change in ΔT.
8. All demand values changed.
9. Only heating demand values changed.
10. Only cooling demand values changed.
11. Used to switch between heating and cooling mode, see Section 4.5.1.
12. Primary side changed to give 20 % change in ΔT.
13. All area values listed in Table 4.1 were changed at once.
14. The storage tank volume and the heat exchanger areas in the solar collector loop were scaled accordingly.
15. The maximum mass flow rates of the BTES circulation pumps were scaled accordingly.

The sensitivity analysis was performed with input data for the year 2015. The results are shown in Figure 6.3.

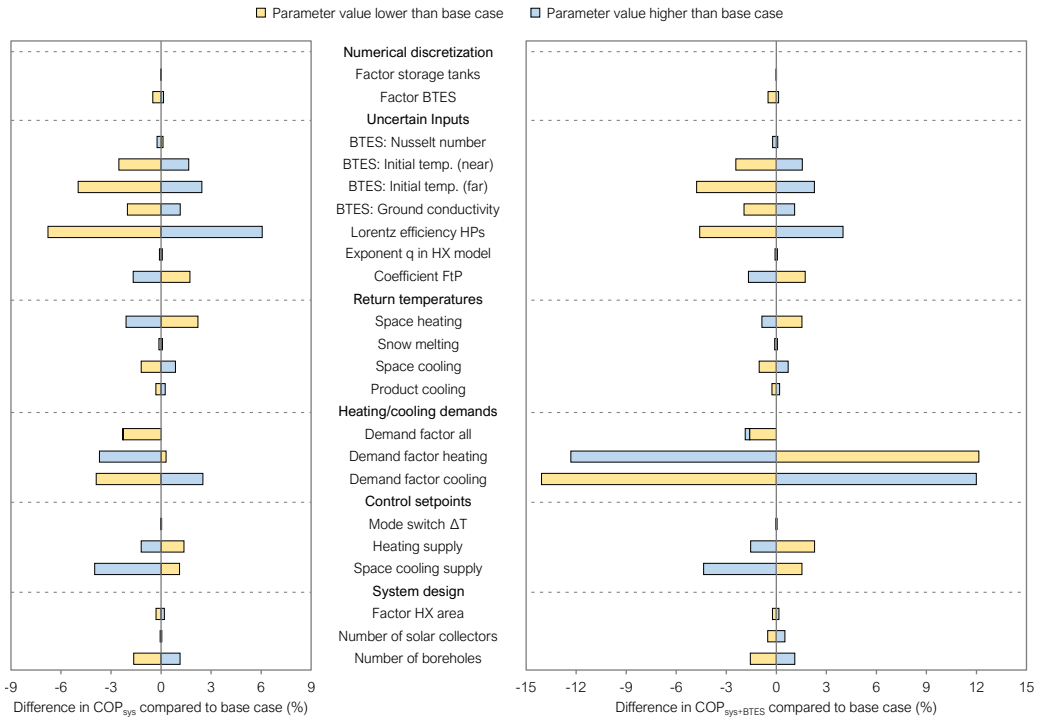

Figure 6.3: Results from the sensitivity analysis.

Increasing the numerical discretization had a negligible effect on the COPs. A reduction in discretization of the BTES led to a decrease of 0.5 %, showing that the chosen values were reasonable.

Some of the uncertain inputs influenced the COPs significantly. The heat pumps were the main electricity users, which is why their efficiency had a strong influence, especially on $\mathrm{COP}_{\mathrm{sys}}$, see Figure 6.3 (left). The initial temperature profile and the conductivity of the ground also showed strong influence on the COPs, while the Nusselt number for natural convection inside the borehole and the heat exchanger exponent q used in Equation (4.16) were less important.

The return temperatures from the buildings' heating and cooling systems (T_{ret}) were assumed constant in this study. The influence of these temperatures on system performance varied. It depended on the total amount of delivered energy for each demand type. Space heating was the largest demand, which is why $T_{\mathrm{ret,SH}}$ had the strongest influence on the COPs.

The heating and cooling demands were based on the available measurements. The cooling demands were heat sources for the IHCS and the heating demands were heat sinks. Therefore, the difference between the total heating demand and the total cooling demand highly influenced the annual heat balance of the BTES. Changing all demands simultaneously thus altered the BTES balance less than changing only heating or cooling demands. This is why changing all demands showed less effect than changing only heating or cooling demands, especially for $\mathrm{COP}_{\mathrm{sys+BTES}}$.

The control setpoint for a mode switch had insignificant influence on the system performance due to the small number of mode switches during a year. The supply temperature setpoints $T_{\mathrm{sup,heat}}$ and $T_{\mathrm{sup,cool}}$ changed the heat pump outlet temperatures and thus affected both the temperature lift of the heat pumps and the mass flow rates of the circulation pumps. Especially an increase of $T_{\mathrm{sup,cool}}$ showed strong influence on the COPs.

The system design parameters showed little effect on the COPs. Only a change in the number of boreholes changed the COPs by more than 1 %. This change in COP was mainly due to the difference in required circulation pump power. The BTES outlet temperature changed slightly when the number of boreholes was

changed, leading to a small change in the heat pump's COP. However, the annual heat balance of the BTES did not change significantly because almost the same amounts of energy had to be injected/extracted each day.

6.3 Ensuring sustainable long-term operation

The analysis described in this section was performed after the calibration of the final system model for Vulkan, which is explained in the previous section. The aim of this analysis was to ensure sustainable long-term operation, i.e. to avoid deterioration of system performance over time. As explained in Section 3.1.3, measurement data from the years 2015 and 2017 were used as input for the analysis. The simulation results with the final system model showed a negative heat balance of the BTES of -469 MWh and -263 MWh for the years 2015 and 2017, respectively as shown in the figures 6.4 and 6.5.

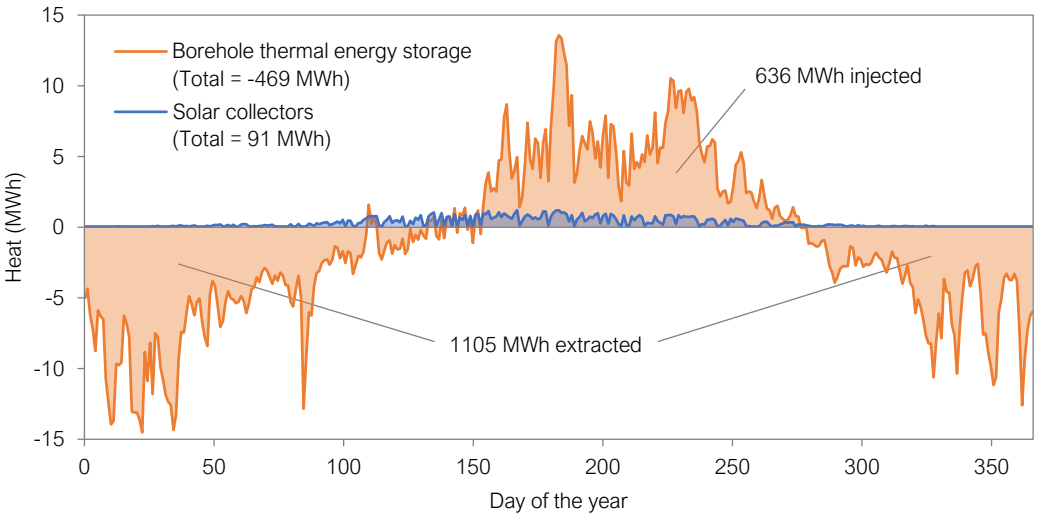

Figure 6.4: Simulated daily heat balance for BTES and solar collectors for 2015.

This is a large difference in the simulated heat balance compared to the results presented in Section 6.1. This difference is due to the issues of the first system model, which are described in Section 4.5.1, especially the neglection of the snow melting demand.

As mentioned in Section 6.1, an unbalanced BTES can lead to decreased long-

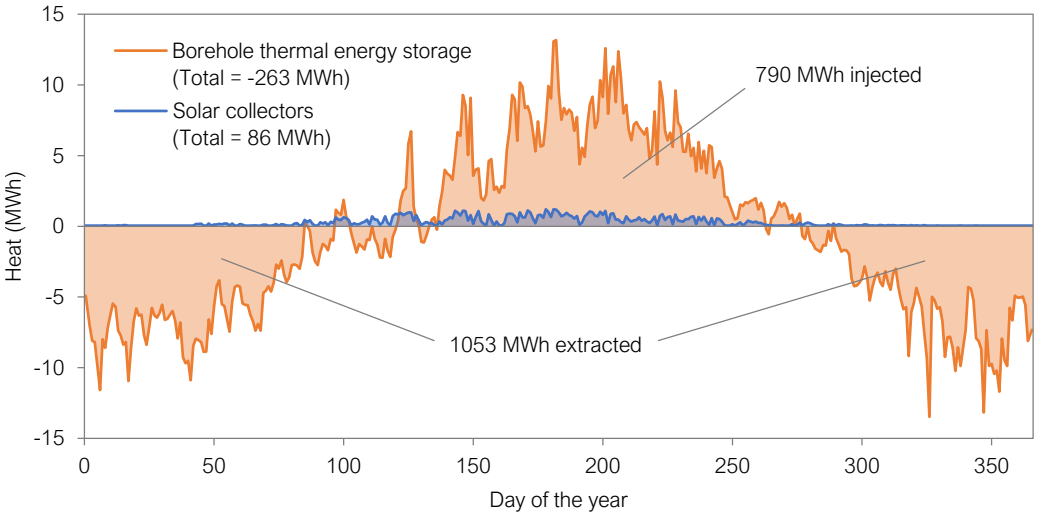

Figure 6.5: Simulated daily heat balance for BTES and solar collectors for 2017.

term performance. The figures 6.4 and 6.5 showed that the charging of the BTES during the summer was insufficient and that the solar collectors only accounted for a small fraction of the charging capacity. Therefore, two solutions to avoid a negative heat balance were analyzed: the installation of more solar collectors and the increase of DH import for DHW heating. These cases are listed in Table 6.5 and described below.

Table 6.5: Defined cases for the analysis of long-term operation.

Case	Number of collectors	Collector area (m^2)	DH import for DHW heating
BAU	140	290	Based on DHW demand
More solar collectors	830	1 719	Based on DHW demand
More DH import	140	290	Reduced by 55 % during cooling mode, zero during heating mode

More solar collectors For this case, the number of solar collectors was increased from 140 to 830 because this increase led to a balanced BTES for the year 2015 as explained in Paper V. There is a lot of roof area at Vulkan suitable for the installation of solar collectors, see Figure 6.1. However, installation possibilities and costs were not analyzed further.

More DH import For this case, the mass flow rate from the IHCS to the DHW heating substation was reduced. This mass flow rate reduction led to an increased amount of DH import for DHW heating. The mass flow rate was reduced by 55 % during cooling mode and by 100 % during heating mode compared to the BAU case. Heat for DHW heating was thus only delivered by the IHCS during cooling mode, when excess heat was available.

To analyze long-term operation, the input data for the years 2015 and 2017 were repeated three times so that a six-year simulation could be performed. The change in total electricity use compared to the first year is shown in Figure 6.6.

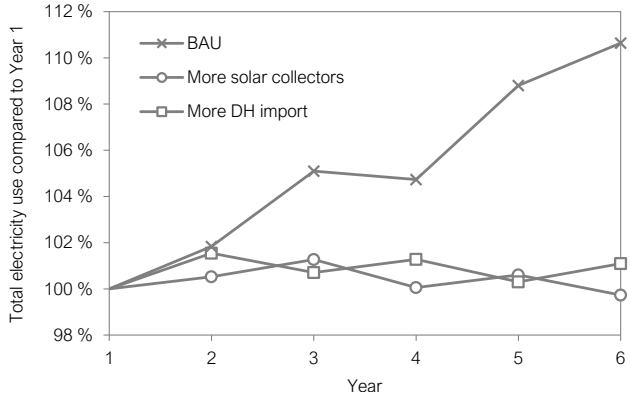

Figure 6.6: Change in total electricity use of the IHCS (input data for 2015 and 2017 repeated).

It can be seen from Figure 6.6, that the total electricity use increased by 10 % during the six simulated years for the BAU case. For the cases "More solar collectors" and "More DH import", the simulated electricity use stayed almost constant. The increase for the BAU case was due to a ground temperature decrease, which led to higher electricity use of the circulation pumps, especially the BTES circulation pump during heating mode as shown in Paper V. The electricity use of all the circulation pumps is shown in Figure 6.7 for the six simulated years.

The electricity use of HP 1/2, see Figure 4.28, also increased over the years for the BAU case due to the lower evaporator inlet temperature. This lower inlet temperature led to a decrease of the calculated COP during heating mode from an average of 3.5 in Year 1 to an average of 3.4 in Year 6.

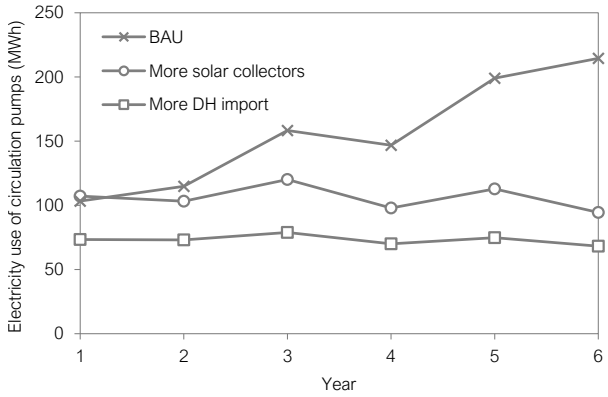

Figure 6.7: Electricity use of circulation pumps (input data for 2015 and 2017 repeated).

The results presented in this section depended highly on the BTES model. The short-term response of the BTES model was validated against experimental data and the heat transfer in the ground was calculated based on established heat transfer theory. However, the idealization of the ground in the BTES model could lead to wrong results, e.g. in the case of groundwater flow. Unfortunately, the simulation results could not be validated because the mass flow rate in the BTES was not measured.

The long-term analysis clearly showed that the simulated system performance decreased for the BAU case. Sustainable operation was achieved with the cases "More solar collectors" and "More DH import". However, the installation of solar collectors would cause installation costs and the import of heat would increase the operating costs. An economic evaluation should therefore be performed, which was outside the scope of this work. Instead, the reduction of electricity use by improving the control setpoints was analyzed. This is explained in the next section.

6.4 Reduction of electricity use

The sensitivity study in Section 6.2.2 showed that the setpoints for $T_{\text{sup,heat}}$ and $T_{\text{sup,cool}}$ influenced the simulated system performance. Therefore, the aim of this analysis was to analyze the control of the IHCS in detail with the objective to reduce the system's electricity use. To this end, the seasonal models for optimization, see Section 5.2.3, were used for dynamic optimizations with JModelica.org as explained in Chapter 5.

To recall, the final system model for Vulkan was not suitable for dynamic optimization. It was therefore reduced and split into seasonal models. The year 2015 was divided into seasonal periods and each period was optimized separately with the corresponding model. The length of each season and the resulting NLP problem size of the respective optimization are listed in Table 6.6.

Table 6.6: Optimization periods and problem sizes.

Days	Seasonal model	Number of finite elements	Number of NLP variables	Number of NLP constraints
1 – 95	`WinterOpt`	4562	$7.2 \cdot 10^5$	$7.8 \cdot 10^5$
96 – 155	`SpringFallOpt`	2883	$4.2 \cdot 10^5$	$4.6 \cdot 10^5$
156 – 260	`SummerOpt`	5043	$6.7 \cdot 10^5$	$7.3 \cdot 10^5$
261 – 290	`SpringFallOpt`	1443	$2.0 \cdot 10^5$	$2.2 \cdot 10^5$
291 – 365	`WinterOpt`	3602	$5.7 \cdot 10^5$	$6.2 \cdot 10^5$

The initial state of the BTES and storage tank models for each season were chosen based on the result of the previous season.

The optimized values for the control variables leading to minimized electricity use are presented in this section. The optimal heat pump power P_{HP} is shown in Figure 6.8, the optimal mass flow rates for the substation circulation pumps are shown in Figure 6.9, and the optimal mass flow rates for the BTES circulation pumps are shown in Figure 6.10.

The optimized values for $T_{\mathrm{sup,heat}}$ and $T_{\mathrm{sup,cool}}$ are shown in Figure 6.11 and Figure 6.12, respectively together with the simulated BAU setpoints. The optimized setpoints were implemented into the final system model for simulation, see Part 3 in Figure 5.1). The resulting energy amounts for the simulated year are shown in Figure 6.13.

It can be seen from Figure 6.13 that the electricity use for the heat pumps and the circulation pumps decreased by 5 % and 14 %, respectively, with the optimized setpoints compared to the BAU case. The amount of heat taken from the long-term storage decreased by 7 %. These reductions would decrease the operating

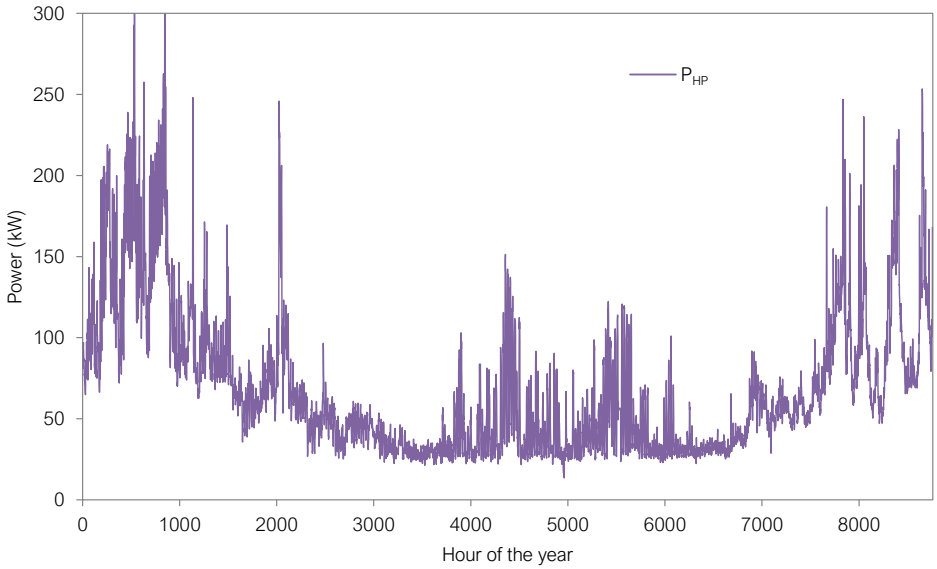

Figure 6.8: Optimized heat pump power.

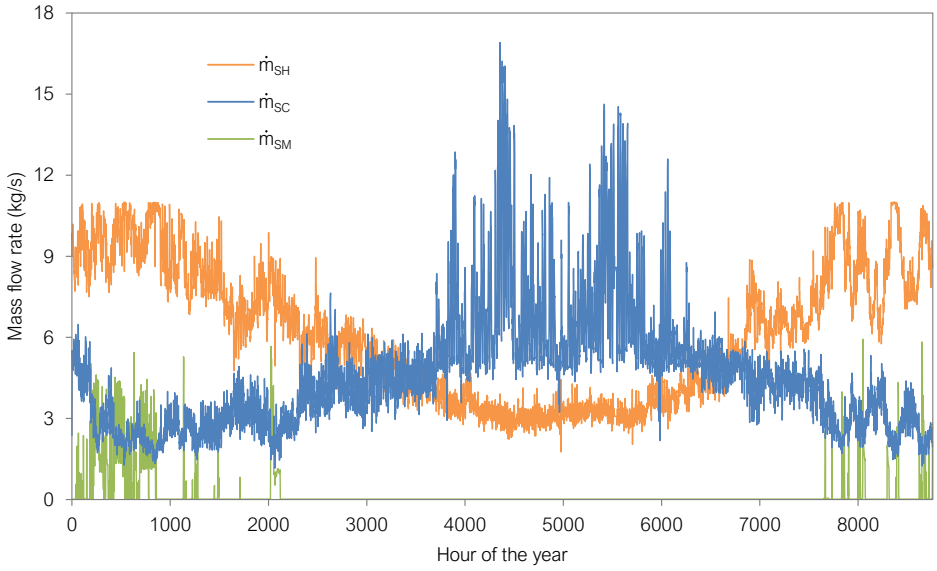

Figure 6.9: Optimized mass flow rates for the substation circulation pumps.

costs significantly. However, the amount of heat imported from DH increased by 12 % for the simulated year. Therefore, the net savings depend on the prices for electricity and DH import. An optimization of the electricity costs is described in the next section.

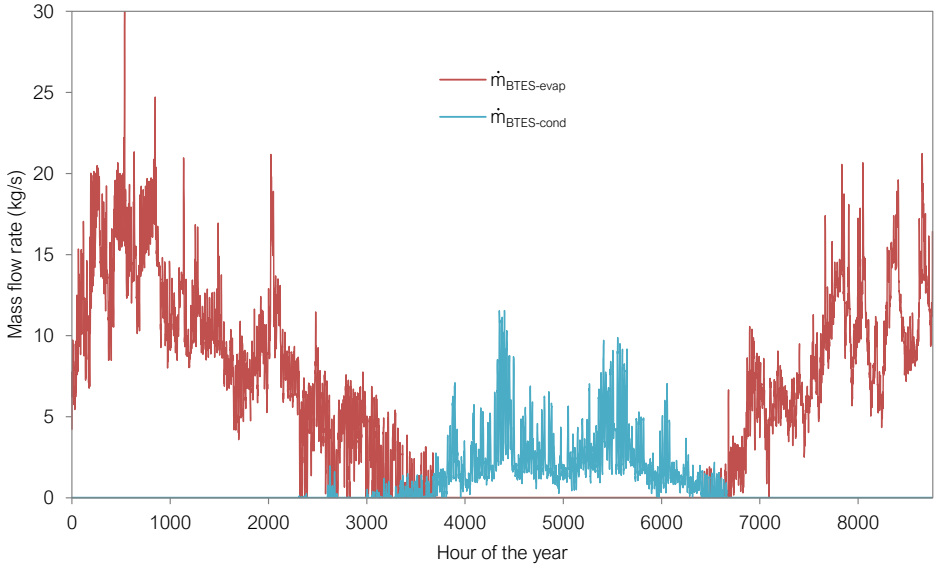

Figure 6.10: Optimized mass flow rates for the BTES circulation pumps.

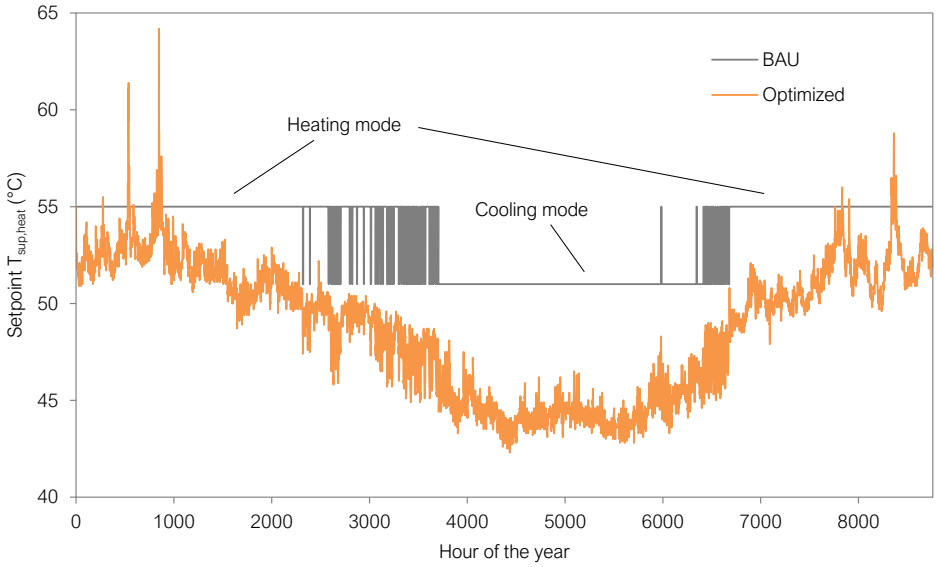

Figure 6.11: Heating supply temperature setpoint.

6.5 Reduction of electricity costs

The storage tanks of the IHCS were relatively small and only used as buffer to even out the supply temperatures of the heating and cooling loop. Storage tanks

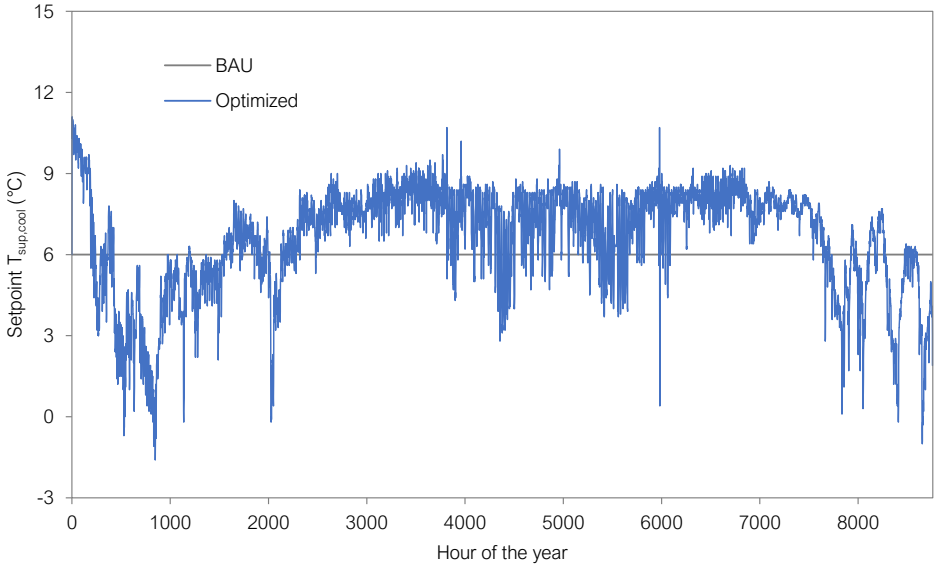

Figure 6.12: Space cooling supply temperature setpoint.

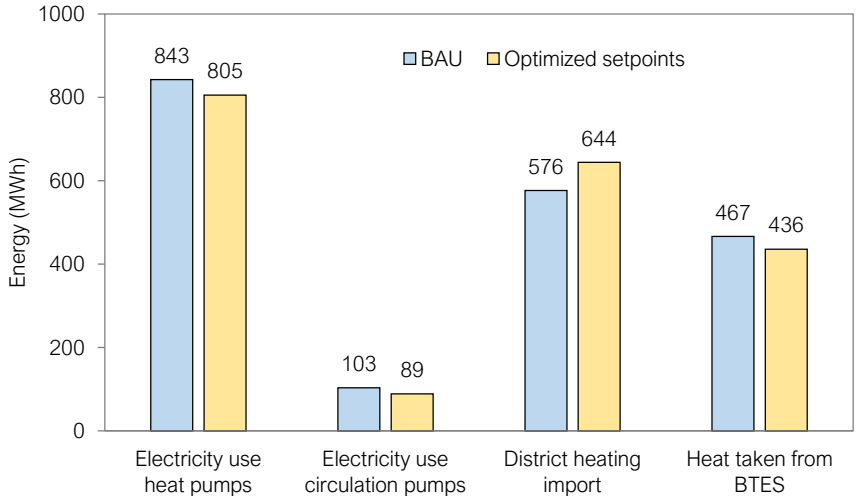

Figure 6.13: Total simulated energy amounts for 2015.

are a relatively cheap component, so the installation of larger tanks was considered as realistic retrofitting option. To investigate the effect of larger storage tanks and optimal control on the cost saving potential, three different tank size combinations were chosen: the installed 10 m^3 and 2 m^3 for the heating and cooling tank, respectively, as well as 100 m^3 and 500 m^3 for both tanks.

In Norway, electricity prices are typically higher during the winter than during the summer due to the market-based electricity price and the high amount of electricity used for space heating. Therefore, the first three months of the year 2015 were chosen for this analysis to limit the number of required optimizations. This way, all the optimizations could be performed with the seasonal model `WinterOpt`, see Section 5.2.3. The electricity spot prices for the location of the IHCS for the first three months of the years 2015 to 2019 are shown in Figure 6.14.

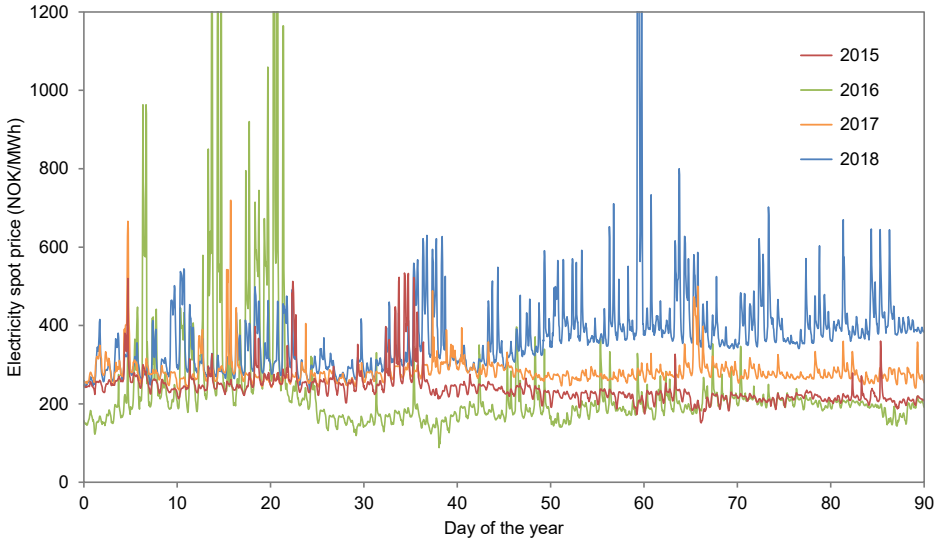

Figure 6.14: Hourly electricity spot prices for Oslo, Norway [69]. Peak values omitted for better readability (max value = 2454).

It can be seen from Figure 6.14 that the electricity price showed relatively little variation in 2015. Therefore, additional price signals were defined with different fluctuations to analyze the influence of the variability of the electricity price (v) on the cost saving potential. The price signals were based on the average price of the first three months of 2015 (239 NOK/MWh) and the original price signal ($e_{Oslo,2015}$). Values of 0, 1, 2, and 3 were chosen for v and the price signals were calculated as follows:

$$e_v(t) = 239 + v \cdot \left(e_{Oslo,2015}(t) - 239\right) \tag{6.6}$$

The four resulting price signals were used for the optimizations and are shown in Figure 6.15.

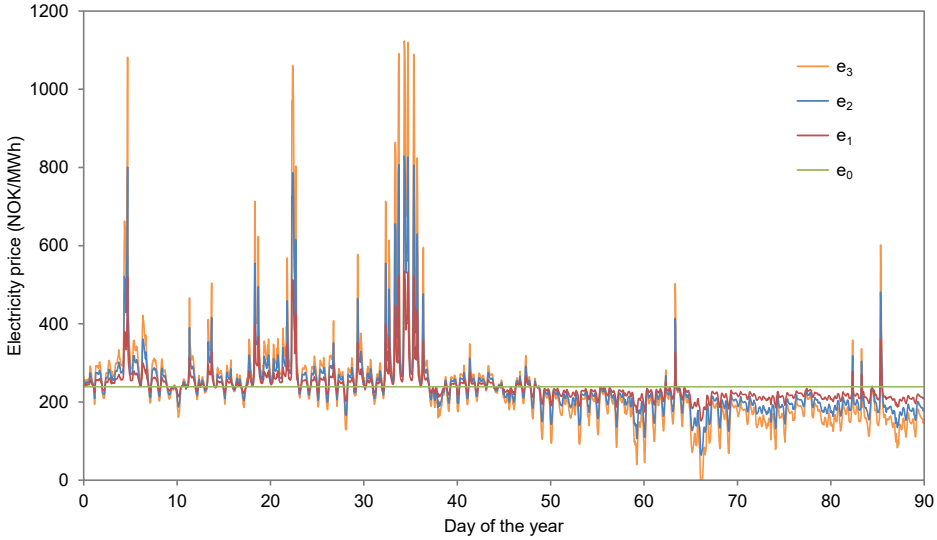

Figure 6.15: Electricity prices used for optimization ($e_1 = e_{Oslo,2015}$).

This approach, similar to the one presented in [70], was chosen instead of using electricity prices from other years to maintain the correlation between the electricity price and the climate conditions. Note that this correlation is not kept for $v = 0$, which corresponds to a constant and thus unrealistic electricity price.

The four different price signals and the three different tank size combinations led to the twelve optimization cases listed in Table 6.7.

Table 6.7: Defined cases for the analysis of electricity cost reduction.

Heating tank volume (m^3)	Cooling tank volume (m^3)	Electricity price signal			
		e_0	e_1	e_2	e_3
10	2	10-2_e_0	10-2_e_1	10-2_e_2	10-2_e_3
100	100	100-100_e_0	100-100_e_1	100-100_e_2	100-100_e_3
500	500	500-500_e_0	500-500_e_1	500-500_e_2	500-500_e_3

All the cases listed in Table 6.7 were optimized separately with the seasonal model `WinterOpt`, see Section 5.2.3. Optimal operation over this period would lead to emptied short-term storages at the end of the period, i.e. the average temperature (T_{avg}) in the hot storage tank would be as low as possible and the average temperature in the cold storage tank would be as high as possible. This

would lead to an unfair comparison, especially when different tank sizes were compared. Therefore, the constraints in Equation (6.7) and Equation (6.8) were added for these twelve optimizations to avoid this effect and thus ensure a fair comparison.

$$T_{\text{tank,heat,avg}}(t_{\text{end}}) \geq T_{\text{tank,heat,avg}}(t_{\text{start}}) \tag{6.7}$$

$$T_{\text{tank,cool,avg}}(t_{\text{end}}) \leq T_{\text{tank,cool,avg}}(t_{\text{start}}) \tag{6.8}$$

Selected result values from the optimizations leading to minimized electricity costs are shown in this section. February 14$^{\text{th}}$ and February 3$^{\text{rd}}$ were days with very different variations in electricity spot price. The price signals for these two days are shown in Figure 6.16 and Figure 6.17, respectively.

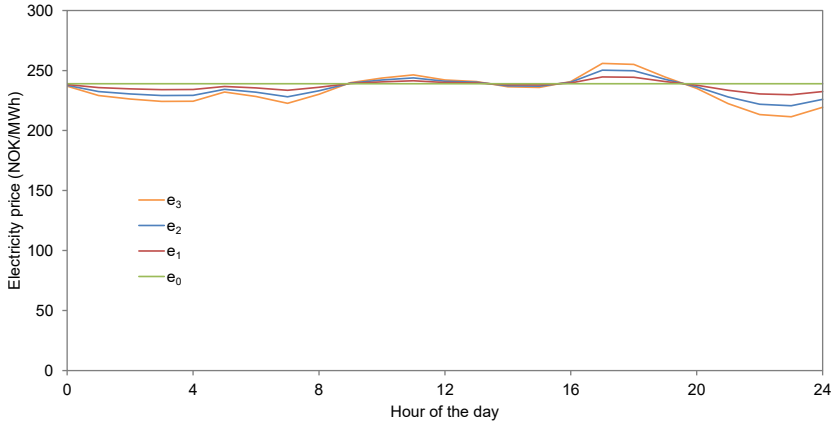

Figure 6.16: Electricity prices for February 14$^{\text{th}}$ ($e_1 = e_{\text{Oslo,2015}}$).

It can be seen from Figure 6.16 that the electricity price was almost constant on February 14$^{\text{th}}$. On the contrary, the electricity price varied significantly on February 3$^{\text{rd}}$ as shown in Figure 6.17 with peak hours in the morning and the afternoon. Detailed results for the optimal heat pump power and temperature setpoints are presented for these two days for selected cases from Table 6.7. The results for February 14$^{\text{th}}$ for the cases with the original electricity price and different tank size combinations are shown in Figure 6.18.

It can be seen from Figure 6.18 that the different tank size combinations

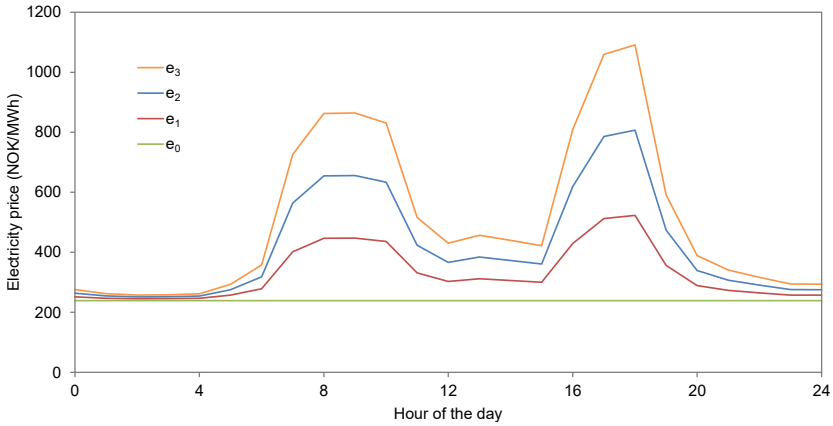

Figure 6.17: Electricity prices for February 3rd ($e_1 = e_{Oslo,2015}$).

yielded very similar results for February 14th. This was expected due to the relatively constant electricity price during that day. The results for February 3rd for the same cases are shown in Figure 6.19.

It can be seen from Figure 6.19 that the optimal control trajectories for February 3rd depended highly on the size of the storage tanks. Larger tanks led to larger variations, due to the possibility to shift electricity use from high-price hours to low-price hours and thus decrease the total electricity costs.

Figure 6.19 clearly shows that the installed tanks (case 10-2_e_1) were too small to take advantage of the electricity price variations. The heat pump power only varied between 150 kW and 270 kW for this case and the temperatures setpoints were relatively constant as well, expect for two short peaks of $T_{sup,heat}$. For the case 100-100_e_1, the heat pump power varied across nearly the entire allowed range from 0 to 300 kW. It was higher during low-price hours to charge the storage tanks, corresponding to high values for $T_{sup,heat}$ and low values for $T_{sup,cool}$. On the contrary, the heat pump power was low during high-price hours and the energy demands of the buildings were to a large extent covered by discharging the tanks. For the case 500-500_e_1, this effect was even more pronounced, leading to the largest variations in the optimal values for $T_{sup,heat}$ and $T_{sup,cool}$.

The results for February 3rd for the cases with the largest tanks and different variability of the electricity price are shown in Figure 6.20.

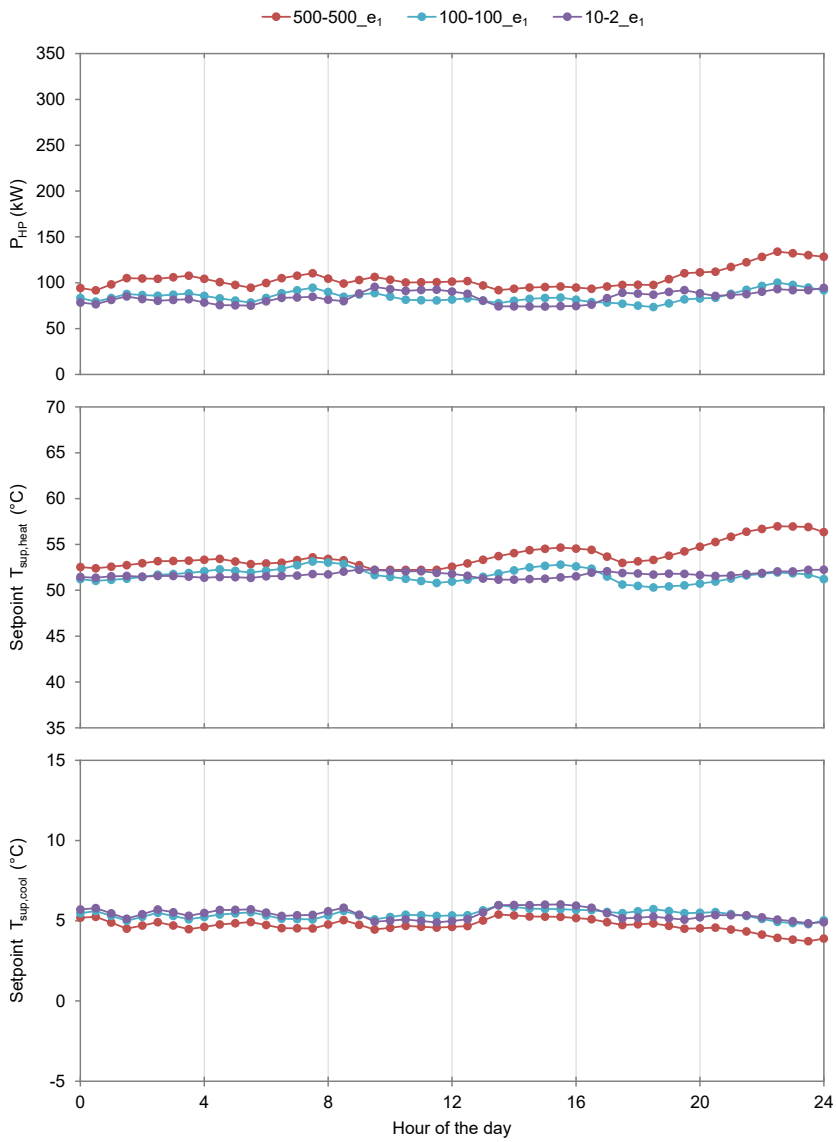

Figure 6.18: Optimization results for February 14$^{\text{th}}$ with different tank size combinations.

It can be seen from Figure 6.20 that there were large differences between the results with a constant electricity price (case 500-500_e_0) and the cases with price variations. Although the costs were optimized for all the cases, the constant price led to a minimization of the total electricity use for the case 500-500_e_0 (i.e. the objective functions Equation (5.9) and Equation (5.10) yielded equal

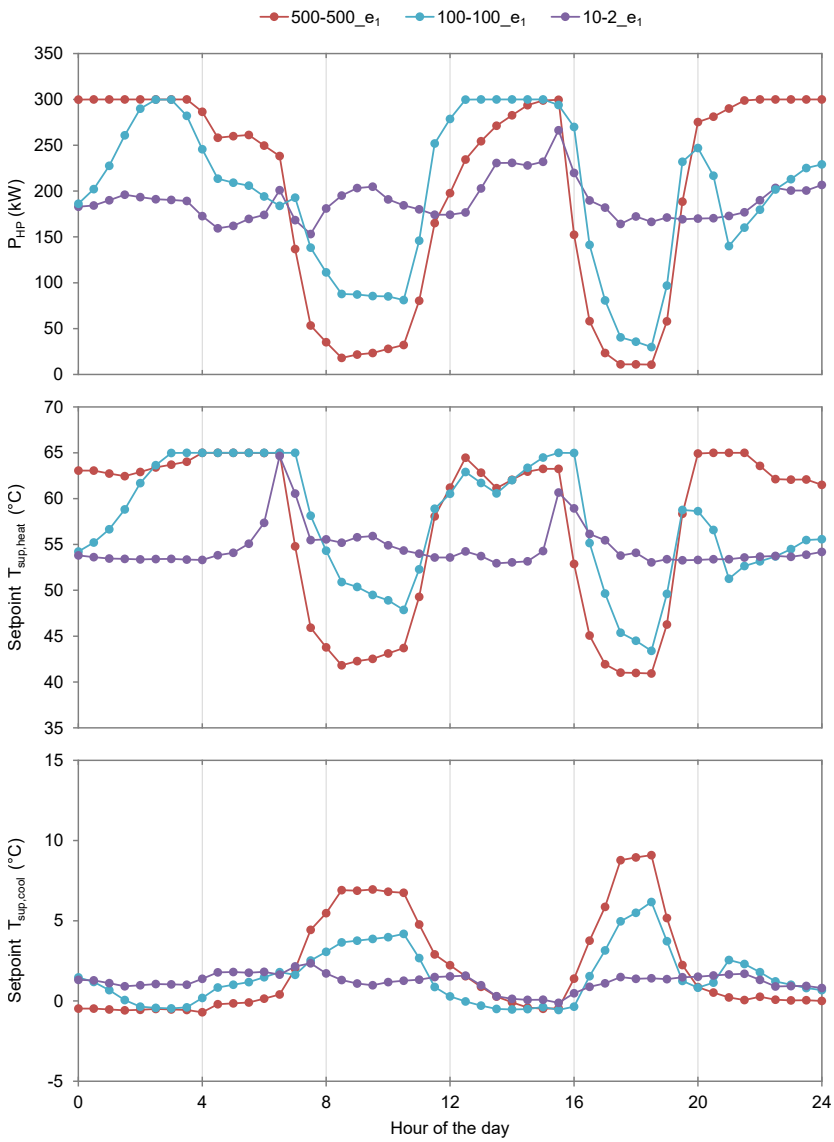

Figure 6.19: Optimization results for February 3rd with different tank size combinations.

results). The control of the heat pump and the circulation pumps were therefore optimized depending on the energy demands of the buildings. For the other three cases, the electricity use was significantly higher during low-price hours. The cases with different variability showed very similar results for February 3rd. The optimal control trajectories became slightly more pronounced for larger values

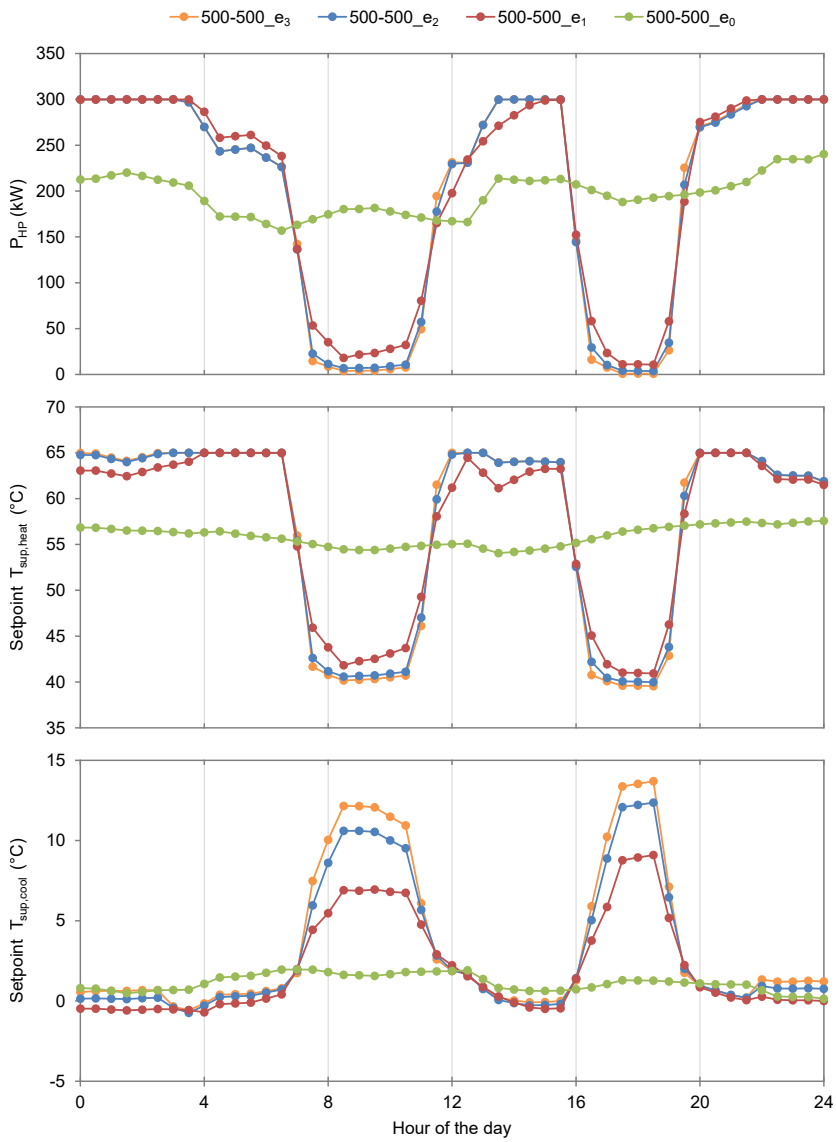

Figure 6.20: Optimization results for February 3rd with different electricity price variability ($e_1 = e_{Oslo,2015}$).

of variability, but only $T_{\text{sup,cool}}$ showed significant differences. This showed that even larger tanks would be required to take advantage of the variations during that day. However, other days showed larger differences between these cases.

The optimized setpoints were implemented into the final system model and a simulation for the first three months of 2015 was performed for all the cases

listed in Table 6.7. The simulated total electricity costs for this period are shown in Figure 6.21. The simulated costs with BAU control were included to show the potential savings. All the results are shown relative to the BAU case because the different price signals led to different costs for the BAU case.

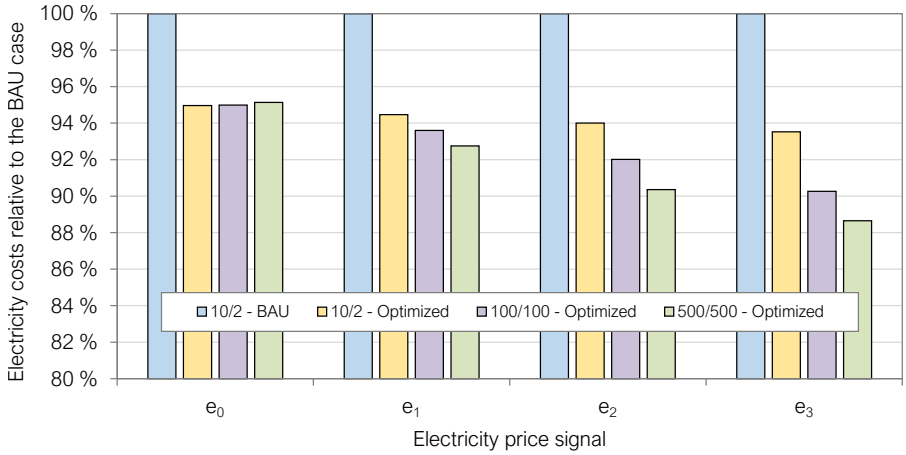

Figure 6.21: Simulated electricity costs for the first three months of 2015 relative to the BAU case ($e_1 = e_{Oslo,2015}$).

It can be seen from Figure 6.21 that all the optimized cases led to lower electricity costs compared to the BAU case. The relative savings were in the range of 5 to 11 %. The relative savings increased with larger variability of the electricity price signal. Larger tanks also led to increased relative savings, except for the cases with constant electricity price (e_0). However, the difference between the BAU case (10/2 - BAU) and the case with the currently installed tanks and optimized setpoints (10/2 - Optimized) was larger than the difference between the cases with different tank sizes and optimized setpoints (10/2 – Optimized vs. 500/500 - Optimized). This means that the optimized control led to higher relative savings than the installation of larger tanks. However, these savings only included the electricity costs and not the costs for DH import. Since the DH import increased for the cases with the optimized setpoints compared to the BAU case, an economic analysis including the calculation of the total operating costs is required to decide if larger storage tanks should be installed. The costs for the advanced control system should be taken into account in such an analysis because the installation of larger tanks would not lead to savings with the BAU control strategy.

It is also worth noting that the electricity costs shown in Figure 6.21 were calculated by multiplying the electricity use of the system by the electricity spot price. However, this is only a part of the actual costs that large customers have to pay in Norway. The electricity grid in Norway is stressed significantly more during the winter than during the rest of the year due to the high use of electricity for space heating. Therefore, the electricity grid prices include additional costs to consider the electricity grid stress. For business customers, this may induce peak-load tariffs and charging for their peak electricity use of each calendar month. This was not taken into account in this study as the measurement data showed that the peak use of the IHCS was almost the same for all the winter months. This cost was therefore assumed fixed and not included in the optimizations. The 25 % taxes that have to be paid were also neglected because they did not affect the relative savings.

7 | Analysis of the case study system Brøset

In this chapter, the results of the case study Brøset are presented. The details about the case study are given in Chapter 3. Different local DH grids were investigated for the given area by means of dynamic simulation. Focus was on LTDH with the motivation to reduce the GHG emissions of the grid by reducing the grid's heat losses and utilizing waste heat sources. In Section 7.1, which is based on Paper III, the effect of different temperature levels on the pumping power and heat losses was analyzed. In Section 7.2, which is based on Paper IV, the inclusion of prosumers in the local LTDH grid was analyzed. As mentioned before, the author of this thesis contributed mostly to the modeling and simulation part of this case study.

7.1 Comparison of different local district heating grids

For this analysis, the first system model for Brøset was used, see Figure 4.32. This system model was built with components from the commercial Modelica library TIL as explained in Section 4.5.2. One-year simulations were performed and the data described in Section 3.2.3 were used as input for this analysis. The main aim of this analysis was to calculate the pumping power and heat losses for different DH system design concepts. The cases listed in Table 7.1 were defined and simulated.

Three different supply temperature levels were considered: 95 °C, 65 °C and 55 °C. 95 °C was chosen because it is the expected temperature at substations of

Table 7.1: Defined cases for the analysis of different local DH grids.

Case	Supply temperature °C	Return temperature °C	Comments
95	95-70	47.5-35.0	Current practice
65	65	32.5	Based on Norwegian legislation
55	55	27.5	Future scenario
55P	55	27.5	Case 55 with 50 % larger pipe diameters
LR	95-70	40.5-28.0	Case 95 with lower return temperature
PS	95-70	47.5-35.0	Case 95 with peak demands reduced by 20 %

the DH grid in Trondheim, 65 °C was considered as a potential future temperature level considering the Norwegian legislation, and 55 °C was included as ultimate goal for LTDH systems. For the 95 °C cases, the supply temperature was outdoor temperature compensated. A constant supply temperature was assumed for the low-temperature cases. Three additional cases were included: a low-temperature case with larger pipe diameters (55P), a high-temperature case with lower return temperature (LR), and a high-temperature case with peak shaving (PS). See Paper III for details.

The pipe diameter was an important input parameter of the pipe model because it affected both the pumping power and the heat losses. The diameter was chosen so that the maximum pressure drop in the grid did not exceed 150 Pa/m for the case 95. To this end, a one-year simulation of the case 95 with uniform pipe diameters was performed to find the maximum mass flow rates for each pipe. These maximum values were then used to set the diameter for each pipe based on the calculated pressure drop as explained in Paper III. All pipe diameters were increased by 50 % for the case 55P.

The main results from the simulations are shown in Figure 7.1 and Figure 7.2 (note that these figures are taken from Paper III and therefore do not follow the notation used in this thesis).

Compared to the case 95, the simulated heat losses were 16 and 31 % lower for

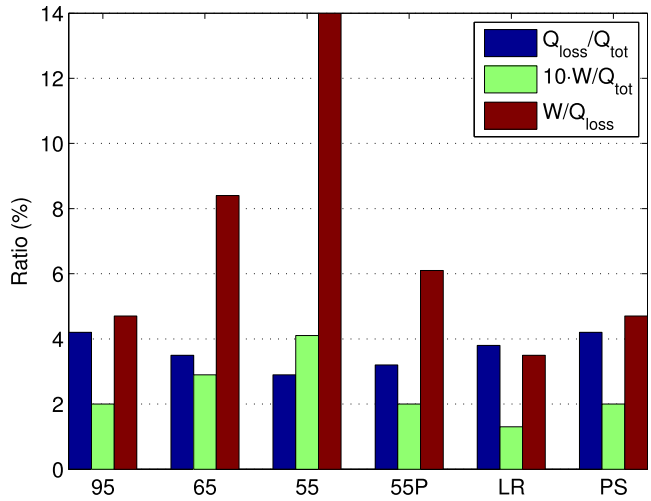

Figure 7.1: Ratios of total heat losses (Q_{loss}), pump energy (W), and delivered heat (Q_{tot}) for all the cases (taken from Paper III).

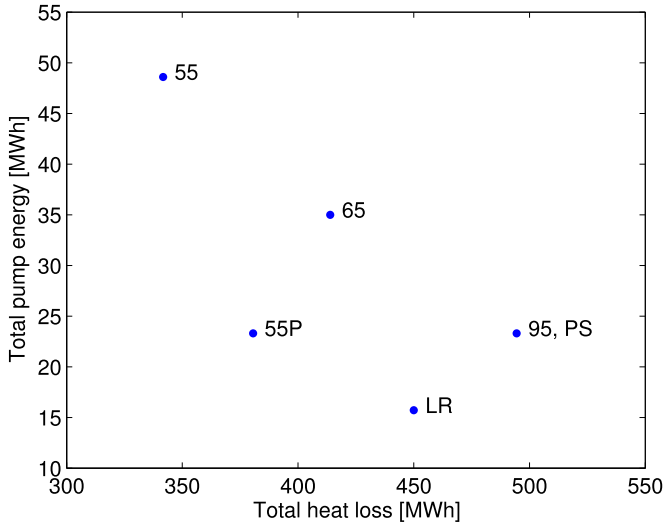

Figure 7.2: Total pump energy and heat losses for all the cases (taken from Paper III).

the cases 65 and 55, respectively as shown in the figures 7.1 and 7.2. The required pump energy increased significantly for the low-temperature cases compared to the case 95, but the total pump energy was an order of magnitude lower than the total heat losses. Therefore, a lower supply temperature had a positive overall environmental impact. The simulation results from the case 55P showed that the heat losses could be reduced without increasing pump energy by using pipes with

larger diameters. The case LR showed that a lower return temperature led to reduced heat losses and reduced pump energy. The case PS showed the same results as the case 95 in terms of heat losses and pump energy. However, the peak heating demand and the maximum pump power were reduced significantly.

Further results can be found in Paper III. These are not presented here due to the issues of the system model used for this study, see Section 4.5.2.

7.2 Including prosumers in local district heating grids

As explained in Section 4.5.2, further development of the first system model led to unacceptably long simulation times. Therefore, the final system model was built based on the simulation models explained in this thesis. One-year simulations were performed with the final system model and the data described in Section 3.2.3 were used as input. The main aim of this analysis was to investigate the effect of including prosumers into the local LTDH grid to reduce GHG emissions. The cases listed in Table 7.2 were defined and simulated.

Table 7.2: Defined cases for the analysis of prosumers in local DH grids.

Case	Supply temperature °C	Comments
HT	115-75	Current high-temperature practice
LT	65	Low-temperature based on Norwegian legislation
LTP1	65	Case LT with low-capacity prosumers
LTP2	65	Case LT with high-capacity prosumers

The supply temperature for the case HT was outdoor temperature compensated and represented the current practice of the main DH grid in Trondheim. For the other cases, a constant supply temperature of 65 °C was assumed as a potential future temperature level considering the Norwegian legislation. For the two cases with prosumers, three distributed prosumers (one data center and two food retail stores) were included in the system model, see Figure 4.33. The waste heat profiles of the prosumers are shown in Figure 3.15. The pipe diameters were different for the cases HT and LT. They were chosen to yield a maximum pressure

drop of 150 Pa/m for each case with the same approach as in the previous section. The diameters from the case LT were also used for the cases with prosumers.

To calculate the GHG emissions, the energy mix of the local DH provider was used as reference. The heat production was divided between the available heat sources, which had given operating limits. Waste incineration was the first priority because the operator gets paid for burning the waste. The remaining heat sources were prioritized based on their emission factors so that the least polluting sources were used first. All heat sources as well as their operating limits and associated emission factors in equivalent $COCO_2$ are listed in Table 7.3.

Table 7.3: Heat sources with operating limits and emission factors.

Heat source	Upper operating limit (kW)	Emission factor kg CO_2e/MWh
Surplus heat from prosumers	-	0
Waste incineration	1 330	11
Bio-oil	1 426	10
Biogas	1 444	11
Recycled wood	1 717	12
Wood chips	1 851	18
Electricity	3 086	110
Liquefied petroleum gas	-	274

The main results from the simulations are presented below (note that the figures are taken from Paper IV and therefore do not follow the notation used in this thesis).

Figure 7.3 shows that the prosumers accounted for a significant share of the total delivered heat, especially during the summer. The share was higher for the case LTP2 due to the higher capacity of the prosumers. To recall, the capacity of the prosumers was based on values from the literature, so the presented results can be considered realistic. However, it should be noted that the prosumers were assumed to be able to deliver heat to the supply line of the grid, i.e. at 65 °C. Due to this relatively high temperature level, a heat pump might be required in a real system to deliver heat to the supply line.

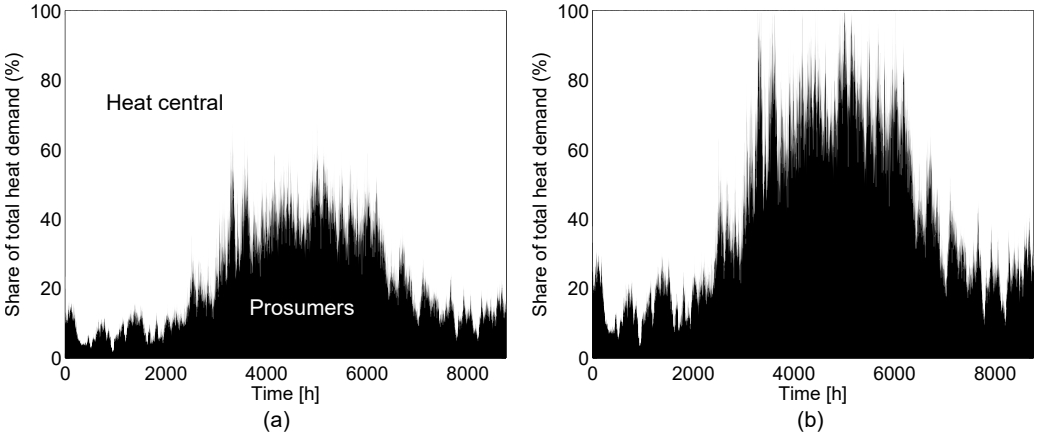

Figure 7.3: Share of heat delivered by the heat central and the prosumers. Cases: (a) LTP1, (b) LTP2 (taken from Paper IV).

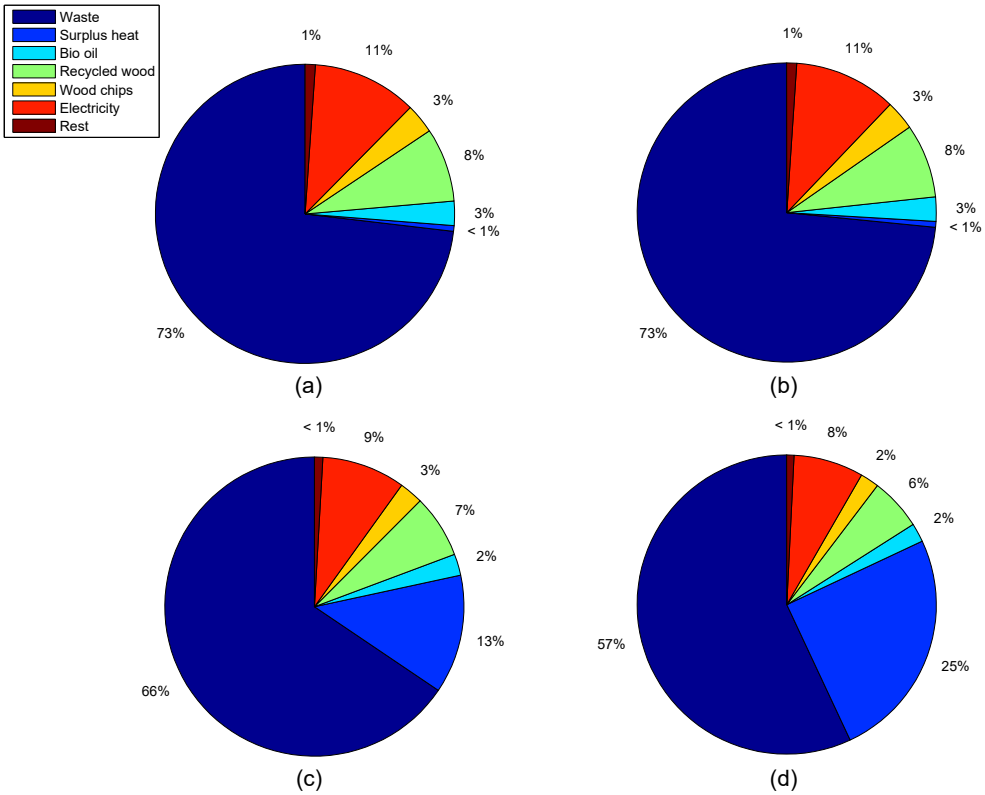

Figure 7.4: The share of heat received from the different heat sources (Rest = Gas). Cases: (a) HT, (b) LT, (c) LTP1, (d) LTP2 (taken from Paper IV).

The resulting share of the heat sources for the local LTDH grid are shown in Figure 7.4 for all simulated cases. The most polluting heat sources are colored in red. It can be seen from Figure 7.4 that the waste heat from the prosumers accounted for 13 % and 25 % for the cases LTP1 and LTP2, respectively. This clearly shows the potential for waste heat utilization in the LTDH grid. The calculated GHG emissions for all the cases are listed in Table 7.4.

Table 7.4: Calculated GHG emissions for all the cases.

Case	Average emissions kg CO_2e/MWh	Reduction compared to the case HT (%)
HT	23.8	0.0
LT	23.6	1.1
LTP1	19.9	16.4
LTP2	17.0	28.9

Table 7.4 shows that significant reductions in GHG emissions were obtained when the emission-free prosumers were included in the grid (16.4 % and 28.9 % for the cases LTP1 and LTP2, respectively). However, most of the waste heat was available during the summer, so the peak heating demand was not reduced significantly. In addition, the heat supply from the prosumers peaked around noon, while the heat demand peaked in the morning due to DHW heating. Reducing peak demands is important for emission reduction because peak heat sources are associated with high emissions. The use of thermal storages for peak shaving could therefore further reduce the GHG emissions of the grid.

Economic aspects were not considered in this study. The inclusion of prosumers was shown to be beneficial in terms of energetic and environmental performance. However, the profitability for the DH supplier depends highly on the applied pricing scheme for waste heat delivery and the investment costs related to prosumer substations.

8 Conclusions and suggestions for further work

8.1 Main conclusions

The main aim of this work was the analysis of both the design and the operation of thermal energy supply systems on neighborhood scale to make these systems more energy- and/or cost efficient. To this end, component and system models were developed in Modelica and used for several analyses. Dynamic simulations with Dymola as well as dynamic optimizations with JModelica.org were successfully performed. Several general conclusions can be drawn from this modeling, simulation, and optimization effort:

1) Modelica-based modeling and simulation are relatively mature and many Modelica libraries with sophisticated simulation models exist. However, an important aspect for system analysis is to ensure that the aim of the analysis and the level of modeling detail are well aligned. No suitable library was available for the planned tasks of this work, i.e. fast simulation of complex thermal energy systems over long time horizons. Therefore, the component models needed to be developed. This was a time-consuming task, but was necessary for successful analysis and can make this work a useful reference for others.

2) Even when suitable component models are available, dynamic simulations can still be a cumbersome task. Entering component model specifications and assembling component models into a system model are usually straightforward tasks. However, the modeling of the control system can be challenging, especially for complex systems with many interconnections. Several simulation performance

issues can arise due to control-related discontinuities, chattering, or algebraic loops. These can make the simulation unnecessary slow or even fail. Efficient system simulation models can therefore only be developed with a certain level of user-experience.

3) Due to the potentially high amount of time required for dynamic system simulation, its use should be carefully evaluated and should not be seen as "low-hanging fruit". However, energy systems are expected to become more complex in the near future - due to the inclusion of fluctuating energy sources, (thermal) energy storages, and more advanced pricing schemes for electricity and district heating – and the operation of such systems cannot be analyzed easily. Dynamic simulations are a suitable tool and are thus expected to be of increasing importance to meet stricter efficiency targets and/or ensure economic operation of future energy systems.

4) JModelica.org, a framework for Modelica-based dynamic optimization, has recently been developed at Lund University and was used in this work. No Modelica library with optimization-ready components for this type of system is available yet. The simulation models developed in this work were therefore used, but had to be adapted due to different handling of the model equations during simulation and optimization. While the required component model changes were minor, the system model complexity had to be reduced. The models were then suitable for dynamic optimization over long time horizons and can therefore be a useful reference for others. However, dynamic optimization is even more advanced than dynamic simulation and can thus be seen as an expert-tool, which is not expected to be widely used outside the research community.

The methodology chosen for this work was shown to be suitable for the analysis of complex thermal energy supply systems with varying load profiles and prices. Reuse of the developed component models was an important aspect and enabled the analysis of different case study systems. Several specific conclusions can be drawn from the analyses of the case study system at Vulkan, Oslo:

1) The annual heat balance of the long-term storage is important for system operation. The current operation might be unsustainable and lead to system performance degradation. Two solutions for sustainable operation were suggested: installing more solar collectors and increasing the heat import from the district

heating grid. These results depended heavily on the simulation model of the long-term storage. Although the short-term response of the model has been validated, a long-term validation could not be performed due to lacking mass flow rate measurements. The installation of flow meters for calibration of the simulation model should be considered to increase the reliability of the results.

2) Changing from constant heating and cooling supply temperature setpoints to variable setpoints could reduce the electricity use of the system. However, the setpoint optimization presented in this work cannot be implemented in a practical manner because the optimized setpoints are adjusted twice an hour. From a practical point of view, operation does not need to be optimal, rather good enough and simple to implement. The optimization approach presented in this work could therefore be used to find practical setpoint adjustments, e.g. outdoor temperature compensated setpoints or setpoints based on daily and/or seasonal schedules. These results depended on the part-load operation of the heat pump. The heat pump COP was only based on the temperature lift of the heat pump during the optimizations in this work. However, a more specific heat pump model considering part-load operation based on advanced circuit simulations was also developed. Using this model could be considered for practical system analyses.

3) Installing larger storage tanks is probably not profitable. Although larger storage tanks could be used for peak shaving and electricity cost reduction, the variability of the electricity price was too low to lead to significant savings for the analyzed period. In addition, savings could only be obtained with a more advanced control system than the one currently implemented. However, higher variability of the electricity price or higher peak load tariffs might lead to a different conclusion.

The simulations of the planned case study system at Brøset, Trondheim confirmed that low-temperature district heating grids are beneficial, especially for new development areas. The pipe diameters were shown to be important for the heat losses in the grid and the required pumping power. The inclusion of prosumers in low-temperature district heating grids was found to reduce greenhouse-gas emissions significantly.

8.2 Suggestions for further work

Recent advances in the development of computational tools for simulation and optimization, supported by increased computational power, have enabled the work presented in this thesis. Due to the high level of individuality of future integrated energy systems and the broadness of the topic, much work remains and some suggestions for further work are given below:

1) Several of the component and system models developed in this work were called "final". Still, many refinements and/or extensions are possible, e.g. the inclusion of pipe models in the system model for Vulkan, a more realistic calculation of the return temperature on the secondary side of the customer substation models, a physical model of the ice thermal energy storage, or a prosumer substation with heat exchangers for more realistic heat supply to the grid. New cases could also be defined and investigated, e.g. charging the borehole thermal energy storage at Vulkan with low-temperature heat from the district heating return line, optimizing the system at Vulkan with a more advanced pricing scheme including district heating prices, or the inclusion of storages and/or solar collectors in the system model for Brøset.

2) The Modelica models developed in this work were tailored to the analyzed case study systems and the aims of the analyses. Developing new models for different types of components would allow the analysis of a wider range of systems and should therefore be considered. Nevertheless, many new use cases for both simulation and optimization have already been defined in the ongoing research projects HighEFF, LTTG+, and LowEmission.

3) Comparing the models developed in this work to the models in the Modelica library IBPSA could give valuable insights. This library is a main part of IBPSA Project 1 (duration 2017 to 2022), which aims at developing a Modelica-based framework for building and community energy system design and operation. This is well within the scope of this work. Optimization with JModelica.org is also part of Project 1 but is, to the best of the author's knowledge, still in an early development phase because many of the simulation models cannot be used for optimization (as was the case in this work). Following the development of the IBPSA library, especially the optimization efforts, is therefore recommended.

4) All the simulation input data were also used as input for the optimizations, i.e. perfect prediction was assumed for the optimization approach presented in this work. Obviously, perfect prediction is not a realistic scenario because energy demands of buildings and the electricity price in Norway both depend on ambient conditions. In practice, the uncertainty of the weather forecast thus makes detailed optimizations over a long prediction horizon obsolete. Repeatedly optimizing a shorter period over a receding horizon, as in Model Predictive Control, is thus a more practical approach. It is therefore suggested to develop Python code for Model Predictive Control in addition to the developed open loop optimization code.

References

[1] European Union (2010). "Directive 2010/31/EU of the European Parliament and of the Council of 19 May 2010 on the energy performance of buildings." *Official Journal of the European Union* L 153, 13–35.

[2] X. Cao, X. Dai, and J. Liu (2016). "Building energy-consumption status worldwide and the state-of-the-art technologies for zero-energy buildings during the past decade." *Energy and Buildings* 128, pp. 198–213. DOI: 10.1016/j.enbuild.2016.06.089.

[3] International Energy Agency (2013). "Heating and Cooling Technologies." In: *Transition to Sustainable Buildings: Strategies and Opportunities to 2050*. Chap. 4. ISBN: 978-92-64-20241-2.

[4] P. Lundqvist (2015). "The role of heat pumps in the smart energy systems." In: *Proceedings of the 24th International Congress of Refrigeration, Yokohama, Japan*. DOI: 10.18462/iir.icr.2015.1009.

[5] D. Schmidt (2018). "Low Temperature District Heating for Future Energy Systems." *Energy Procedia* 149, pp. 595–604. DOI: 10.1016/j.egypro.2018.08.224.

[6] H. Lund et al. (2018). "Future district heating systems and technologies: On the role of smart energy systems and 4th generation district heating." *Energy* 165, pp. 614–619. DOI: 10.1016/j.energy.2018.09.115.

[7] L. Belussi et al. (2019). "A review of performance of zero energy buildings and energy efficiency solutions." *Journal of Building Engineering* 25, p. 100772. DOI: 10.1016/j.jobe.2019.100772.

[8] C. Lausselet, V. Borgnes, and H. Brattebø (2019). "LCA modelling for Zero Emission Neighbourhoods in early stage planning." *Building and Environment* 149, pp. 379–389. DOI: 10.1016/j.buildenv.2018.12.034.

[9] F. Jorissen et al. (2018). "Implementation and verification of the IDEAS building energy simulation library." *Journal of Building Performance Simulation* 11 (6), pp. 669–688. DOI: 10.1080/19401493.2018.1428361.

[10] G. Schweiger et al. (2018). "District energy systems: Modelling paradigms and general-purpose tools." *Energy* 164, pp. 1326–1340. DOI: 10.1016/j.energy.2018.08.193.

[11] A. Brand et al. (2015). "Beyond authorship: attribution, contribution, collaboration, and credit." *Learned Publishing* 28 (2), pp. 151–155. DOI: 10.1087/20150211.

[12] M. Lanahan and P. C. Tabares-Velasco (2017). "Seasonal Thermal-Energy Storage: A Critical Review on BTES Systems, Modeling, and System Design for Higher System Efficiency." *Energies* 10 (6). DOI: 10.3390/en10060743.

[13] G. Alva, Y. Lin, and G. Fang (2018). "An overview of thermal energy storage systems." *Energy* 144, pp. 341–378. DOI: 10.1016/j.energy.2017.12.037.

[14] J. Heier, C. Bales, and V. Martin (2015). "Combining thermal energy storage with buildings – a review." *Renewable and Sustainable Energy Reviews* 42, pp. 1305–1325. DOI: 10.1016/j.rser.2014.11.031.

[15] A. R. Mazhar, S. Liu, and A. Shukla (2018). "A state of art review on the district heating systems." *Renewable and Sustainable Energy Reviews* 96, pp. 420–439. DOI: 10.1016/j.rser.2018.08.005.

[16] A. Afram and F. Janabi-Sharifi (2014). "Theory and applications of HVAC control systems – A review of model predictive control (MPC)." *Building and Environment* 72, pp. 343–355. DOI: 10.1016/j.buildenv.2013.11.016.

[17] R. Ooka and S. Ikeda (2015). "A review on optimization techniques for active thermal energy storage control." *Energy and Buildings* 106, pp. 225–233. DOI: 10.1016/j.enbuild.2015.07.031.

[18] J. Clauß et al. (2019). "Predictive rule-based control to activate the energy flexibility of Norwegian residential buildings: Case of an air-source heat pump and direct electric heating." *Applied Energy* 237, pp. 500–518. DOI: 10.1016/j.apenergy.2018.12.074.

[19] P. Rockett and E. A. Hathway (2017). "Model-predictive control for non-domestic buildings: a critical review and prospects." *Building Research and Information* 45 (5), pp. 556–571. DOI: 10.1080/09613218.2016.1139885.

[20] K. Rupp (2018). *"42 Years of Microprocessor Trend Data"*. www.karlrupp.net/2018/02/42-years-of-microprocessor-trend-data. Accessed 05/2019.

[21] G. Augenbroe (2011). "The role of simulation in performance based building." In: *Building Performance Simulation for Design and Operation*. Spon Press. Chap. 2, pp. 15–36. ISBN: 978–0–415–47414–6.

[22] M. Trčka and J. L. M. Hensen (2010). "Overview of HVAC system simulation." *Automation in Construction* 19 (2), pp. 93–99. DOI: 10.1016/j.autcon.2009.11.019.

[23] M. Wetter, M. Bonvini, and T. S. Nouidui (2016). "Equation-based languages – A new paradigm for building energy modeling, simulation and optimization." *Energy and Buildings* 117, pp. 290–300. DOI: 10.1016/j.enbuild.2015.10.017.

[24] Modelica Association (2017). "Modelica - A Unified Object-Oriented Language for Systems Modeling." *Language Specification Version 3.4*. URL: www.modelica.org/documents/ModelicaSpec34.pdf.

[25] Modelica Association. *"Modelica Libraries"*. www.modelica.org/libraries. Accessed 03/2019.

[26] J. Allegrini et al. (2015). "A review of modelling approaches and tools for the simulation of district-scale energy systems." *Renewable and Sustainable Energy Reviews* 52, pp. 1391–1404. DOI: 10.1016/j.rser.2015.07.123.

[27] Modelica Association. *"Modelica Tools"*. www.modelica.org/tools. Accessed 03/2019.

[28] S. Dutta (2016). "A Brief Discussion on Optimization." In: *Optimization in Chemical Engineering*. Cambridge University Press. Chap. 1, p. 7. ISBN: 978-1-107-09123-8.

[29] D. H. Wolpert and W. G. Macready (1997). "No Free Lunch Theorems for Optimization." *IEEE Transactions on Evolutionary Computation* 1 (1), pp. 67–82. DOI: 10.1109/4235.585893.

[30] L. T. Biegler (2010). "Simultaneous Methods for Dynamic Optimization." In: *Nonlinear Programming*. MOS-SIAM Series on Optimization. Chap. 10, pp. 287–324. ISBN: 978-0-89871-702-0.

[31] F. Magnusson and J. Åkesson (2015). "Dynamic Optimization in JModelica.org." *Processes* 3 (2), p. 471. DOI: 10.3390/pr3020471.

[32] J. A. E. Andersson et al. (2019). "CasADi: a software framework for nonlinear optimization and optimal control." *Mathematical Programming Computation* 11 (1), pp. 1–36. DOI: 10.1007/s12532-018-0139-4.

[33] A. Wächter and L. T. Biegler (2006). "On the implementation of an interior-point filter line-search algorithm for large-scale nonlinear programming." *Mathematical Programming* 106 (1), pp. 25–57. DOI: 10.1007/s10107-004-0559-y.

[34] J. Åkesson (2008). "Optimica - An Extension of Modelica Supporting Dynamic Optimization." In: *Proceedings of the 6th International Modelica Conference*.

[35] F. Belkhir et al. (2015). "Optimal Startup Control of a Steam Power Plant Using the JModelica Platform." *IFAC-PapersOnLine* 48 (1), pp. 204–209. DOI: 10.1016/j.ifacol.2015.05.050.

[36] A. Holmqvist and F. Magnusson (2016). "Open-loop optimal control of batch chromatographic separation processes using direct collocation." *Journal of Process Control* 46, pp. 55–74. DOI: 10.1016/j.jprocont.2016.08.002.

[37] S. Barsali et al. (2017). "Optimised operation of storage systems integrated with MV photovoltaic plants, considering the impact on the battery lifetime." *Journal of Energy Storage* 12, pp. 178–185. DOI: 10.1016/j.est.2017.05.003.

[38] Y. Cao et al. (2017). "Real-time feasible multi-objective optimization based nonlinear model predictive control of particle size and shape in a batch crystallization process." *Control Engineering Practice* 69, pp. 1–8. DOI: 10.1016/j.conengprac.2017.08.008.

[39] A. Sellberg et al. (2018). "Multi-flowrate Optimization of the Loading Phase of a Preparative Chromatographic Separation." *Computer Aided Chemical Engineering* 43, pp. 1619 –1624. DOI: 10.1016/B978-0-444-64235-6.50282-5.

[40] F. Audino et al. (2019). "Systematic optimization approach for the efficient management of the photo-Fenton treatment process." *Science of The Total Environment* 646, pp. 902–913. DOI: 10.1016/j.scitotenv.2018.07.057.

[41] R. De Coninck et al. (2016). "Toolbox for development and validation of grey-box building models for forecasting and control." *Journal of Building Performance Simulation* 9 (3), pp. 288–303. DOI: 10.1080/19401493.2015.1046933.

[42] G. Schweiger et al. (2017). "District heating and cooling systems – Framework for Modelica-based simulation and dynamic optimization." *Energy* 137, pp. 566–578. DOI: 10.1016/j.energy.2017.05.115.

[43] F. Jorissen, W. Boydens, and L. Helsen (2019). "TACO, an automated toolchain for model predictive control of building systems: implementation and verification." *Journal of Building Performance Simulation* 12 (2), pp. 180–192. DOI: 10.1080/19401493.2018.1498537.

[44] B. Knudsen, H. Kauko, and T. Andresen (2019). "An optimal-control scheme for coordinated surplus-heat exchange in industry clusters." *Energies* 12 (10). DOI: 10.3390/en12101877.

[45] Norwegian Institute of Bioeconomy Research. *"Weather Data for Norway"*. https://lmt.nibio.no/agrometbase/getweatherdata_new.php. Accessed 03/2018.

[46] Trondheim Municipality (2013). *"Områdeplan for Brøset. Vedlegg 4 - illustrasjonsplan"*. www.trondheim.kommune.no/globalassets/10-bilder-og-filer/10-byutvikling/byplankontoret/temaplaner/omradeplan-for-broset/vedlegg-4---illustrasjonsplan-04.04.13.pdf. Accessed 04/2019.

[47] Trondheim Municipality (2011). *"Områdeplan for Brøset. Vedlegg 19 - energiløsninger" (in Norwegian)*. www.trondheim.kommune.no/globalassets/10-bilder-og-filer/10-byutvikling/byplankontoret/temaplaner/omradeplan-for-broset/vedlegg-19---energilosninger.pdf. Accessed 04/2019.

[48] H. Lund et al. (2014). "4th Generation District Heating (4GDH): Integrating smart thermal grids into future sustainable energy systems." *Energy* 68, pp. 1–11. DOI: 10.1016/j.energy.2014.02.089.

[49] T. Tereshchenko and N. Nord (2018). "Future Trends in District Heating Development." *Current Sustainable/Renewable Energy Reports* 5 (2), pp. 172–180. DOI: 10.1007/s40518-018-0111-y.

[50] TLK-Thermo GmbH. *"TIL Suite – Simulates thermal systems"*. https://www.tlk-thermo.com/index.php/en/software-products/til-suite. Accessed 06/2019.

[51] M. Wetter et al. (2014). "Modelica Buildings library." *Journal of Building Performance Simulation* 7 (4), pp. 253–270. DOI: 10.1080/19401493.2013.765506.

[52] F. Jorissen, M. Wetter, and L. Helsen (2015). "Simulation Speed Analysis and Improvements of Modelica Models for Building Energy Simulation." In: *Proceedings of the 11th International Modelica Conference*. DOI: 10.3384/ecp1511859.

[53] I. H. Bell et al. (2014). "Pure and Pseudo-pure Fluid Thermophysical Property Evaluation and the Open-Source Thermophysical Property Library CoolProp." *Industrial and Engineering Chemistry Research* 53 (6), pp. 2498–2508. DOI: 10.1021/ie4033999.

[54] H. Sofrata (1993). "Carnot and Lorenz cycles for dual absorption system." *Wärme - und Stoffübertragung* 28 (3), pp. 107–116. DOI: 10.1007/BF01541106.

[55] F. P. Incropera et al. (2007). "Heat Exchangers." In: *Fundamentals of Heat and Mass Transfer*. John Wiley & Sons. Chap. 11. ISBN: 978-0-471-45728-2.

[56] J. Yang, A. Jacobi, and W. Liu (2017). "Heat transfer correlations for single-phase flow in plate heat exchangers based on experimental data." *Applied Thermal Engineering* 113, pp. 1547–1557. DOI: 10.1016/j.applthermaleng.2016.10.147.

[57] F. Ruiz-Calvo et al. (2015). "Experimental validation of a short-term Borehole-to-Ground (B2G) dynamic model." *Applied Energy* 140, pp. 210–223. DOI: 10.1016/j.apenergy.2014.12.002.

[58] D. Bauer et al. (2011). "Thermal resistance and capacity models for borehole heat exchangers." *International Journal of Energy Research* 35 (4), pp. 312–320. DOI: 10.1002/er.1689.

[59] P. Stephan (2010). "Fundamentals of Heat Transfer." In: *VDI Heat Atlas*. Springer Berlin Heidelberg. Chap. B1, pp. 15–30. ISBN: 978-3-540-77876-9.

[60] B. Sibbitt et al. (2012). "The Performance of a High Solar Fraction Seasonal Storage District Heating System – Five Years of Operation." *Energy Procedia* 30, pp. 856–865. DOI: 10.1016/j.egypro.2012.11.097.

[61] R. A. Beier, M. D. Smith, and J. D. Spitler (2011). "Reference data sets for vertical borehole ground heat exchanger models and thermal response test analysis." *Geothermics* 40 (1), pp. 79–85. DOI: 10.1016/j.geothermics.2010.12.007.

[62] F. Mosallat et al. (2013). "Modeling, Simulation and Control of Flat Panel Solar Collectors with Thermal Storage for Heating and Cooling Applications." *Procedia Computer Science* 19, pp. 686–693. DOI: 10.1016/j.procs.2013.06.091.

[63] A. C. Hindmarsh et al. (2005). "SUNDIALS: Suite of nonlinear and differential/algebraic equation solvers." *ACM Transactions on Mathematical Software* 31 (3), pp. 363–396. DOI: 10.1145/1089014.1089020.

[64] F. Magnusson and J. Åkesson (2018). "Symbolic elimination in dynamic optimization based on block-triangular ordering." *Optimization Methods and Software* 33 (1), pp. 92–119. DOI: 10.1080/10556788.2016.1270944.

[65] HSL. *"A collection of Fortran codes for large scale scientific computation"*. www.hsl.rl.ac.uk. Accessed 03/2018.

[66] Sivilingeniør Carl Christian Strømberg AS. *"Solar potential of roof areas in Norway"*. https://solkart.no. Accessed 04/2019.

[67] H. Holmberg et al. (2016). "Numerical model for non-grouted borehole heat exchangers, Part 2 - Evaluation." *Geothermics* 59, pp. 134–144. DOI: 10.1016/j.geothermics.2014.11.002.

[68] R. K. Ramstad et al. (2015). "Thermal conductivity map of the Oslo region based on thermal diffusivity measurements of rock core samples." *Bulletin of Engineering Geology and the Environment* 74 (4), pp. 1275–1286. DOI: 10.1007/s10064-014-0701-x.

[69] Nord Pool AS. *"Historical Market Data"*. https://www.nordpoolgroup.com/historical-market-data/. Accessed 02/2019.

[70] D. Fischer et al. (2016). "Impact of PV and variable prices on optimal system sizing for heat pumps and thermal storage." *Energy and Buildings* 128, pp. 723–733. DOI: 10.1016/j.enbuild.2016.07.008.